HARMONICS FORECASTING FOR WIND AND SOLAR RENEWABLE ENERGY RESOURCES-BASED ELECTRICAL POWER SYSTEMS

by

Fawaz Masoud Al Hadi

Submitted in partial fulfilment of the requirements
for the degree of Doctor of Philosophy

at

Dalhousie University
Halifax, Nova Scotia
November 2023

Dedication

I dedicate this thesis to my parents (Masoud and Saadah),
my wife (Amani), my children (Kinda, Mohammad, and Jasser),
and all my family.

Table of Content

List of Tables viii

List of Figures ix

Abstract xii

List of Abbreviations and Symbols Used xiii

Acknowledgement xv

Chapter 1: Introduction 1

1.1 Thesis Motivation 1

1.2 Significance of Harmonics Forecasting 2

1.3 Thesis Aim 6

1.4 Thesis Outline 9

1.5 Thesis Contribution 10

1.6 List of Publications 11

Chapter 2: Literature Survey 13

2.1 Power Quality 13

2.2 Harmonics 16

2.2.1 Definition, Causes, and Impacts of Harmonics 16

2.2.2 Interharmonics 17

2.2.3 Harmonics Distortion Sources in RESs 17

2.2.4 Harmonics Analysis and Fourier Series 18

2.2.5 Total Harmonic Distortion (THD) 22

2.2.6 Total Demand Distortion (TDD) 23

2.2.7 Individual Harmonic Distortion (IHD) 24

2.3 IEEE Standard 519-2014 for Voltage and Current Harmonics 24
2.4 Harmonics Mitigation and Rationale for Studying Harmonics Forecasting.. 26
2.5 Rationale for Building a Hybrid Model Combining Multilayered-ANN with ANFIS for Harmonics Forecasting..... 38
2.5.1 Complementary Strengths of ANN and ANFIS 38
2.5.2 Capturing Nonlinearities and Complex Relationships..... 39
2.5.3 Improved Forecasting Accuracy and Robustness 39
2.5.4 Adaptability and Generalization 40
2.5.5 Model Transparency and Interpretability..... 40
2.5.6 Summary 40
2.6 Rationale for Building a Hybrid Model Combining LSTM with ANFIS for Harmonics Forecasting..... 42
2.6.1 Capturing Temporal Dependencies..... 42
2.6.2 Fuzzy Logic-Based Reasoning 42
2.6.3 Handling Nonlinearities..... 43
2.6.4 Incorporating Domain Knowledge 43
2.6.5 Enhanced Interpretability..... 43
2.6.6 Robustness and Generalization..... 44
2.6.7 Summary 44
2.7 Summary 45
Chapter 3: Models and Harmonics Forecasting Techniques 46
3.1 Overview 46
3.2 Generator Models..... 46
3.2.1 Hybrid Wind-DFIG Solar Energy System..... 46

3.2.2 Hybrid Wind-PMSG Solar Energy System 48
3.3 Artificial Neural Networks and Proposed Algorithm 48
3.3.1 Introduction 48
3.3.2 Single and Multilayered Feed-Forward Neural Network 49
3.3.3 Cascaded, Recurrent and Hybrid Neural Networks 52
3.3.4 Three-Layered Recurrent Cascaded Neural Network with Local Feedback . 53
3.3.5 Three-Layered Cascaded Recurrent Neural Network with Global Feedback 54
3.3.6 Three-Layered Cascaded Recurrent Neural Network with Local and Global Feedback 55
3.3.7 Network Training 57
3.4 Adaptive Neuro Fuzzy Inference System (ANFIS) 57
3.4.1 Introduction 57
3.4.2 ANFIS Structure and Working Principle 58
3.4.3 Learning Algorithm 60
3.5 Long Short-Term Memory Network (LSTM) 60
3.5.1 Introduction 60
3.5.2 Architecture of LSTM 61
3.6 Novel Hybrid Forecasting Models 63
3.6.1 Introduction 63
3.6.2 Model-1 – 3LCRNNL-ANFIS 63
3.6.3 Model-2 – 3LCRNNG-ANFIS 63
3.6.4 Model-3 – 3LCRNNGL-ANFIS 64
3.6.5 Model 4 – ANFIS-3LCRNNL 64

3.6.6 Model-5 – ANFIS-3LCRNNG Model 65
3.6.7 Model-6 – ANFIS-3LCRNNGL 65
3.6.8 Model-7 – LSTM-ANFIS 66
3.6.9 Model-8 – ANFIS-LSTM 66
3.7 K-Fold Cross-Validation 66
3.8 Implementation of Hybrid Forecasting Models 68
3.8.1 Data Generation from Generator Models 68
3.8.2 Selection of Inputs 69
3.8.3 Data Pre-processing 72
3.8.4 Network Training and Forecasting Methodology 74
3.8.4.1 Application of Artificial Neural Networks 74
3.8.4.2 Application of Adaptive Neuro Fuzzy Inference System 77
3.8.4.3 Application of Long Short-Term Memory Network 80
3.8.4.4 Application of K-Fold Cross-Validation 81
3.8.4.5 Models 1-3: 3LCRNNL-ANFIS, 3LCRNNG-ANFIS, and 3LCRNNGL-ANFIS 84
3.8.4.6 Models 4-6: ANFIS-3LCRNNL, ANFIS-3LCRNNG, and ANFIS-3LCRNNGL 85
3.8.4.7 Models 7-8: LSTM-ANFIS and ANFIS-LSTM 85
3.8.5 Evaluation of the Forecasting Models 86
3.8.5.1 Root Mean Squared Error (RMSE) 86
3.8.5.2 Mean Absolute Error (MAE) 87
3.8.6 Use of Software 87
3.8.7 Conclusion 87

Chapter 4: Results and Discussion 89
4.1 Overview 89
4.2 Generator Models 89
4.3 Voltage Harmonics Results for Generator Models 95
4.4 Current Harmonics Results for Generator Models 99
4.5 Utilization of Artificial Neural Networks 101
4.6 Utilization of the Long Short-Term Memory Network 102
4.7 Utilization of an Adaptive Neuro-Fuzzy Inference System 102
4.8 Harmonics Forecasting Results and Analysis – Wind-DFIG-PV 103
4.8.1 Voltage Harmonics 103
4.8.2 Current Harmonics 108
4.9 Harmonics Forecasting Results – Wind-PMSG-PV Model 114
4.9.1 Voltage Harmonics 114
4.9.2 Current Harmonics 118
4.9.3 Conclusion 123
Chapter 5: Conclusions, and Future Works 126
5.1 Conclusions 126
5.2 Future Works 127
References 129
Appendix A: NON-EXCLUSIVE DISTRIBUTION LICENSE 141

List of Tables

Table 1: Principal Phenomena Causing Electromagnetic Disturbances as Classified by the IEC [18] 14
Table 2: Categories and Typical Characteristics of Power System Electromagnetic Phenomena as defined in IEEE Std 1159-2009 [18] 15
Table 3: IEEE Std 519-2014 Voltage Distortion Limits [6] 25
Table 4: IEEE Std 519-2014 Current Distortion Limits Rated 120V Through 69kV [6]. 25
Table 5: IEEE Std 519-2014 Current Distortion Limits Rated 69kV Through 161kV [6]26
Table 6: Strengths and Weaknesses of Forecasting Models 35
Table 7: Rationale for ANN-ANFIS-based Hybrid Model Summary 41
Table 8: Rationale for LSTM-ANFIS-based Hybrid Model Summary 44
Table 9: Statistical Parameters for Wind-DFIG-PV Generator Voltage Harmonics 97
Table 10: Statistical Parameters for Wind-PMSG-PV Generator Voltage Harmonics 98
Table 11: Statistical Parameters for Wind-DFIG-PV Generator Current Harmonics 100
Table 12: Statistical Parameters for Wind-PMSG-PV Generator Current Harmonics... 101
Table 13: Forecasting Result Comparison Voltage Harmonics – Wind-DFIG-PV 106
Table 14: Best Forecasting Model for Voltage Harmonics – Wind-DFIG-PV 108
Table 15: Forecasting Result Comparison Current Harmonics – Wind-DFIG-PV 112
Table 16: Best Forecasting Model for Current Harmonics – Wind-DFIG-PV 113
Table 17: Forecasting Result Comparison Voltage Harmonics – Wind-PMSG-PV 116
Table 18: Best Forecasting Model for Voltage Harmonics – Wind-PMSG-PV 118
Table 19: Forecasting Results Comparison for Current Harmonics – Wind-PMSG-PV 121
Table 20: Best Forecasting Model for Current Harmonics – Wind-PMSG-PV 123

List of Figures

Figure 1: Power Quality Issues 16
Figure 2: Fourier Series Representation 20
Figure 3: Fast Fourier Transform Depicting Frequency Spectrum 22
Figure 4: Artificial Neuron Model [69] 49
Figure 5: Single-Layered Perceptron Network [69] 50
Figure 6: Multi-Layered Perceptron Network [69] 51
Figure 7: Three-Layered Cascaded Neural Network 52
Figure 8: Recurrent Neural Network with Local Feedback 53
Figure 9: Recurrent Neural Network with Global Feedback 53
Figure 10: Three-Layered Cascaded Recurrent Neural Network with Local Feedback (3LCRNNL) 54
Figure 11: Three-Layered Cascaded Recurrent Neural Network with Global Feedback (3LCRNNG) 55
Figure 12: Three-Layered Cascaded Recurrent Neural Network with Local and Global Feedback (3LCRNNGL) 56
Figure 13: First-Order Sugeno Fuzzy Inference System 58
Figure 14: ANFIS Architecture [74] 59
Figure 15: 3LCRNNL-ANFIS Model 63
Figure 16: 3LCRNNG-ANFIS Model 64
Figure 17: 3LCRNNGL-ANFIS Model 64
Figure 18: ANFIS-3LCRNNL Model 65
Figure 19: ANFIS-3LCRNNG Model 65
Figure 20: ANFIS-3LCRNNGL Model 65
Figure 21: LSTM-ANFIS Model 66
Figure 22: ANFIS-LSTM Model 66
Figure 23: Total Harmonic Distortion Curves for Wind-DFIG PV Model 71
Figure 24: THD vs Wind Speed and Solar Irradiation for Wind-DFIG-PV (Day 5) 71
Figure 25: THD vs Wind Speed and Solar Irradiation for Wind-DFIG-PV (Day 4) 72

Figure 26: Superimposed Hyperbolic Function over Sigmoid Function 75
Figure 27: Structure of LSTM Model 81
Figure 28: K-Fold Data Split Using Expanding Window for Time Series 82
Figure 29: K-Fold Cross-Validation Methodology 83
Figure 30: Forecasting Using K-Fold Cross-Validation for Model Training (for All Models) 83
Figure 31: Wind-DFIG PV Model 91
Figure 32: Wind-PMSG PV Model 91
Figure 33: Sample Voltage Waveform for Wind-DFIG-PV Model (Phases 1 & 2) 92
Figure 34: Sample Voltage Waveform for Wind-DFIG-PV Model (Phases 1 & 3) 93
Figure 35: Sample Current Waveform for Wind-DFIG-PV Model (Phases 1 & 2) 94
Figure 36: Sample Current Waveform for Wind-DFIG-PV Model (Phases 1 & 3) 95
Figure 37: THD for Wind-DFIG-PV Model 96
Figure 38: THD for Wind-DFIG-PV Model, Days 3 to 5 96
Figure 39: THD for Wind-PMSG-PV Model 97
Figure 40: TDD for Wind-DFIG-PV Model 99
Figure 41: TDD for Wind-DFIG-PV Model, Days 3 to 5 99
Figure 42: TDD for Wind-PMSG-PV Model 100
Figure 43: THDV – Actual vs Forecast Curves Wind-DFIG-PV 103
Figure 44: Voltage 7th Harmonic – Actual vs Forecast Curves Wind-DFIG-PV 104
Figure 45: Voltage 11th Harmonic – Actual vs Forecast Curves Wind-DFIG-PV 104
Figure 46: Voltage 13th Harmonic – Actual vs Forecast Curves Wind-DFIG-PV 105
Figure 47: TDD – Actual vs Forecast Curves Wind-DFIG-PV 109
Figure 48: Current 7th Harmonic – Actual vs Forecast Curves Wind-DFIG-PV 109
Figure 49: Current 11th Harmonic – Actual vs Forecast Curves Wind-DFIG-PV 110
Figure 50: Current 13th Harmonic – Actual vs Forecast Curves Wind-DFIG-PV 110
Figure 51: THDV – Actual vs Forecast Curves Wind-PMSG-PV Model 114
Figure 52: Voltage 7th Harmonic – Actual vs Forecast Curves Wind-PMSG-PV 115
Figure 53: Voltage 11th Harmonic – Actual vs Forecast Curves Wind-PMSG-PV 115
Figure 54: Voltage 13th Harmonic – Actual vs Forecast Curves Wind-PMSG-PV 116

Figure 55: TDD – Actual vs Forecast Curves Wind-PMSG-PV Model..... 119
Figure 56: Current 7th Harmonic – Actual vs Forecast Curves Wind-PMSG-PV..... 120
Figure 57: Current 11th Harmonic – Actual vs Forecast Curves Wind-PMSG-PV..... 120
Figure 58: Current 13th Harmonic – Actual vs Forecast Curves Wind-PMSG-PV..... 121

Abstract

The practice of harmonics forecasting plays an integral role in the development of mitigation devices aimed at lessening the adverse effects of harmonic disturbances in electrical systems. This doctoral research endeavours to contribute to this field by introducing a novel hybrid forecasting model capable of generating precise and reliable harmonics predictions for Renewable Energy Systems (RESs). To attain this objective, multi-layered Advanced Neural Networks (ANNs), the Adaptive Neuro Fuzzy Inference System (ANFIS), and the Long Short-Term Memory (LSTM) network were harnessed to formulate eight innovative hybrid forecasting models, which are the integral components of this study.

Within the scope of the research, three distinct ANN structures featuring three layers each—Cascaded Recurrent Neural Network with Local feedback (3LCRNNL), Cascaded Recurrent Neural Network with Global feedback (3LCRNNG), and Cascaded Recurrent Neural Network with Local and Global feedback (CRNNLG)—are combined with ANFIS to create the initial six hybrid forecasting models (Models 1-6). The integration of the ANFIS-LSTM techniques results in the formulation of two additional hybrid models (Models 7-8).

In conjunction with these modelling efforts, two renewable generator models are employed to generate harmonics. The first model involves a grid-connected Double-Fed Induction Generator (DFIG) driven by a wind turbine and integrated with a Solar Photovoltaic (PV)-based power generator. The second generator model combines a Solar-PV generator with a wind turbine-linked Permanent Magnet Synchronous Generator (PMSG) interconnected to a shared grid. The harmonics generated by these generator models are utilized to construct comprehensive training and testing datasets that are subsequently employed to generate forecasts using the novel hybrid forecasting models proposed in this research.

To rigorously evaluate the performance and effectiveness of these models, a systematic comparison is conducted against benchmark studies available in the literature. The findings highlight the exceptional performance consistency of model-8, which not only outperforms all of the other proposed models in the study, but also significantly surpasses the capabilities of existing techniques in the literature. Moreover, this study underscores the superiority of hybrid forecasting models over individual forecasting techniques typically used as benchmarks, thereby reaffirming the value of hybrid modelling in the context of harmonics forecasting for RESs.

List of Abbreviations and Symbols Used

3LCRNNG	Three-Layered Cascaded Recurrent Neural Network with Global Feedback
3LCRNNGL	Three-Layered Cascaded Recurrent Neural Network with Local and Global Feedback
3LCRNNL	Three-Layered Cascaded Recurrent Neural Network with Local Feedback
ANFIS	Adaptive Neuro Fuzzy Interference Systems
ANN	Artificial Neural Network
CNN	Cascaded Neural Network
DFIG	Double Fed Induction Generator
DFT	Discrete Fourier Transform
DTW	Dynamic Time Wrapping
EMD	Empirical Mode Decomposition
EPS	Electrical Power System
FFT	Fast Fourier Transform
FIS	Fuzzy Inference System
HAPF	Hybrid Active Power Filter
IEC	International Electrotechnical Commission
IEEE	Institute for Electrical and Electronics Engineers
IHD	Individual Harmonic Distortion
JRC	Joint Research Centre
LED	Light Emitting Diode
LMS	Least Mean Square
LSTM	Long Short-Term Memory
LV	Low Voltage
MAE	Mean Absolute Error
MLP	Multilayer Perceptron
MLPN	Multilayer Perceptron Network
MW	Mega Watt

NLMS	Normalized LMS
PCC	Point of Common Coupling
PMSG	Permanent Magnet Synchronous Generator
PQ	Power Quality
PV	Photovoltaic
RES	Renewable Energy Systems
RMS	Root Mean Square
RMSE	Root Mean Square Error
RNN	Recurrent Neural Network
SLFNN	Single-Layer Feed-Forward Neural Network
SLP	Single Layer Perceptron
SVR	Support Vector Regression
TDD	Total Demand Distortion
THD	Total Harmonic Distortion
UDR	Univariate Dimension Reduction
VLLMS	Variable Leaky Least Mean Square
VSC	Voltage Source Converter

Acknowledgement

All thanks to Allah, who gives and grants me this success and this degree. I am very grateful to my sponsor, Technical and Vocational Training Corporation (TVTC), for giving me the opportunity to study abroad and continue my Ph.D. I also wish to acknowledge the Saudi Arabian Cultural Bureau (SACB) in Ottawa, Canada, for its generous support.

In particular, I wish to express my deepest gratitude to Dr. Timothy Little, my Ph.D. supervisor, for his invaluable advice, continuous encouragement, and superhuman patience during my Ph.D. study. I am truly grateful for his help. Also, it is difficult to find words to express my gratitude to Dr. Hamed Aly, my co-supervisor. His impressive knowledge and vast experience have guided me throughout my academic research, and for that I will forever be grateful to him.

I must as well show my appreciation for the efforts of my first supervisor, Dr. Mohamed El-Hawary, who supervised my Master and Ph.D. work until his passing on July 26, 2019. Additionally, I would like to thank Dr. Guy Kember for agreeing to be one of the committee members at the last minute because of Dr. William Phillips' sickness, and Dr. Jason Gu, for serving as a committee member for both my Master and Ph.D. degrees. Also, I am immensely thankful to the external examiner, Dr. Sherif Faried of the University of Saskatchewan, Canada, for his valuable time and for agreeing to evaluate my thesis and join the defence. Finally, I am extremely grateful to Mrs. Saly Michael at the SACB for facilitating my administrative procedures throughout my academic studies in Canada.

Chapter 1: Introduction

1.1 Thesis Motivation

The generation of electrical energy from renewable energy resources has significantly increased in recent decades, making it one of the most important research topics today. Solar and wind energy-based Renewable Energy Systems (RESs) are one of the most rapidly growing technologies for generating electric energy as a means of producing clean energy, meeting energy demands, and preserving rapidly depleting fossil fuel sources [1]. New ideas such as smart grids and microgrids have emerged as a result of the rising penetration of renewable/sustainable energy generation technologies on the Electrical Power System (EPS) [2]. The unpredictable and uncontrollable nature of these RESs in terms of power output is a fundamental challenge in achieving EPS stability, as it results in the deterioration of its power quality (PQ). RESs have different characteristics than conventional power sources, with the main ones being that they are less controllable, generate undesirable power flow patterns, and result in non-sinusoidal current and voltage waveforms.

Furthermore, the grid integration of RESs involves various types of power electronics-based converters and inverters, which converts Direct Current (DC) to Alternating Current (AC) or vice versa for control and regulation. These electronic devices at their terminals produce both current and voltage harmonics, which are transferred to the remainder of the grid. The presence of harmonics could cause transformers to overheat, circuit breakers to trip, or protection devices to malfunction, resulting in a reduction in the life of connected equipment [3], [4], [5]. Therefore,

harmonics are one of the most important characteristics that must be kept to a minimum to secure network power quality, as per IEEE 519-2014 guidelines [6].

For large-scale integration of renewable energy into a secure and efficient system, harmonics estimation is an important tool that could help reduce harmonics distortion. If an accurate estimation of harmonics could be made, it could lead to developing solutions that effectively reduce the impact of harmonics on the system. The next section will address the subject of harmonics estimation and its significance for harmonics mitigation.

1.2 Significance of Harmonics Forecasting

Harmonics are the integer multiples of fundamental frequencies and depict a distorted waveform. They have a significant impact on the power system and load as well as the operational efficiency and dependability of the protective relay [7], [8]. Power system losses rise dramatically when harmonics are present. Voltage disturbances originate from a harmonic voltage drop across system impedances, causing other linear loads to draw a harmonic current. Another major side-effect of harmonics is communications interferences [9].

As a result, the harmonics problem necessitates much consideration for accurate prediction and reliable mitigation. In this context, many standards, guidelines, and suggestions have been implemented, including IEEE standard 519-2014 [6] and the IEC 61000 family of standards [10], [11], [12]. To quantify the level of distortions contained in the original signal, some indices have been established, such as Total Harmonic Distortion (THD) and Total Demand Distortion (TDD), which are used for voltage and current harmonics [13]. For instance, voltage THD should be less than or equivalent to

a 5% limit in the Point of Common Coupling (PCC), as per IEEE 519-2014. In order to reduce harmonics, their forecasting is one of many techniques used to design harmonic mitigation devices.

The term "harmonics forecasting" refers to the identification of frequency components in a signal, as well as the prediction of their amplitudes and phases. Harmonics prediction is critical for constructing harmonics mitigation devices and other controllers, since it allows identification of the harmonics components and their magnitudes. Harmonics forecasting should be rapid enough for real-time use, highly accurate for greater reliability, simple to apply in practice, and cost-effective. Because power systems are highly dynamic, network topologies and characteristics are constantly changing. As a result, harmonics prediction should be adaptive. It should also be resistant to noise and transients, which are common in measured data.

In order to achieve harmonics forecasting, various techniques have been employed by different researchers. These techniques can be divided into parametric and non-parametric methods [14]. Non-parametric methods forecast the spectrum directly from the signal, usually in terms of the coefficients (i.e., amplitude) of a collection of known functions, referred to as the basis function. Depending on the approach utilized, the forecasted signal can be time-independent or time-dependent. Parametric methods represent the signal with an appropriate model and then estimate the model's parameters from the available data points. The predicted parameters are then applied to the chosen model to determine the signal's harmonic content.

This thesis will adopt the parametric method, as the datapoints generated will adjust the model parameters to perform forecasts. Namely, the Adaptive Neuro Fuzzy

Inference System (ANFIS), three-layered cascaded and recurrent Artificial Neural Network (ANN) with local and global feedbacks, and Long Short-Term Memory (LSTM) network will be utilized to achieve harmonics forecasting. Additionally, eight hybrid forecasting models will be proposed in an effort to produce and further improve the forecasting accuracy of the results.

Furthermore, the significance of this work extends beyond its immediate objectives and contributes to the broader context of harmonic mitigation within the realm of renewable energy systems. Harmonic mitigation is a critical aspect of power system engineering, aiming to minimize undesirable harmonic distortions in electrical waveforms. Standard techniques employed in harmonic mitigation include:

1. **Passive Filters:** Passive filters, such as harmonic filters and tuned filters, are commonly used to absorb specific harmonic frequencies and prevent their propagation through the power system.
2. **Active Filters:** Active filters dynamically adjust their characteristics to counteract harmonics in real-time, offering a more flexible and responsive solution compared to passive filters.
3. **Variable Frequency Drives (VFDs):** VFDs are employed in motor control applications and can inadvertently introduce harmonics. Techniques such as multilevel inverter control are used to mitigate these harmonics.
4. **Transformers with Low Harmonic Content:** Specialized transformers designed to minimize harmonic distortion in their output waveforms are utilized to mitigate harmonics in power distribution systems.

5. **Power Factor Correction:** Improving power factor through power factor correction devices can reduce harmonic distortions in the power system.

The novel contribution of harmonic forecasting, as presented in this work, lies in its potential application as a predictive tool to enhance the effectiveness of these standard harmonic mitigation techniques. By forecasting the occurrence and characteristics of harmonics, power system operators can implement preemptive measures to mitigate harmonics before they significantly impact the system. The role of harmonic forecasting in the harmonic mitigation process can be outlined as follows:

1. **Proactive Planning:** Harmonic forecasting provides insights into the expected harmonic content over time. This information allows for proactive planning, enabling the deployment of appropriate mitigation techniques in anticipation of periods with heightened harmonic levels.
2. **Optimized Resource Allocation:** Armed with harmonic forecasts, operators can allocate resources more efficiently. For instance, they can optimize the deployment of active filters or switch between different mitigation strategies based on the predicted harmonic profile.
3. **Early Detection of Anomalies:** Harmonic forecasting can serve as an early warning system by detecting deviations from expected harmonic patterns. This allows for timely investigation and intervention to address potential issues before they escalate.
4. **Integration with Smart Grids:** Harmonic forecasting aligns with the goals of smart grid integration. By incorporating forecasting capabilities into control

systems, smart grids can dynamically adapt to changing harmonic conditions, enhancing overall system resilience.

In summary, the incorporation of harmonic forecasting into the broader context of harmonic mitigation enhances the adaptability and efficiency of conventional mitigation techniques. This proactive approach aligns with the evolving landscape of smart grid technologies and contributes to the advancement of strategies aimed at ensuring the stability and reliability of power systems in the presence of harmonics.

1.3 Thesis Aim

Harmonics forecasting is crucial for predicting the future behavior of time series data marked by periodic patterns or harmonics. The importance of harmonics prediction in enhancing power quality within electrical systems has been well-documented through extensive research efforts. Researchers have also explored various methodologies to achieve precise predictions. This study's central objective revolves around pioneering a novel forecasting model characterized by accuracy and reliability for harmonics forecasting.

To advance this goal, a two-fold hybrid renewable generator approach is implemented using real-world data as the input. The selection of these generators is grounded in the emphasis on harmonics forecasting within renewable energy systems. The initial hybrid model utilizes a Doubly-Fed Induction Generator (DFIG) operated by a wind turbine in conjunction with photovoltaic (PV) panels (Wind-DFIG-PV). The second model adopts a hybrid configuration incorporating both wind and PV systems, employing a Permanent Magnet Synchronous Generator (Wind-PMSG-PV). The primary intention in this context is to produce authentic output waveforms for voltage

and current that faithfully replicate real-world conditions. Subsequently, these output waveforms undergo analysis to extract harmonics data, which in turn forms the basis for forecasting within our innovative hybrid forecasting models.

ANFIS, ANN, and LSTM techniques are chief among those used by researchers to produce harmonics forecasting. The aim of this work is to develop and evaluate a hybrid forecasting model that effectively captures complex harmonics patterns in time series data and provides accurate predictions. The research focuses on integrating a forecasting model that combines the strengths of ANFIS, ANN, and LSTM to improve the accuracy and robustness of harmonics forecasting. The integrated ANFIS-ANN and ANFIS-LSTM models are expected to effectively capture the complex harmonics patterns in time series data and provide accurate predictions.

This thesis has the following objectives:

1. Review and analyse ANFIS, ANN, and LSTM techniques: To do so, the thesis conducts a comprehensive literature review to understand the principles, capabilities, and limitations of ANFIS, ANN, LSTM, and other forecasting techniques in the context of time series forecasting and harmonics analysis. This review helps identify their respective strengths and weaknesses and provides insights into how they can be combined to create a hybrid model.
2. Design and develop the hybrid forecasting model: Based on the insights from the literature review, the research proposes a hybrid model that integrates ANFIS, ANN, and LSTM in different combinations. The proposed models leverage the fuzzy logic-based inference capabilities of ANFIS to capture the nonlinear and complex relationships in harmonics patterns. Multi-layered ANN provides the

ability to learn and model the intricate dynamics of the data, while LSTM is proficient at capturing temporal dependencies and patterns in time series data. The thesis focuses on designing the architecture and structure of the hybrid models to harness the strengths of these methods.

3. Data preprocessing and feature extraction: The thesis explores appropriate data preprocessing techniques for handling time series data with harmonics patterns. This may involve detrending and normalizing the data. Additionally, the research investigates feature extraction methods specifically tailored to capture the unique characteristics of harmonics patterns in the data.
4. Integration and optimization of ANFIS, ANN and LSTM: The hybrid models integrate ANFIS-ANN and ANFIS-LSTM techniques. The research focuses on developing strategies to effectively combine the outputs of ANFIS, ANN, and LSTM in the prediction process. Furthermore, the K-Fold cross-validation technique is utilized to decrease the training error and improve forecasting efficiency.
5. Evaluation and comparative analysis: The developed hybrid models are evaluated using simulations of RES generators based on real-world data (wind speed and solar irradiation) and extracting harmonics patterns. The research compares the performance of the hybrid models and forecasting techniques used by other authors in the literature to validate the results of the proposed models. The evaluation metrics Mean Absolute Error (MAE) and Root Mean Squared Error (RMSE) are employed to assess the effectiveness of the hybrid models.

By accomplishing these objectives, the research aims to contribute to the field of harmonics forecasting by developing a hybrid model that combines either ANFIS-ANN or ANFIS-LSTM techniques. The research findings will help enhance the understanding and application of hybrid models in harmonics forecasting and provide insights into the potential benefits of combining these techniques for improved accuracy and robustness.

1.4 Thesis Outline

Chapter 1 commences the research work by providing a comprehensive insight into the driving force behind this study, which centres around the concept of harmonics forecasting and its pivotal role in addressing harmonics issues. It delineates the objectives of the thesis and underscores its contributions.

Chapter 2 provides an overview and conducts a review of the literature pertaining to the impact of harmonics, harmonics forecasting, and the methodologies involved. It also elucidates the permissible limits set by relevant standards to facilitate a better understanding of current and voltage harmonics. Additionally, it expounds upon the rationale behind employing a fusion of ANFIS-ANN and ANFIS-LSTM techniques for the creation of hybrid forecasting models.

Chapter 3 explains the two hybrid generator models (Wind-DFIG-PV and Wind-PMSG-PV) utilized in this study for harmonics generation based on real-world data. Additionally, it introduces forecasting techniques, namely ANFIS, ANN, and LSTM, followed by the presentation of eight novel hybrid models devised to enhance forecasting precision. Each proposed model comprises unique combinations of either ANFIS-ANN or ANFIS-LSTM components. The chapter also offers a concise overview of K-Fold cross-validation and its application.

Chapter 4 showcases the outcomes of the proposed harmonics forecasting models. It defines the forecasting methodology and introduces performance metrics against which the results derived from forecasting models are assessed and juxtaposed. Moreover, it conducts a comparative analysis between the proposed hybrid forecasting models and those employed by researchers in existing literature. This validation process not only authenticates the results but also underscores the advantages of employing the hybrid model.

Chapter 5 offers some concluding remarks, summarises the thesis' contributions, and provides recommendations for future research endeavours.

1.5 Thesis Contribution

This research makes a significant contribution by introducing eight innovative hybrid forecasting models. Among these models, six employ a synergistic combination of three distinct ANN architectures in conjunction with ANFIS, while two models integrate ANFIS-LSTM techniques. These models were developed within a MATLAB environment.

To enhance adaptability and accuracy, the ANN architecture was designed using three different combinations of cascade and recurrent inputs. The utilization of hyperbolic tangent transfer functions assists in precise weight adjustment, and subtractive clustering is applied within ANFIS to capture the trends and impacts associated with input variations. The implementation of the K-Fold cross-validation technique further enhances the training process of these proposed hybrid models.

In these models' construction, three incorporate ANN and ANFIS in stages 1 and 2, with the reverse configuration adopted for the remaining three models. Similarly, the

two ANFIS-LSTM hybrid models leverage LSTM in stage 1 and ANFIS in stage 2, and vice versa, creating a well-rounded set of forecasting models.

Furthermore, this research conducts a comprehensive comparative analysis of the proposed hybrid models and those employed in the existing literature. This comparative study elucidates the advantages and benefits of utilizing hybrid forecasting models in the context of harmonics forecasting, ultimately contributing valuable insights to the field.

1.6 List of Publications

C1- Optimal Filter Placement and Sizing Using Ant Colony Optimization in Electrical Distribution System, 2017 IEEE Electrical Power and Energy Conference.

C2- An Overview of Wind-Solar System Output Power, 2019 IEEE 32nd Canadian Conference of Electrical and Computer Engineering (CCECE).

C3- An Overview of Active Power Filters for Harmonics Mitigation of Renewable Energies Resources, 2019 IEEE 10th Annual Information Technology, Electronics and Mobile Communication Conference (IEMCON).

C4- A Proposed Adaptive Intelligent Controllers for Tidal Currents Turbine Driving DDPMSG for Improving the Output Power Generated, 2019 IEEE Electrical Power and Energy Conference.

C5- A Proposed Adaptive Filter for Harmonic Mitigation Based on Adaptive Neuro Fuzzy Inference System Model for Hybrid Wind Solar Energy System, 2022 IEEE 35th Canadian Conference of Electrical and Computer Engineering (CCECE).

C6- Harmonic Prediction and Mitigation Based on Adaptive Neuro Fuzzy Inference System Model Using Hybrid of Wind Solar Driven by DFIG, 2022 IEEE 13th

Annual Information Technology, Electronics and Mobile Communication Conference (IEMCON).

J1- Harmonics forecasting of Wind and Solar Hybrid Model Driven by DFIG and PMSG using ANN and ANFIS; published in June 2023 in Journal of IEEE Access.

J2- Harmonics Forecasting of Wind and Solar Hybrid Model Based on Deep Machine Learning; published in September 2023 in Journal of IEEE Access.

J3- Harmonics Forecasting of Renewable Energy System using Hybrid Model based on LSTM and ANFIS; submitted in August 2023 in journal of Electric Power Systems Research, Elsevier.

Chapter 2: Literature Survey

2.1 Power Quality

The phrase "power quality" has many definitions depending on the authors' point of view [15, 16, 17]. Some publications associate power quality with voltage, current, supply, service, and consumption quality [15], while others [16] define power quality as a set of electrical boundaries that allow a piece of equipment to function as designed without suffering severe performance or life expectancy degradation. Still others define power quality as the system's reliability [17].

In this thesis, power quality is defined as the monitoring, analysis, and improvement of a voltage, current, and frequency in order to maintain a sinusoidal waveform at rated values of magnitude and frequency, which allows all electrical devices on the network to operate properly. As per IEEE standard 1159, "[t]he term *power quality* refers to a wide variety of electromagnetic phenomena that characterize the voltage and current at a given time and at a given location on the power system" [18].

The International Electrotechnical Commission (IEC) and the Institute for Electrical and Electronics Engineers (IEEE) produced important power quality issue classifications based on specific characteristics of electromagnetic phenomena. The IEC and IEEE standard 1159 have categorized the electromagnetic phenomena, as presented in Table 1 and Table 2, respectively [18]. One of the key reasons for the development of multiple categories of electromagnetic phenomena is that different solutions to power quality problems exist based on the specific variation that is of relevance.

To classify power quality issues, the duration of the occurrence as well as the size and frequency range of the signal waveforms are used [18]. Figure 1 presents an overview of power quality issues [16]. This thesis, however, focuses on the analysis and techniques of mitigating the power system harmonics, which is one of the main causes of the deterioration of power quality in Electrical Power Systems (EPSs) based on Renewable Energy Systems (RESs).

Table 1 – Principal Phenomena Causing Electromagnetic Disturbances, as Classified by the IEC [18]

Group	Examples
Conducted low-frequency phenomena	Harmonics, interharmonics
	Signal systems (power line carrier)
	Voltage fluctuations
	Voltage dips and interruptions
	Voltage imbalance
	Power-frequency variations
	Induced low-frequency voltages
	DC in AC networks
Radiated low-frequency phenomena	Magnetic fields
	Electric fields
Conducted high-frequency phenomena	Induced continuous wave (CW) voltages or currents
	Unidirectional transients
	Oscillatory transients
Radiated high-frequency phenomena	Magnetic fields
	Electric fields
	Electromagnetic fields
	Continuous waves
	Transients
Electrostatic discharge phenomena (ESD)	—
Nuclear electromagnetic pulse (NEMP)	—

Table 2 – Categories and Typical Characteristics of Power System Electromagnetic Phenomena, as Defined in IEEE Std 1159-2009 [18]

Categories	Typical Spectral Content	Typical Duration	Typical Voltage Magnitude
1.0 Transients			
1.1 Impulsive			
1.1.1 Nanosecond	5 ns rise	< 50 ns	
1.1.2 Microsecond	1 μs rise	50 ns – 1 ms	
1.1.3 Millisecond	0.1 ms rise	> 1 ms	
1.2 Oscillatory			
1.2.1 Low frequency	< 5 kHz	0.3–50 ms	0–4 pu[a]
1.2.2 Medium frequency	5–500 kHz	20 μs	0–8 pu
1.2.3 High frequency	0.5–5 MHz	5 μs	0–4 pu
2.0 Short-duration root-mean-square (RMS) variations		0.5–30 cycles	0.1–0.9 pu
2.1 Instantaneous		0.5–30 cycles	1.1–1.8 pu
2.1.1 Sag			
2.1.2 Swell			
2.2 Momentary		0.5 cycles – 3	
2.2.1 Interruption		s 30 cycles – 3	< 0.1 pu
2.2.2 Sag		s 30 cycles – 3	0.1–0.9 pu
2.2.3 Swell		s	1.1–1.4 pu
2.3 Temporary			
2.3.1 Interruption		>3 s – 1 min	< 0.1 pu
2.3.2 Sag		>3 s – 1 min	0.1–0.9 pu
2.3.3 Swell		>3 s – 1 min	1.1–1.2 pu
3.0 Long-duration RMS variations			
3.1 Interrupted, sustained		> 1 min	0.0 pu
3.2 Undervoltages		> 1 min	0.8–0.9 pu
3.3 Overvoltages		> 1 min	
3.4 Current overload		> 1 min	1.1–1.2 pu
4.0 Imbalance			
4.1 Voltage		steady state	0.5–2%
4.2 Current		steady state	1.0–30%
5.0 Waveform distortion			
5.1 DC offset		steady state	0–0.1%
5.2 Harmonics	0–9 kHz	steady state	0–20%
5.3 Interharmonics	0–9 kHz	steady state	0–2%
5.4 Notching			
5.5 Noise	Broadband	steady state	0–1%
		steady state	
6.0 Voltage fluctuations	< 25 Hz	intermittent	0.1–7%
			0.2–2 P_{st}[b]
7.0 Power frequency variations		< 10 s	± 0.10 Hz

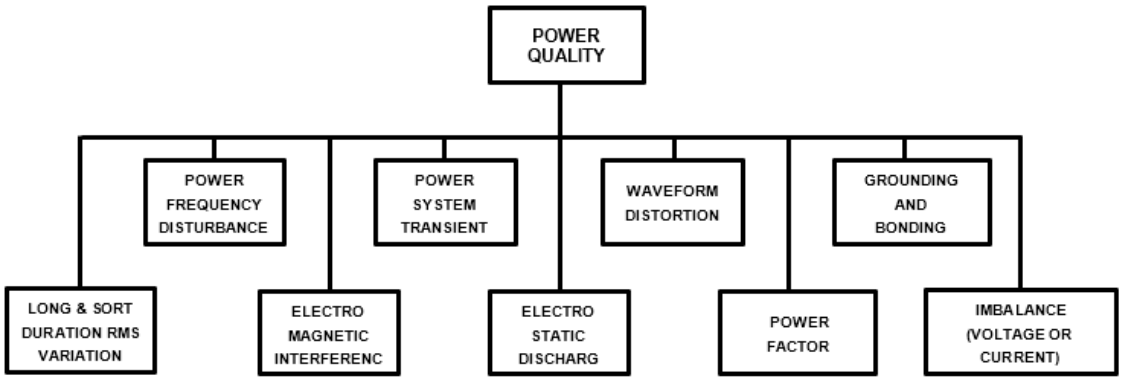

Figure 1: Power Quality Issues

2.2 Harmonics

2.2.1 Definition, Causes, and Impacts of Harmonics

Harmonics, as defined in [15-19], are sinusoidal voltages or currents with frequencies that are integer multiples of the fundamental frequency (typically 50 Hz or 60 Hz) at which the supply system is supposed to operate. The waveform distortion in currents or voltages generates harmonics. The nonlinear features of devices and loads on the power system inject harmonic currents and cause harmonic distortion. These currents generate nonlinear voltage dips across the system impedance, resulting in voltage distortion.

In power systems, industrial nonlinear loads (e.g., drives, rectifiers, inverters), load-generating electric arcs (e.g., arc furnaces, welding machines, lighting), residential loads with switch-mode power supplies (e.g., television sets, computers), and fluorescent and energy-saving lamps are the main sources of harmonics [15], [19]. Additionally, harmonics have numerous negative consequences, including control device malfunction; additional losses in capacitors, transformers, and rotating machines;

additional noise from motors and other apparatuses; telephone interference; and the possibility of causing parallel and series resonance frequencies (due to the power factor correction capacitor and cable capacitance), resulting in voltage amplification even at a distance from the distorting load [15], [17], [20].

2.2.2 Interharmonics

Interharmonics are voltages or currents with frequency components that are not integer multiples of the supply system's operating frequency. They take the form of individual frequencies or a broad spectrum. Interharmonics can be observed in all voltage classes of networks. Static frequency converters, cycloconverters, induction furnaces, and arcing devices, especially those whose operation is not synchronized with the power supply frequency, are the principal sources of interharmonic waveform distortion. Interharmonics' effects are not well understood [15-19] and so will not be considered here. The IEC categorizes background noise phenomena as interharmonic in IEC 61000-2-2:2002 [21], which is discussed separately as a unique electromagnetic phenomenon.

2.2.3 Harmonics Distortion Sources in RESs

Voltage source converters (VSCs) are used to integrate RESs to the grid. One of the major drawbacks of VSCs is that they increase the number of harmonics fed into the power system. Harmonics have an impact on the system's capacity to perform at its best by increasing power losses, creating device malfunctions, and producing undesirable tripping. These negative consequences affect electricity users and system operators. Researchers have devoted significant resources to finding ways to reduce the negative

impacts of harmonics on the power grid by creating mitigation strategies and upgrading equipment as needed [22-23].

2.2.4 Harmonics Analysis and Fourier Series

Harmonically distorted waveforms that are periodic (i.e., identical from one cycle to the next) can be represented as a sum of pure sine waves, with each sinusoid's frequency being an integer multiple of the distorted wave's fundamental frequency. The harmonic (h) of the fundamental is the name given to this multiple. The process of estimating the magnitudes and phases of the fundamental and high-order harmonics of periodic waveforms is known as harmonic analysis. The series that results, which is known as the Fourier series, establishes a relationship between a time-domain function and a frequency-domain one [24].

The Fourier series is defined as the sum of sinusoids and contains only odd harmonics when both the positive and negative half cycles of a waveform have the same shape. Because most typical harmonic-producing devices appear the same in both polarities, this simplifies most power system analyses even further. Low-power electrical gadgets may experience interference, but the power system is normally unaffected. To express the Fourier series, a periodic function $x_{(t)}$ is defined as one in which $x_{(t)} = x_{(t+T)}$. A trigonometric series of components can be used to depict this function, which includes a direct current (DC) component and additional element with frequencies that include the fundamental component and its integer multiple frequencies. This is the case when the following conditions known as Dirichlet requirements are met [19]:

- Over the period T, $x_{(t)}$ has a finite number of discontinuities if it is a discontinuous function.
- Over the period T, $x_{(t)}$ has a finite mean value.
- If there are a finite number of positive and negative maximum values for $x_{(t)}$, the trigonometric series $f_{(t)}$ has the following expression:

$$x(t) = \frac{a_0}{2} + \sum_{h=1}^{\infty} [a_h \cos(h\omega t) + b_h \sin(h\omega t)] \quad (2.1)$$

where

$\omega = \frac{2\pi}{T}$,

a_0 = amplitude of fundamental harmonic, and

a_h, b_h = Fourier coefficients.

Harmonics can be divided into three broad types. The classification of harmonics can be stated as follows: f is the fundamental frequency, f_h is the harmonic frequency, and h is the harmonic number.

- Integer harmonics $f_h = hf$, where h is an integer and h>1.
- Inter harmonics $f_h = hf$, where h is a non-integer number and h>1.
- Subharmonics $f_h = hf$, where h is a non-integer number and 0<h<1.

A periodic distorted waveform can be decomposed into an infinite series, including a DC component, a fundamental component (50/60 Hz for power systems), and its integer multiples, known as harmonic components, using Fourier analysis. The harmonic number (h) usually refers to a harmonic component whose frequency is proportional to the fundamental frequency [25]. Equation 2.1 could be further simplified as follows [24], [26]:

$$x(t) = c_0 + \sum_{h=1}^{\infty} c_h \sin(h\omega t + \phi_h)] \tag{2.2}$$

where

$c_0 = \frac{a_0}{2}$ = magnitude of the DC component,

$c_h = \sqrt{{a_h}^2 + {b_h}^2}$ = magnitude of nth harmonic component, and

$\phi_h = tan^{-1}\left(\frac{a_h}{b_h}\right)$ = phase angle of the nth harmonic.

Equation 2.2 could further be expressed in complex form as follows:

$$x(t) = \sum_{h=1}^{\infty} c_h e^{jh\omega t} \tag{2.3}$$

The fundamental component is the one with n = 1. The resultant waveform x(t) is determined by the magnitude and phase angle of each harmonic. Figure 2 depicts the Fourier series representation of a distorted signal:

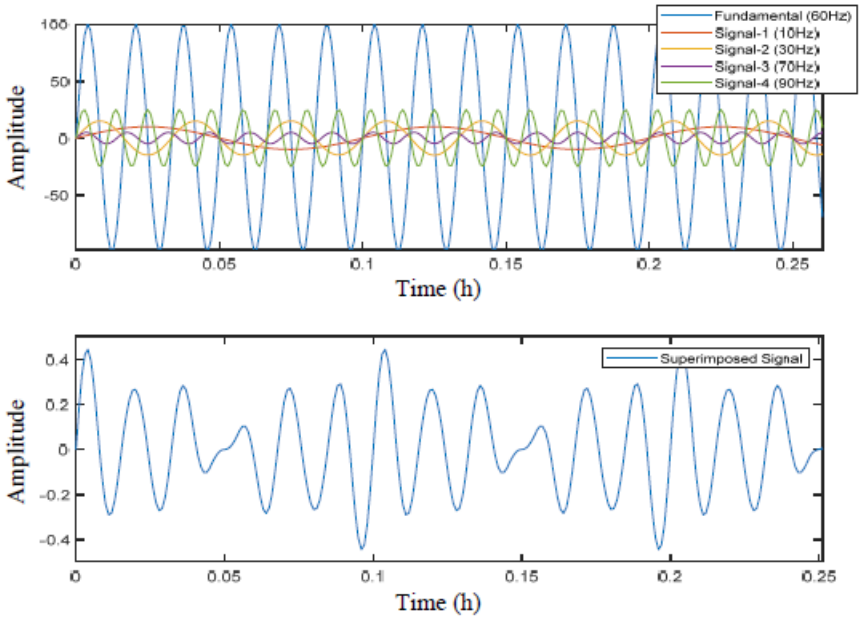

Figure 2: Fourier Series Representation

The top half of Figure 2 contains a plot of five signals, including a signal with a fundamental frequency (60Hz), along with four signals with different frequencies and amplitudes. The bottom half of Figure 2 shows the superimposed signal, where the effect of all signals is added to the fundamental signal.

Furthermore, Discrete Fourier Transform (DFT) establishes a relationship between the time domain and the frequency domain representation. Fast Fourier Transform (FFT) is a highly efficient numerical approach for implementation of DFT with computational techniques to reduce complexity [27]. The frequency spectrum of a discrete/sampled signal can be calculated as:

$$X(k) = \sum_{n=0}^{N-1} x(n) e^{-j2\frac{k}{N}n} \tag{2.4}$$

where

N = the number of samples over the period *T*,

x(n) = the amplitude at each sample, and

k = 0, 1, 2, ..., N-1.

Each frequency here is also separated by 1/T, with the highest frequency component at k = *N/2.* An FFT plot depicting the frequency spectrum for signal x(t) is shown in Figure 3. As can be seen, FFT is applied to the superimposed signal in the bottom half of Figure 2, which results in the presentation of a frequency spectrum of x(t).

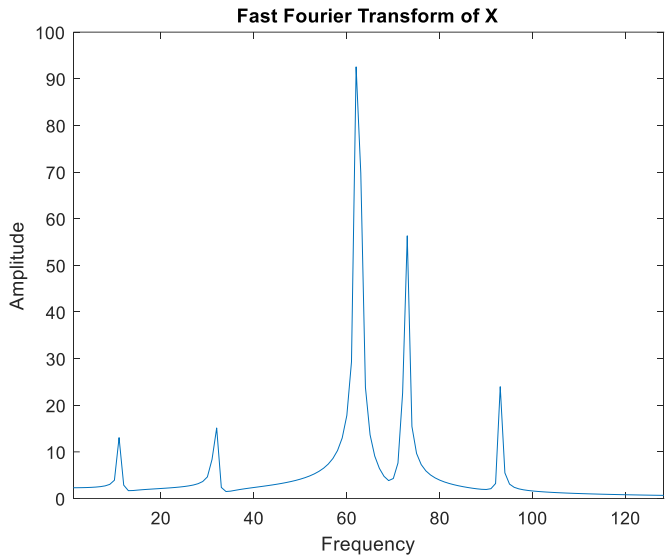

Figure 3: Fast Fourier Transform Depicting Frequency Spectrum

2.2.5 Total Harmonic Distortion (THD)

Total Harmonic Distortion (THD) is a measurement of the effective value of a distorted waveform's harmonic components. It is the harmonics' potential heating value in relation to the fundamental [17]. THD is calculated by dividing the Root-Mean-Square (RMS) value of harmonics by the RMS value of the fundamental and multiplying by 100%, as indicated in Equation 2.5 [15], [26], [28]:

$$THD(\%) = \frac{\sqrt{\sum_{h>1}^{h_{max}} M_h^2}}{M_1} \times 100 \tag{2.5}$$

where

M_h = RMS value of harmonic component h of the quantity M.

The voltage and current THD can be expressed as in Eqs. 2.6 and 2.7:

$$THD_V(\%) = \frac{\sqrt{\sum_{h>1}^{h_{max}} V_h^2}}{V_1} \times 100 \quad (2.6)$$

$$THD_I(\%) = \frac{\sqrt{\sum_{h>1}^{h_{max}} I_h^2}}{I_1} \times 100 \quad (2.7)$$

where

THD_V = THD for voltage expressed as the total of the squares of all harmonics generated by a single load divided by the nominal 50/60 Hz (V_1) waveform value. This amount depicts a relationship between the fundamental and distorted waveforms.

THD_I = THD for current is also referred to as Total Demand Distortion.

V_1 = The load current measured at the fundamental frequency.

I_1 = The load current measured at the fundamental frequency.

Voltage harmonic distortion is most commonly described using the THD index. Harmonic voltages are virtually always based on the waveform's fundamental value at the time of sampling. The voltage THD is nearly always a useful value because fundamental voltage varies by only a few percentage points [15], [17].

2.2.6 Total Demand Distortion (TDD)

The THD value can be used to describe current distortion levels, but it can be deceiving. A current with low amplitude may have a high THD that is not a substantial threat. One way to get around this problem is by referring to the THD as the fundamental of the peak demand load current rather than the fundamental of the current sample [15], [29]. This is called the Total Demand Distortion (TDD) and is expressed in Eq. 2.8:

$$TDD(\%) = \frac{\sqrt{\sum_{h=2}^{h_{max}} I_h^2}}{I_L} \times 100 \quad (2.8)$$

I_L is the peak, or maximum, demand load current measured at the Point of Common Coupling (PCC) at the fundamental frequency component. It can be estimated as the average of the maximum demand current for the previous 12 months if there is already a load in the system. This calculation is as simple as averaging the peak demand readings over a 12-month period. However, for a new facility, I_L must be calculated based on expected load profiles [15].

2.2.7 Individual Harmonic Distortion (IHD)

Individual harmonic distortion (IHD) is the ratio of the individual harmonic's RMS value to the fundamental's RMS value.

$$h_N = \frac{V_N}{V_1} \; OR \; \frac{I_N}{I_1} \quad (2.9)$$

where h_N = the individual harmonic distortion of the Nth harmonic

2.3 IEEE Standard 519-2014 for Voltage and Current Harmonics

The IEEE 519 harmonics standards are the most widely utilized harmonics standards in the research community for power quality restrictions, as seen in Tables 1 and 2. IEEE 519 specifies best practices and regulations for harmonics control in electric power systems. A THD of less than 5% is typically deemed acceptable [6]. For renewable energy, the THD should be as small as possible, as renewable resources are limited and our objective is to achieve the most efficient power system. As per standard

IEEE 519, the allowable limits for voltage and current harmonics are presented in Tables 3, 4, and 5.

Table 3: IEEE Std 519-2014 Voltage Distortion Limits [6]

Bus Voltage *V* at PCC	Individual Harmonics (%)	Total Harmonics Distortion (THD) (%)
$V \leq 1.0$ kV	5.0	8.0
1 kV < $V \leq 69$ kV	3.0	5.0
69 kV < $V \leq 161$ kV	1.5	2.5
161 kV < V	1.0	1.5[a]

[a] High-voltage systems can have up to 2.0% THD due to an HVDC terminal whose effects will have attenuated at points in the network where future users may be connected.

Table 4: IEEE Std 519-2014 Current Distortion Limits Rated 120V Through 69kV [6]

Maximum Harmonics Current Distortion in Percent of IL						
Individual Harmonics Order (Odd harmonics) [a, b]						
I_{SC}/I_L	$3 \leq h < 11$	$11 \leq h < 17$	$17 \leq h < 23$	$23 \leq h < 35$	$35 \leq h \leq 50$	TDD
< 20[c]	4.0	2.0	1.5	0.6	0.3	5.0
20 < 50	7.0	3.5	2.5	1.0	0.5	8.0
50 < 100	10.0	4.5	4.0	1.5	0.7	12.0
100 < 1000	12.0	5.5	5.0	2.0	1.0	15.0
> 1000	15.0	7.0	6.0	2.5	1.4	20.0

Table 5: IEEE Std 519-2014 Current Distortion Limits Rated 69kV Through 161kV [6]

Maximum Harmonics Current Distortion in Percent of IL						
Individual Harmonics Order (Odd harmonics)[a, b]						
I_{SC}/I_L	**$3 \leq h < 11$**	**$11 \leq h < 17$**	**$17 \leq h < 23$**	**$23 \leq h < 35$**	**$35 \leq h \leq 50$**	**TDD**
< 20	2.0	1.0	0.75	0.3	0.15	2.5
20 < 50	3.5	1.75	1.25	0.5	0.25	4.0
50 < 100	5.0	2.25	2.0	0.75	0.35	6.0
100 < 1000	6.0	2.75	2.5	1.0	0.5	7.5
> 1000	7.5	3.5	3.0	1.25	0.7	10.0

[a] Even harmonics are limited to 25% of the odd harmonics limits above.

[b] Current distortions that result in a DC offset, e.g., half-wave converters, are not allowed.

[c] All power generation equipment is limited to these values of current distortion, regardless of actual Isc/I_L.

where

Isc = maximum short-circuit current at PCC, and

I_L = maximum demand load current (fundamental frequency component) at the PCC under normal load operating conditions.

2.4 Harmonics Mitigation and Rationale for Studying Harmonics Forecasting

Traditionally, utility companies would know the precise industry of the customers responsible for the dominant harmonics sources. Based on this knowledge, the harmonics problems were compensated by employing a passive harmonics filter at the PCC of major distorting loads to ensure the effectiveness of the filters [30-32]. In recent years, however, the significant expansion of power electronics-based loads in power systems has fostered substantial distortion in power system signals. Nonlinear loads such as power electronics devices (e.g., cycloconverters) and arcing loads (e.g., welding machines and arc furnaces), which are frequently utilized in industry, are the main

generators of harmonics in EPSs [33]. Furthermore, the grid integration of renewable energy sources, which involves various types of power electronics-based converters, has also been found to increase the number of harmonics in the power system [34], [35]. Hence, in order to anticipate and mitigate problems caused by the existence of harmonics, utilities must be able to predict their expected impact in order to evaluate the compensation required and avoid the consequences caused by harmonics. In this regard, efforts have been made by authors to use harmonics forecasting to maintain power quality and ensure harmonics levels under acceptable limits [103].

Pablo in [36] introduced a methodology for forecasting of voltage THD for low-voltage (LV) busbars of residential distribution feeders based on data from a small number of smart meters. Using only the existing monitoring infrastructure required for demand response operation, the methodology gives important power quality indicators to system operators. Different voltage THD forecasting techniques, namely autoregressive and feed-forward ANNs, were utilized. The proposed methodology employs a small number of smart meters with sub-metering functionality to first anticipate demand disaggregation into linear and nonlinear loads and then predict the THD at various busses throughout the network. This technique allows additional features to be integrated into existing monitoring devices in order to forecast current or future harmonic distortion. It was demonstrated that a network of advanced smart meters with a minimal number of advanced smart meters is sufficient for accurate harmonic predictions [36].

Ray, Puhan and Panda in [37] proposed a harmonics forecasting technique based on a Variable Leaky Least Mean Square (VLLMS) algorithm. The proposed method

used a leak compensation method to prevent parameter drift. In this procedure, the step size was also adjusted to improve the rate of convergence. A real-time power system was simulated utilizing various instances, demonstrating the superiority of the proposed method over other systems presented in the paper [37].

In [38], Ivry examined the impact of uncertainty on harmonic prediction in a power system with numerous Voltage Source Converters (VSCs). The study focused on predicting harmonic distortion levels in numerous VSCs when some system or design parameters were only known within certain restrictions. The Univariate Dimension Reduction (UDR) method was used to forecast the level of harmonic distortion of the VSCs measured at the PCC to the grid. In predicting the THD at the PCC, the suggested prediction approach (UDR) ensured full interactions between the harmonic sources (VSCs) and the entire power system. The study found that electricity companies/design engineers can use the lower UDR to help them choose parameters [38].

In his research, Hussam [39] proposed the concept of adaptive filters that use real-time harmonics prediction algorithms by applying LMS, Normalised LMS (NLMS) and Recursive Least Square (RLS) methods. The author showed that an active filter was able to mitigate the time delay produced by the harmonics information acquisition process. The LMS method was found to have a slow convergence rate and data-dependent behaviour. In this work, a comparison of the LMS, NLMS, and RLS approaches was performed. A single load computer desktop was used to collect data for a fixed-point operation harmonics source. In terms of Mean Squared Error (MSE), the RLS and NLMS algorithms performed better than the LMS method [39].

The THD of each load cannot be used to compute the THD of the current in a feeder. Depending on the phase angle, each harmonic order of current can range from cancellation to addition. A method for predicting current distortions of nonlinear loads operating simultaneously is proposed by Braga and Jota in [40]. This method makes use of a model that can forecast the amplitude and phase of current in non-linear loads. The experimental data in the study is used in a simplified practical technique that is carried out in the frequency domain. The model is based on an admittance matrix that is harmonically connected. Harmonics in static converters are analysed using these matrices. The research presented in this study is based on load tests using a Light Emitting Diode (LED) in conjunction with fluorescent bulbs. The model's predictions are compared against actual data. The suggested method can forecast the current waveform of nonlinear loads working simultaneously at different fundamental voltage levels, as evidenced by comparisons between measured and anticipated results. The model may be used to forecast the rms value of current THD, and magnitude and phase spectra of a practical power system with sufficient accuracy for expected operation conditions [40].

Dong, Zhang, and Li in [41] introduced a nonlinear load harmonic prediction approach based on the combination of Distribution Internet of Things (IoT) and deep learning networks to fulfil the demand for high accuracy for nonlinear load harmonic prediction and analysis in a distribution system. This method uses the harmonic coupling admittance matrix model based on measured data at the edge of Power Distribution IoT to realize the mathematical modelling of user-side load data and to solve the modelling problems caused by complex electrical structure and parameters.

This aim was accomplished with the support of the architecture of Power Distribution IoT based on nonlinear load harmonic prediction. Simultaneously, on the cloud side of the network, the Dynamic Time Wrapping – Long Short-Term Memory (DTW-LSTM) algorithm was used to build the load harmonic prediction and analysis model, which effectively reduced the number of load prediction models, ensured the prediction model's strong generalization ability, and realized the efficient analysis of nonlinear load harmonic in the distribution system. Finally, the high-efficiency performance of the suggested method for nonlinear load harmonic prediction was verified using the general dataset, demonstrating that the proposed method has clear advantages in processing accuracy and speed [41].

Panoiu and Ghiormez in [42] presented a study on the modelling and prediction of the total harmonic distortion of current emerging in an electric arc furnace's medium voltage installation. ANFIS in MATLAB were used for modelling. According to the findings, ANFIS showed a good understanding of how to adjust the THD. As a result of the system's ability to read 800 data points, it was able to provide THD variations for another 400 samples with a very low error rate. The authors also attempted to train the system with different numbers of samples. However, the system failed to model appropriately when the number of samples used in training was less than the number used in testing [42].

Harmonics may cause damage to power system equipment, which is why it is critical for power system operators to understand harmonic behaviour. Harmonics, however, exhibit several complicated features, such as nonlinearity and abrupt changes. As a result, by using traditional methods for Mega Watt (MW) demand forecasting, it

is difficult to forecast them. The research carried out by Mori, Suga, et al. [43] presented a method for predicting power system harmonic voltages based on ANNs. In the research, harmonic dynamics were handled using recurrent neural networks, with the fifth harmonic voltage being predicted using four recurrent neural networks. In terms of accuracy and computational effort, the four models (Jordan, Elman, Noda, and Nagao) were then compared. The results suggest that Elman's approach is more effective than the other models, as demonstrated by the example [43].

Shengqing et al. [44] proposed the Hybrid Active Power Filter (HAPF) harmonics current prediction method based on the Empirical Mode Decomposition (EMD)-Support Vector Regression (SVR) theory to solve microgrid power quality problems. This strategy first explores harmonic currents for each harmonic using EMD, and then predicts the next step of the harmonics current at different times using SVR's varied kernel functions. After that, the predicted value of each harmonic weighted summation is determined. The simulation results demonstrated the EMD decomposition for all harmonics. The authors concluded that by adopting this combination of EMD-SVR, the harmonics currents at the next time step could be accurately predicted, resulting in harmonics current minimum error compensation [44].

Kuyunani, Hasan, Shongwe, et al. [45] used the LSTM deep learning method in their paper. A total of 8,103 voltage harmonics measured at the Jeffreys Bay Wind Farm in Eastern Cape Province were employed in the study. The suggested model extracted key information from voltage harmonics signals in two steps, with the moving window segmentation being used to derive the mean voltage amplitude. The prediction of voltage harmonics generation using LSTM was based on the voltage properties

extracted. The proposed model only had one LSTM layer with 128 hidden neurons for simplicity. To train the model in MATLAB, the researchers used 8,103 computed sample mean values as expected data. With a low RMSE, the LSTM model was able to predict the next 3,800 sample mean values. The proposed model is thought to be a good contender for forecasting harmonics and hence assisting in the search for solutions to suppress them [45].

Žnidarec [46] proposed long-term current harmonic distortion prediction models in order to monitor the effects of current harmonics generated by PV systems. In order to forecast current harmonics, the suggested models use a Multilayer Perceptron Neural Network (MLPNN), a form of ANN with input parameters that are straightforward to measure. The models were trained using data from a year of power quality measurements (1 January to 31 December 2018) at the PCC of the 10-kW PV system and the distribution network. Meteorological data (solar irradiance and ambient temperature) was also collected at the test location. In terms of the number of hidden layers and input parameters, six distinct models were constructed, tested, and verified. A three-phase, grid-tied, PV plant inverter was used with the MLPNN to predict the 5th, 7th, 11th, and 13th. The results of the MLPNN model prediction demonstrate that adding the third input parameter (time of day) to the models improved performance to a small extent. Otherwise, no general conclusion was reached as to whether the MLPNN with one or two hidden layers performs better. When it comes to overall harmonic prediction performance, MLPNN 6 with three input parameters (solar irradiance, ambient temperature, and time of day) and two hidden layers achieved the best accuracy.

Hatata, Eladawy, et. al [79] combined a nonlinear autoregressive network with an exogenous inputs (NARX) network as a potential approach for predicting the load current harmonics induced in electric power systems. The suggested technology was used on a micro-grid at the Khalda – Main Razzak (MRZK) power station in west Egypt, which is a petroleum site. An Electrical Submersible Pump (ESP) that was powered by an induction motor and managed by a Variable Speed Drive (VSD) served as the test nonlinear load. The method for creating the suggested NARX network to simulate nonlinear loads and determine their THD of currents was described in the authors' paper [79].

For the purpose of determining the genuine harmonic current of the load and the nonlinearity of each load, the planned network was tested using both simulated pure sinusoidal voltage waveform and standalone measured voltage. By comparing the suggested method with a Recurrent Neural Network (RNN)-based method, it was determined that the suggested NARX method was quicker and more accurate than the RNN-based technique. The tested load's real current and voltage waveforms were collected from the field measurement data of an ESP powered by a stand-alone generator and controlled by VSD, and the THD was assessed in relation to the output of the suggested NARX network. The results validated the precision and dependability of the suggested method by showing good performance for ESP current harmonic prediction.

Pang and Li [80] developed a method of Stack Auto Encoder (SAE) Neural Network-based short-term harmonics forecasting and evaluation affected by electrified trains on the power grid. According to their findings, the goal of harmonics forecasting

was achieved and the harmonic value was measured using harmonic assessment techniques. The authors' study offers a theoretical frame of reference for the harmonic analysis of the impact of the railroad, which can help enhance the power quality in a power network.

Zavala et. al [81] provided a statistical framework for examining model behaviour, trend extraction, and forecasting based on Dynamic Harmonic Regression (DHR). Synthetic and observational data were both used to evaluate the model's performance. Wind power generation measurements were employed to test the practical applicability of this technique under diverse data gathering settings. The forecasting function of the DHR model was shown to be a useful tool that could compete with other techniques already in use, exhibiting a low error in forecasting data that could be decreased further by an appropriate selection of the moving window.

Most authors in the reviewed literature are aware of the significance of harmonics forecasting in mitigating harmonics and improving power quality. Accordingly, they applied different techniques to achieve accurate harmonics forecasting. Some authors [36], [43] used these predictions to allow the system operators to understand the behaviour of harmonics, while others [40], [41] utilized the forecast results to monitor the impact of nonlinear loads of distribution networks. Harmonics forecasting was also utilized in the reviewed literature for parameters selection for control of VSCs [38] or design filters [39], [44]. Moreover, some authors presented a range of different forecasting techniques in order to accomplish better and more accurate forecasting results [37], [42], [45], [46]. A comparison showing the strengths and weaknesses of each method discussed is summarized in Table 6.

Table 6: Strengths and Weaknesses of Forecasting Models

Method	Strengths	Weaknesses	References
Variable Leaky Least Mean Square (VLLMS)	- Ability to track and adapt to changes in the underlying data distribution - Reduced sensitivity to initialization parameters	- Limited robustness against outliers or non-stationary data - Requires careful tuning of hyperparameters	[37]
Univariate Dimension Reduction (UDR)	- Capability to handle high-dimensional and correlated time series data - Effective in capturing relevant features and reducing dimensionality	- Limited interpretability compared to other methods - Complexity in determining the optimal number of principal components	[38]
Feed-forward Artificial Neural Networks (ANN)	- Ability to capture nonlinear relationships and patterns in time series data - Flexible architecture that can handle various input features and time series characteristics	- May suffer from overfitting if not properly regularized - Prone to sensitivity in parameter initialization and network architecture design	[36], [43], [46]
Least Mean Square (LMS)	- Simplicity and ease of implementation - Low computational complexity	- Slow convergence rate, especially in non-stationary or highly correlated data - Sensitivity to step size (learning rate) selection	[39]
Normalized LMS (NLMS)	- Robustness against varying input signal power - Low computational complexity	- Vulnerable to noise amplification - Requires careful tuning of the step size parameter	[39]
Recursive Least Square (RLS)	- Enhanced adaptability and faster convergence compared to LMS methods - Robustness against noise and non-stationary data	- Higher computational complexity compared to LMS methods - Sensitivity to the selection of the forgetting factor and initial covariance matrix	[39]
Dynamic Time Wrapping – Long Short-Term Memory (DTW-LSTM) algorithm	- Ability to handle time series data with varying lengths and temporal alignments - Effective in capturing long-term dependencies and sequential patterns	- Increased computational complexity compared to other methods - Requires careful tuning of hyperparameters, such as the number of LSTM layers, hidden units, and learning rate	[41]
Adaptive Neuro Fuzzy Interference Systems (ANFIS)	- Ability to handle nonlinear relationships and uncertainty in time series data through fuzzy logic and inference mechanisms - Capability to adapt and learn from data to optimize the fuzzy model parameters	- Complexity in designing and tuning the fuzzy inference system, including rule base construction and membership function design - Limited interpretability compared to other methods	[42]

Support Vector Regression (SVR) method	- Effective in handling high-dimensional data and capturing nonlinear relationships - Good generalization capabilities	- Sensitivity to parameter settings and kernel selection - Limited interpretability compared to other methods	[44]
Long Short-Term Memory (LSTM)	- Ability to model temporal dependencies and capture sequential patterns in time series data - Flexibility in handling various types of time series data and input features.	- Suffers from vanishing/exploding gradient problems and long training times. - Prone to sensitivity in parameter initialization and network architecture design	[45]
Nonlinear Autoregressive Network with Exogenous Inputs (NARX)	- Capability to capture nonlinear relationships and incorporate exogenous inputs in time series forecasting - Ability to handle time-delayed relationships	- Complexity in determining the optimal network architecture and handling long input sequences - Prone to overfitting if not properly regularized	[79]
Stack Auto Encoder (SAE)	- Effective in capturing hierarchical and abstract representations of time series data - Robustness against noise and missing data	- Increased computational complexity due to the stacked architecture - Requires careful tuning of hyperparameters such as the number of layers and hidden units	[80]
Dynamic Harmonic Regression (DHR)	- Capability to capture seasonal and harmonic components in time series data - Robustness against missing data and outliers	- Limited ability to handle complex patterns and long-term dependencies - Complexity in determining the appropriate number of harmonic components and modelling their interactions	[81]

Furthermore, several efforts have been made by researchers to improve the forecasting accuracy by using hybrid forecasting models for harmonics forecasting in renewable energy systems [47-65] [105-120]. In continuation of the above works, the main goal of this research is to introduce novel hybrid forecasting model for precise and reliable harmonics forecasting. It has been observed that hybrid models perform better compared to traditional methods alone. The most prominent methods utilized in literature for forecasting are Artificial Neural Networks (ANNs), Adaptive Neuro Fuzzy Interference Systems (ANFIS), and Long-Short Term Memory (LSTM) networks. In order to forecast harmonics, several hybrid models will be introduced with different

combinations of cascaded and recurrent three-layered ANN with local and global feedbacks with ANFIS to achieve high accuracy and suitability for real-time applications. The advantage of employing a hybrid of ANN and ANFIS lies in the synergy of their strengths, which effectively mitigates each other's weaknesses. ANFIS contributes its expertise in handling nonlinear relationships and uncertainty in time series data through fuzzy logic and learning from data for fuzzy model optimization. Meanwhile, ANN brings its capability to capture intricate nonlinear patterns and adapt to various input features and time series characteristics. This hybridization can result in an efficient forecasting approach that leverages ANFIS's robustness and interpretability, along with ANN's modelling prowess, to address challenges such as overfitting, sensitivity to parameter initialization, and complex fuzzy inference system design. Consequently, such a hybrid will enhance forecast accuracy by accommodating a broader spectrum of data patterns and uncertainties while retaining some level of interpretability.

A combination of LSTM and ANFIS will also be introduced and tested. The utilization of a hybrid model that combines the strengths of ANFIS and LSTM presents a distinct advantage by effectively compensating for each other's limitations. ANFIS excels in managing nonlinear relationships and handling uncertainty within time series data through its fuzzy logic-based adaptable parameter learning, while LSTM demonstrates expertise in modeling temporal dependencies and capturing sequential patterns across a range of time series data types. This hybridization is expected to enhance forecast accuracy by amalgamating the robustness and adaptability of ANFIS with the temporal modeling capabilities of LSTM, thus effectively addressing

challenges such as mitigating vanishing/exploding gradients, reducing protracted training times, alleviating sensitivity to parameter initialization and network architecture design, simplifying complex fuzzy system design intricacies, and enhancing interpretability. Consequently, this hybrid approach can optimize forecasting efficiency, offering a holistic solution capable of effectively accommodating diverse characteristics found within time series data, ultimately culminating in improved forecast accuracy.

2.5 Rationale for Building a Hybrid Model Combining Multilayered-ANN with ANFIS for Harmonics Forecasting

Harmonics forecasting is an important task in various fields, most importantly for the improvement of power quality and grid integration of renewable energy generators. The objective is to predict the behaviour of harmonics components so they can serve as inputs for RES integration to the grid. To improve the accuracy and reliability of harmonics forecasting, a hybrid model that combines multilayered ANN with ANFIS and LSTM is considered here. This approach offers several benefits and provides a robust solution to harmonics forecasting problems. The rationale behind building such a hybrid model is discussed below.

2.5.1 Complementary Strengths of ANN and ANFIS

ANNs are powerful computational models capable of learning complex nonlinear relationships between inputs and outputs. They excel at recognizing patterns and capturing hidden dependencies in the data. ANNs can efficiently handle large volumes of training data and can generalize well to make predictions on unseen data. On the other hand, ANFIS combine the strengths of fuzzy logic and neural networks. They can model

fuzzy rules, linguistic variables, and expert knowledge to provide transparent and interpretable results. ANFIS can handle uncertain and imprecise data effectively and capture the nonlinear relationships present in the data. Thus, combining ANNs and ANFIS in a hybrid model can benefit from the complementary strengths of both techniques. ANNs can handle complex patterns and capture intricate nonlinear relationships, while ANFIS can incorporate expert knowledge and provide interpretable results.

2.5.2 Capturing Nonlinearities and Complex Relationships

Harmonics forecasting often involves dealing with nonlinearities and complex relationships between harmonics components and other variables. ANNs are well-suited for capturing such nonlinear relationships due to their ability to model complex functions. By training a multilayered ANN on a dataset containing harmonics measurements and other relevant variables, its capability to capture the intricate relationships between the variables and the harmonics behaviour can be exploited.

ANFIS, with its fuzzy rule-based structure, can handle linguistic variables and expert knowledge effectively. By integrating ANFIS into the hybrid model, domain expertise and fuzzy logic-based rules can be incorporated, which can enhance the forecasting accuracy by capturing underlying linguistic patterns in the data.

2.5.3 Improved Forecasting Accuracy and Robustness

The combination of ANN and ANFIS in a hybrid model can lead to improved forecasting accuracy and robustness. ANNs can learn from historical data patterns and

make accurate predictions, while ANFIS can provide interpretability and handle uncertainties. The hybrid model can leverage the strength of both techniques, leading to more reliable and accurate harmonics forecast.

2.5.4 Adaptability and Generalization

The hybrid model can adapt to different datasets and generalize well to unseen data. ANNs are known for their ability to adapt to new patterns and data variations, enabling the model to capture changing harmonics behaviours over time. ANFIS can adapt its fuzzy rules and linguistic variables based on the input data, making the hybrid model adaptable to different operating conditions and system configurations.

2.5.5 Model Transparency and Interpretability

The transparency and interpretability of the hybrid model are crucial in harmonics forecasting applications. ANFIS, with its fuzzy rule-based structure, provides a transparent framework that allows experts to understand and interpret the model's decision-making process. This interpretability can aid in identifying the factors contributing to harmonics variations and assessing the model's reliability.

2.5.6 Summary

Table 7 presents a summary of the model components and their specific contributions to building a hybrid model based on combining multilayered ANN and ANFIS for harmonics forecasting.

Table 7: Rationale for ANN-ANFIS-Based Hybrid Model Summary

Rationale	ANN	ANFIS
Nonlinear Relationship Capture	ANNs excel at capturing complex nonlinear relationships between inputs and outputs. They can learn from historical data patterns and identify intricate dependencies.	ANFIS combines fuzzy logic and neural networks, enabling it to model fuzzy rules and linguistic variables. It incorporates expert knowledge into the model, capturing underlying linguistic patterns and handling uncertainties effectively.
Handling Large Volumes of Data	ANNs can efficiently handle large volumes of training data. They can process and learn from extensive datasets, which is essential in harmonics forecasting tasks where significant amounts of data are involved.	ANFIS can handle uncertain and imprecise data effectively. It can process data with varying degrees of uncertainty, providing robust predictions even in the presence of noise or incomplete information.
Adaptability and Generalization	ANNs are known for their adaptability to new patterns and variations in data. They can adjust their internal parameters and learn from evolving harmonics behaviours over time.	ANFIS can adapt its fuzzy rules and linguistic variables based on the input data. It can adjust its structure to accommodate different operating conditions and system configurations, ensuring the model's adaptability and generalization capability.
Interpretability	ANN models typically lack interpretability and are often considered as "black boxes." The complex relationships they capture can be challenging to interpret.	ANFIS provides transparency and interpretability by employing fuzzy rule-based structures. It incorporates expert knowledge and linguistic variables, allowing experts to understand and explain the decision-making process. The model's output can be easily explained using linguistic terms and fuzzy rules, making it more interpretable and explainable.
Integration of Domain Knowledge	ANN models rely primarily on data-driven learning and may not explicitly incorporate domain knowledge or expert insights.	ANFIS can incorporate domain expertise and expert knowledge into the model by defining fuzzy rules and linguistic variables. This integration helps capture the underlying dynamics and linguistic patterns specific to harmonics forecasting, enhancing the accuracy and reliability of predictions.

In conclusion, developing a hybrid model for harmonics forecasting that combines multilayered ANNs and ANFIS offers several benefits. The model may incorporate expert information, handle uncertainties, capture nonlinear relationships, and produce findings that are easy to understand. The hybrid model can improve accuracy, resilience, flexibility, and generalisation by taking advantage of the complimentary capabilities of both methodologies, which makes it an appealing option for harmonics forecasting applications.

2.6 Rationale for Building a Hybrid Model Combining LSTM with ANFIS for Harmonics Forecasting

The benefits and capabilities of each technique are the foundation for why a hybrid model for harmonic forecasting integrating LSTM and ANFIS should be constructed. It is possible to increase the forecasting model's accuracy and robustness by combining these two approaches and taking advantage of their respective benefits. Aspects for considering the hybrid strategy are presented in the following sections.

2.6.1 Capturing Temporal Dependencies

LSTM is a powerful deep learning technique that excels in capturing long-term dependencies in time series data. It can effectively model the complex patterns and relationships within a sequence. By using LSTM, the hybrid model can leverage its ability to learn from historical harmonics data and capture the temporal dynamics of harmonics components.

2.6.2 Fuzzy Logic-Based Reasoning

ANFIS is a fuzzy logic-based inference system that can handle uncertain and imprecise information. It combines the advantages of fuzzy logic and neural networks to create a hybrid model that can reason with linguistic rules and make inference based on fuzzy logic principles. This makes ANFIS suitable for handling complex, nonlinear relationships and incorporating expert knowledge into the model.

2.6.3 Handling Nonlinearities

Harmonics forecasting often involves dealing with nonlinear relationships between different variables and factors. LSTM, with its deep learning capabilities, can capture nonlinear patterns in the data. ANFIS, on the other hand, excels at modelling complex, nonlinear relationships through fuzzy inference. By combining these two techniques, the hybrid model can better handle the nonlinearities present in harmonic forecasting.

2.6.4 Incorporating Domain Knowledge

ANFIS allows the integration of expert knowledge in the form of linguistic rules. In the context of harmonics forecasting, domain experts may have insights and expertise that can contribute to accurate predictions. ANFIS can capture this expert knowledge and incorporate it into the forecasting process, complementing the data-driven approach of LSTM.

2.6.5 Enhanced Interpretability

ANFIS models are known for their interpretability. They provide linguistic rules that can be understood and analysed by domain experts. This can be particularly useful in harmonics forecasting, where stakeholders may require explanations or justifications for the predictions. The hybrid model can provide interpretable results while benefiting from the powerful predictive capabilities of LSTM.

2.6.6 Robustness and Generalization

Combining different modelling techniques can enhance the robustness and generalization ability of the model. LSTM and ANFIS have different strengths and weaknesses, and by integrating them, the hybrid model can potentially overcome limitations and improve overall forecasting performance.

2.6.7 Summary

A description of the model elements and their individual contributions to developing a hybrid model based on fusing LSTM and ANFIS for harmonic forecasting can be found in Table 8.

Table 8: Rationale for LSTM-ANFIS-Based Hybrid Model Summary

Rationale	LSTM	ANFIS
Complementary strengths	Captures long-term dependencies and temporal patterns in sequential data.	Handles linguistic variables and interprets complex nonlinear relationships in tabular data.
Improved accuracy	Enhances forecasting accuracy by leveraging LSTM's ability to capture temporal relationships.	Incorporates tabular features and fuzzy logic to capture additional contextual information.
Feature extraction and interpretation	Automatically learns feature representations from harmonic time series.	Utilizes tabular features directly and provides interpretability through fuzzy rules.
Robustness to data characteristics	Adapts to various data characteristics, such as seasonality and nonlinear trends.	Models complex nonlinear relationships and adapts to linguistic variables in tabular data.
Ensemble effect	Harnesses ensemble benefits by combining LSTM with ANFIS for improved predictions.	Reduces the risk of overfitting and increases robustness and generalization performance.
Flexibility and customization	Enables customization by adjusting LSTM and ANFIS weights based on their performance.	Allows for customization according to specific harmonic forecasting requirements.

It is worth noting that the success of a hybrid LSTM-ANFIS model for harmonics forecasting depends on the specific dataset, problem domain, and modelling approach. Careful experimentation, validation, and fine-tuning of the model will be essential to

achieve the desired forecasting accuracy and performance. As detailed above, combining LSTM and ANFIS in a hybrid model for harmonics forecasting provides complementary strengths, improved accuracy, feature extraction and interpretation capabilities, robustness to data characteristics, ensemble benefits, and customization flexibility. These justifications make the hybrid model an attractive choice for performing harmonics forecasting.

2.7 Summary

This chapter presented a definition of power quality and explained the relationship between power quality and harmonics. Various phenomena causing power quality issues were stated, as per IEC and IEEE 1159 standards. Harmonics, along with their causes and effects, were also discussed, showing how they degrade power quality and endanger the power system and other electrical equipment. For proper regulation of renewable energy provided by wind turbines and PV to the grid, modern EPS rely heavily on power electronic converters.

In addition, this chapter reviewed the relevant literature and included some applicable standards, such as the IEEE 519 standard on harmonics limits and the IEEE 1159 standard for categorizing power quality issues, to provide an understanding of harmonics generated by different harmonics sources. The literature review was conducted to highlight the importance of harmonics forecasting and its application to mitigate issues caused by harmonics. The review was followed by a detailed rationale explaining why ANFIS-ANN and ANFIS-LSTM-based hybrid models should be used.

Chapter 3: Models and Harmonics Forecasting Techniques

3.1 Overview

This chapter discusses the models used in this thesis, including a modelling of wind speed and solar irradiation. As well, a brief explanation of ANN, ANFIS and LSTM will be provided, followed by an introduction of novel forecasting models adopted in this thesis to forecast harmonics.

3.2 Generator Models

3.2.1 Hybrid Wind-DFIG Solar Energy System

The hybrid wind DFIG-PV generator model have been utilized in this work to produce the current and voltage waveforms. The inputs for generator model are known values of wind speed and solar irradiation as recorded by European Commission, Joint Research Centre (JRC) [66]. In this way the output produced by the generator model depicts the real-world scenario. The model was created by combining a DFIG model in MATLAB with a PV model so it could be fed into the common grid. The total capacity of the Wind-DFIG PV generator model is 3 MW, which includes a 1.5 MW Wind-DFIG generator and a 1.5 MW PV array. The hybrid Wind-DFIG-PV model contains 1.5 MW-rated wind turbines using a wound rotor DFIG coupled with an AC/DC/AC IGBT-based PWM converter [83]. In this model, the wind speed signal is generated using a signal generator block. The values for wind speeds (m/s) are actual wind speed data recorded at Halifax, Nova Scotia, Canada, between June 1 and June 30, 2015 by the European Commission, Joint Research Centre (JRC) [66]. Additionally, the hybrid model consists

of a 1.5 MW-rated PV array containing 518 parallel strings. Each string has seven SunPower SPR-415E modules connected in series, and each solar cell capacity is 415 Watts. Hence, the seven-cell series connected in a solar panel for a total of 518 panels make up the 1.5 MW capacity of the solar plant. The PV model's input irradiance and temperature are generated from a signal generator block and are considered the real irradiance and temperature of Halifax as recorded on June 1-30, 2015 [66].

The selection of a 1.5 MW power rating for both wind and photovoltaic (PV) power systems was driven by a combination of practical considerations and standardization within the context of the study. Choosing a consistent power rating, in this case, 1.5 MW, allows for a meaningful and fair comparative analysis between the wind power and PV power systems. Standardization is often employed in research to ensure that differences in outcomes can be attributed to the inherent characteristics of the systems being studied rather than variations in their capacities. Furthermore, A 1.5 MW power rating aligns with the typical commercial scale for both wind turbines and PV arrays. This choice reflects a common capacity range seen in practical applications and facilitates the extrapolation of findings to real-world scenarios, enhancing the relevance of the study. Moreover, while larger power ratings might be found in certain installations, a 1.5 MW rating strikes a balance between being representative of commercial-scale systems and ensuring computational feasibility. It allows for a sufficiently detailed analysis without overwhelming computational resources.

The output of generator model is connected to a grid is modelled as a typical distribution grid which exports power to a 120 kV, 60 Hz grid through a 25 kV feeder. As the inputs are supplied to the model, it was simulated for 30 days (June 1-30, 2015).

Results from this model are used to extract harmonics which are later divided into training and test datasets to be used as inputs for the forecasting models discussed in subsequent section in this chapter.

3.2.2 Hybrid Wind-PMSG Solar Energy System

Like the Wind-DFIG-PV model, the hybrid PMSG-PV model was created by merging the PMSG model available in the MATLAB file exchange [67] with the PV model to be interconnected to the common grid. The model contains 1.5 MW wind turbines directly coupled with a multipole PMSG without a gearbox. The same PV, wind speed and solar irradiance models are utilized, as explained in a previous section. The model was simulated for 30 working days (June 1-30, 20215). All of the mentioned days were working days. The results achieved are used as input data for forecasting models discussed later in this chapter.

3.3 Artificial Neural Networks and Proposed Algorithm

3.3.1 Introduction

Artificial neural networks are based on how the human brain functions. The human brain's ability to remember, recall, correlate, interpret, recognize, and reason has made it appealing for researchers to create robots that mimic its performance in order to model, simulate, and perform a range of jobs. The human brain is made up of billions of neurons, defined as parallel computing elements. A network of axons, synapses, and dendrites connects them. As a result, the human brain resembles a large network of interconnected neurons.

McCulloch and Pitts were the first to describe a model of an artificial neuron that can mimic the behaviour of a biological neuron in [68]. An artificial neuron model in real life executes a sum of products ‘n’ of inputs denoted by ‘p’ and weights ‘w’ connected to them, as well as bias ‘b’. To generate the output, this sum is passed into a nonlinear transfer function ‘f(.)’. The weights ‘w’ and bias ‘b’ are variables that can be changed. Figure 4 shows a model of an artificial neuron [69]:

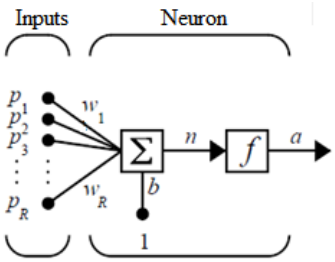

Figure 4: Artificial Neuron Model [69]

Mathematically, *n* is given by the following equations:

$$n = w_1 p_1 + w_2 p_2 + \cdots + w_R p_R + b \tag{3.1}$$

$$n = \sum_{j=1}^{R} w_j p_j + b \tag{3.2}$$

where R is the number of inputs. The neuron's output is given by:

$$a = f(n) = f\left(\sum_{j=1}^{R} w_j p_j + b\right) \tag{3.3}$$

3.3.2 Single and Multilayered Feed-Forward Neural Network

The Single-Layer Feed-Forward Neural Network (SLFNN), also known as the Single-Layer Perceptron (SLP), has only one level of neuron connectivity. It simply adjusts the weights ‘w’ to simulate the relationship between the input vector ‘p’ and the

output vector ‘a.’ A SLP can be made up of many neurons. Figure 5 depicts a simple SLP:

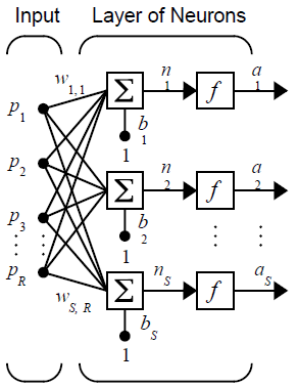

Figure 5: Single-Layer Perceptron Network [69]

The output vector can be determined using the following equation:

$$n_S = \sum_{j=1}^{R} w_{Sj} p_j + b_S \tag{3.4}$$

$$a_S = f(n_S) = f\left(\sum_{i=1}^{S}\sum_{j=1}^{R} w_{ij} p_j + b_S\right) \tag{3.5}$$

where R is the number of inputs and S is the number of neurons. The above expression can be written in vector form as:

$$a = Wp + b \tag{3.6}$$

The input, weight, bias, and output matrices are given by:

$$p = [p_1 \dots p_R],\ W = \begin{bmatrix} 1,1 & \cdots & w_{1,R} \\ \vdots & \ddots & \vdots \\ w_{S,1} & \cdots & w_{S,R} \end{bmatrix},\ b = [b_1 \dots b_S]\ \&\ a = [a_1 \dots a_S]$$

Multiple layers of neurons make up a Multi-Layer Feed-Forward Network, also known as a Multi-Layer Perceptron (MLP). The number of neurons in each layer can be the same or different. Between the input and output layers, there are one or more hidden layers. The activation functions and weight vectors of each layer can be the same or different. Every layer's output becomes an input for the following concealed layer until it reaches the output layer. An MLP network with two hidden layers is shown in Figure 6:

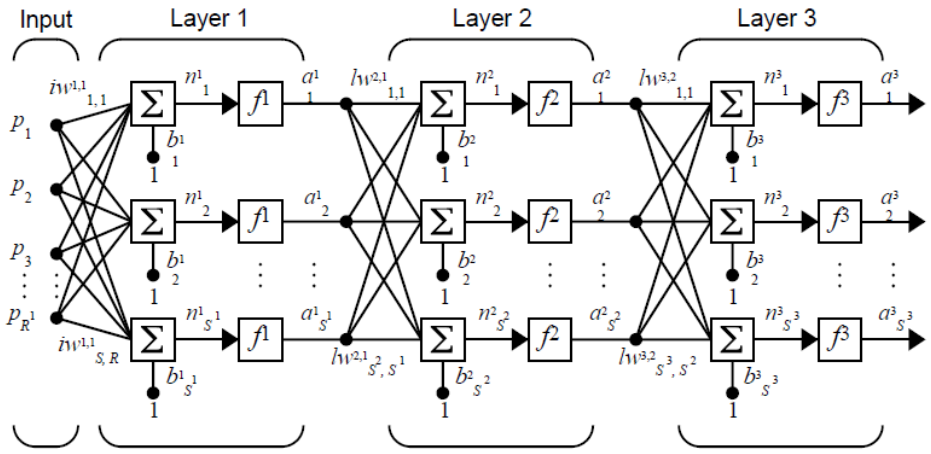

Figure 6: Multi-Layer Perceptron Network [69]

If we let l denote the number of hidden layers and $l = L$ for the output layer, the equations for the outputs of every hidden layer and the final output can be expressed by the following equations:

Hidden layer 1 ($l = 1$):

$$a_{1S^1} = f_1(n_{1S^1}) = f_1\left(\sum_{i=1}^{S^1}\sum_{j=1}^{R} w_{ij}p_j + b_{1S^1}\right) \tag{3.7}$$

Here, S^l denotes the number of neurons in layer l:

Hidden layer 2 to output layer ($l = 2 \ldots L$):

$$a_{lS^l} = f_l(n_{lS^l}) = f_l\left(\sum_{i=1}^{S^l}\sum_{j=1}^{S^{l-1}} w_{ij}a_{(l-1)j} + b_{lS^l}\right) \tag{3.8}$$

since in the above figure, L = 3:

$$a_{3S^3} = f_3(n_{3S^3}) = f_3\left(\sum_{i=1}^{S^3}\sum_{j=1}^{S^2} w_{ij}a_{2j} + b_{3S^3}\right) \tag{3.9}$$

$$a_{3S^3} = f_3\left(\sum_{i=1}^{S^3}\sum_{j=1}^{S^2} w_{ij}\, f_2\left(\sum_{i=1}^{S^2}\sum_{j=1}^{S^1} w_{ij} f_1\left(\sum_{i=1}^{S^1}\sum_{j=1}^{R} w_{ij}p_j + b_{1S^1}\right) + b_{2S^2}\right) + b_{3S^3}\right) \tag{3.10}$$

3.3.3 Cascaded, Recurrent and Hybrid Neural Networks

The Cascaded Neural Network (CNN) architecture is a type of MLP network in which each input and output of every hidden layer is cascaded to the next layer. Figure 7 demonstrates a three-layered CNN:

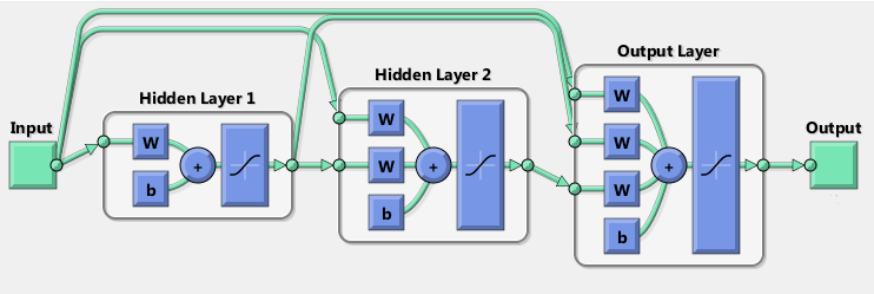

Figure 7: Three-Layered Cascaded Neural Network

A Recurrent Neural Network (RNN) has a feedback loop from the output to the input, as well as the weights that go with it. Many different forms of RNNs that are utilized for prediction have been discussed in the literature. Local feedback and global feedback are the two main types of feedback pathways. The recurrent path within the hidden layer provides local feedback, whereas the network's output and input provide global feedback [70]. Both local and global RNNs are depicted in Figures 8 and 9:

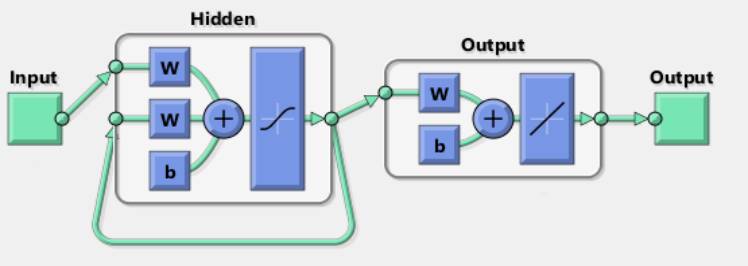

Figure 8: Recurrent Neural Network with Local Feedback

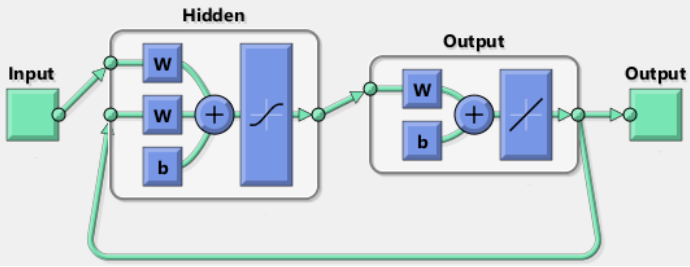

Figure 9: Recurrent Neural Network with Global Feedback

Hybrid neural network architectures integrate CNN with recurrent networks. These networks have a cascaded input-output layer link as well as local or global feedback routes and have been discussed in the literature [70]. The purpose of this thesis is to introduce a hybrid architecture and apply it to forecast harmonics to procure accurate prediction results. The next section discusses the novel hybrid neural networks that are created and utilized in this thesis in a MATLAB environment.

3.3.4 Three-Layered Recurrent Cascaded Neural Network with Local Feedback

A hybrid three-layered recurrent neural network with cascaded inputs of local feedback is portrayed in Figure 10. The equation evaluating and depicting the output of the network is expressed in Eq. 3.13. This multilayered-ANN ANFIS combination is called Three-layered Cascaded Neural Network with Recurrent Local feedback (3LCRNNL) [102-104]. Figure 10 below shows the 3LCRNNL feedback architecture.

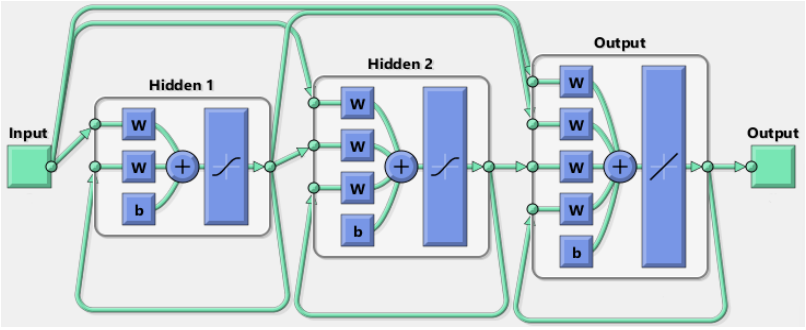

Figure 10: Three-Layered Cascaded Recurrent Neural Network with Local Feedback

The output equation of the 3LCRNNL is derived as follows:

$$a_{1S^1}(t) = f_1(n_{1S^1}) = f_1\left(\sum_{i=1}^{S^1}\sum_{j=1}^{R} w_{ij}p_j + \sum_{i=1}^{S^1}\sum_{j=1}^{S^1} w_{ij}a_{1j}(t-1) + b_{1S^1}\right) \tag{3.11}$$

$$a_{2S^2} = f_2(n_{2S^2}) = f_2\left(\sum_{i=1}^{S^2}\sum_{j=1}^{R} w_{ij}p_j + \sum_{i=1}^{S^2}\sum_{j=1}^{S^1} w_{ij}a_{1j} + \sum_{i=1}^{S^2}\sum_{j=1}^{S^2} w_{ij}a_{2j}(t-1) + b_{2S^2}\right) \tag{3.12}$$

$$\begin{aligned} a_{3S^3} = f_3(n_{3S^3}) = f_3\Bigg(&\sum_{i=1}^{S^3}\sum_{j=1}^{R} w_{ij}p_j \\ &+ \sum_{i=1}^{S^3}\sum_{j=1}^{S^1} w_{ij} f_1\left(\sum_{i=1}^{S^1}\sum_{j=1}^{R} w_{ij}p_j + \sum_{i=1}^{S^1}\sum_{j=1}^{S^2} w_{ij}a_{1j}(t-1) + b_{1S^1}\right) \\ &+ \sum_{i=1}^{S^3}\sum_{j=1}^{S^2} w_{ij} f_2\left(\sum_{i=1}^{S^2}\sum_{j=1}^{R} w_{ij}p_j + \sum_{i=1}^{S^2}\sum_{j=1}^{S^1} w_{ij}a_{1j} + \sum_{i=1}^{S^2}\sum_{j=1}^{S^2} w_{ij}a_{2j}(t-1)\right. \\ &\left. + b_{2S^2}\right) + \sum_{i=1}^{S^3}\sum_{j=1}^{S^3} w_{ij}a_{3j}(t-1) + b_{3S^3}\Bigg) \end{aligned} \tag{3.13}$$

3.3.5 Three-Layered Cascaded Recurrent Neural Network with Global Feedback

The second hybrid network combines the 3LCRNNG to create Three-layered Cascaded Neural Network with Recurrent Global feedback (3LCRNNG) [102], as shown in Figure 11.

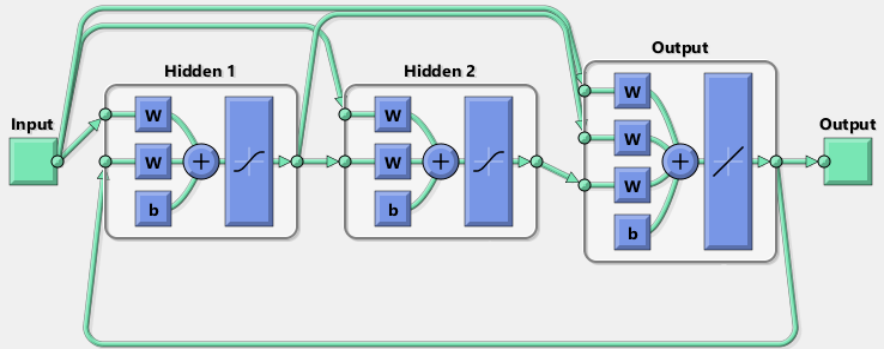

Figure 11: Three-Layered Cascaded Recurrent Neural Network with Global Feedback (3LCRNNG)

The output of 3LCRNNG is given as follows:

$$a_{1S^1}(t) = f_1(n_{1S^1}) = f_1\left(\sum_{i=1}^{S^1}\sum_{j=1}^{R} w_{ij}p_j + \sum_{i=1}^{S^1}\sum_{j=1}^{S^3} w_{ij}a_{3j}(t-1) + b_{1S^1}\right) \tag{3.14}$$

$$a_{2S^2} = f_2(n_{2S^2}) = f_2\left(\sum_{i=1}^{S^2}\sum_{j=1}^{R} w_{ij}p_j + \sum_{i=1}^{S^2}\sum_{j=1}^{S^1} w_{ij}a_{2j} + b_{2S^2}\right) \tag{3.15}$$

$$\begin{aligned} a_{3S^3} = f_3(n_{3S^3}) = f_3\Bigg(&\sum_{i=1}^{S^3}\sum_{j=1}^{R} w_{ij}p_j \\ &+ \sum_{i=1}^{S^3}\sum_{j=1}^{S^1} w_{ij} f_1\left(\sum_{i=1}^{S^1}\sum_{j=1}^{R} w_{ij}p_j + \sum_{i=1}^{S^1}\sum_{j=1}^{S^3} w_{ij}a_{2j}(t-1) + b_{1S^1}\right) \\ &+ \sum_{i=1}^{S^3}\sum_{j=1}^{S^2} w_{ij} f_2\left(\sum_{i=1}^{S^2}\sum_{j=1}^{R} w_{ij}p_j + \sum_{i=1}^{S^2}\sum_{j=1}^{S^1} w_{ij}a_{2j} + b_{2S^2}\right) + b_{3S^3}\Bigg) \end{aligned} \tag{3.16}$$

3.3.6 Three-Layered Cascaded Recurrent Neural Network with Local and Global Feedback

In order to improve accuracy in network integration, the inputs are cascaded to the next layers and each layer also receives feedback from its output as well as from the output layer. Figure 12 shows the architecture of a Three-Layered Cascaded Recurrent Neural Network with Local and Global feedback (3LCRNNGL) [102].

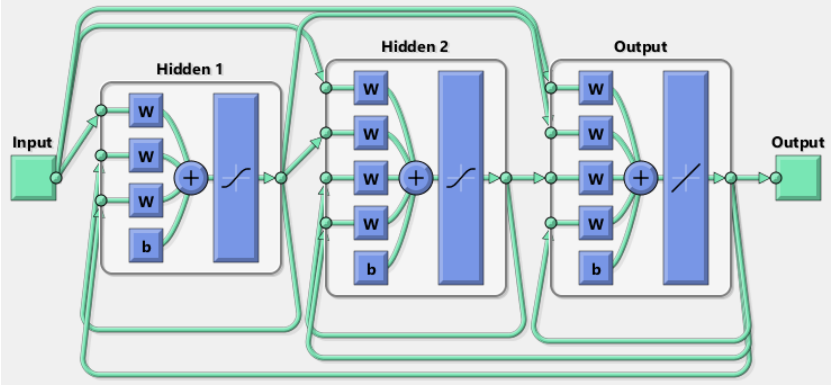

Figure 12: 3- Layered Cascaded Recurrent Neural Network with Local and Global Feedback (3LCRNNGL)

The equation governing the output of 3LCRNNGL can be expressed as follows:

$$a_{1S^1}(t) = f_1(n_{1S^1}) = f_1\left(\sum_{i=1}^{S^1}\sum_{j=1}^{R} w_{ij}p_j + \sum_{i=1}^{S^1}\sum_{j=1}^{S^1} w_{ij}a_{1j}(t-1) + \sum_{i=1}^{S^1}\sum_{j=1}^{S^3} w_{ij}a_{3j}(t-1) + b_{1S^1}\right) \tag{3.17}$$

$$\begin{aligned} a_{2S^2} = f_2(n_{2S^2}) = f_2\Bigg(&\sum_{i=1}^{S^2}\sum_{j=1}^{R} w_{ij}p_j + \sum_{i=1}^{S^2}\sum_{j=1}^{S^1} w_{ij}a_{2j} + \sum_{i=1}^{S^2}\sum_{j=1}^{S^2} w_{ij}a_{2j}(t-1) \\ &+ \sum_{i=1}^{S^2}\sum_{j=1}^{S^3} w_{ij}a_{3j}(t-1) + b_{2S^2}\Bigg) \end{aligned} \tag{3.18}$$

$$a_{3S^3} = f_3(n_{3S^3})$$

$$= f_3\left(\begin{array}{l} \sum_{i=1}^{S^3}\sum_{j=1}^{R} w_{ij}p_j + \\ \sum_{i=1}^{S^3}\sum_{j=1}^{S^1} w_{ij}f_1\left(\sum_{i=1}^{S^1}\sum_{j=1}^{R} w_{ij}p_j + \sum_{i=1}^{S^1}\sum_{j=1}^{S^1} w_{ij}a_{1j}(t-1) + \sum_{i=1}^{S^1}\sum_{j=1}^{S^3} w_{ij}a_{3j}(t-1) + b_{1S^1}\right) + \\ \sum_{i=1}^{S^3}\sum_{j=1}^{S^2} w_{ij}f_2\left(\sum_{i=1}^{S^2}\sum_{=1}^{R} w_{ij}p_j + \sum_{i=1}^{S^2}\sum_{j=1}^{S^1} w_{ij}a_{2j} + \sum_{i=1}^{S^2}\sum_{j=1}^{S^2} w_{ij}a_{2j}(t-1) + \right. \\ \left. \sum_{i=1}^{S^2}\sum_{j=1}^{S^3} w_{ij}a_{3j}(t-1) + b_{2S^2}\right) + \\ \sum_{i=1}^{S^3}\sum_{j=1}^{S^3} w_{ij}a_{3j}(t-1) + b_{3S^3} \end{array}\right) \tag{3.19}$$

3.3.7 Network Training

Neural network training is the process of altering network architecture and updating link weights and biases so that a network response can follow a specific behaviour. Various learning methods are utilized to accomplish this objective. A learning algorithm's goal is to reduce the error function by changing network parameters and using previous data as samples. When a solution is reached, the finalized parameters are stored, which means that network has learned how to respond to new information received for a particular application. In this thesis, the Levenberg-Marquardt Back Propagation (LMBP) algorithm is used to train the neural network architectures, due to its fast convergence and stability [71], [72].

3.4 Adaptive Neuro Fuzzy Inference System (ANFIS)

3.4.1 Introduction

The Adaptive Neuro-Fuzzy Inference System (ANFIS) was introduced in the early 1990s by Jang Roger, who proposed integrating Adaptive Neural Networks (ANNs) and fuzzy logic. Based on the Takagi–Sugeno Fuzzy Inference System, ANFIS combines ANN’s capability of self-learning with a fuzzy system’s logical inference ability, robustness, and ease in implementing the rule bases. The ANFIS systems are extremely effective and easy to implement, especially in cases of nonlinearity and uncertainty in the data [73].

In the MATLAB environment, the toolbox function ANFIS is fed by a given set of input/output data on the basis of which it constructs a Fuzzy Inference System (FIS). The membership function parameters of this FIS are tuned using a combination of back

propagation algorithms with a least squares type of method. In this way, the fuzzy systems learn from the data modelled [74]. Additionally, a neural network-type structure is generated that maps inputs through associated parameters and input membership functions and outputs via associated parameters and output membership functions. In this way the input/output map is interpreted for further processing and prediction [102].

3.4.2 ANFIS Structure and Working Principle

The ANFIS structure consists of a fuzzy Sugeno model which is set in an adaptive system framework [73]. A typical fuzzy rule in a Sugeno fuzzy model has the following format:

$$\boldsymbol{IF\ x\ is\ A\ and\ y\ is\ B, THEN\ z = f(x, y)} \tag{3.20}$$

where A and B are fuzzy sets and z = f (x, y) is a crisp function defining the output. The function f (x, y) is typically a polynomial, which describes the output based on the input variables x and y within the fuzzy region specified by the fuzzy sets of the rule. Figure 13 shows a first-order Sugeno FIS containing two rules.

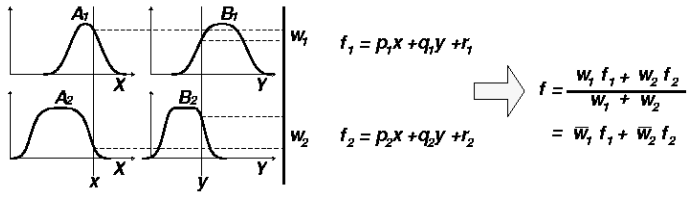

Figure 13: First-Order Sugeno Fuzzy Inference System

$$\begin{aligned}&\boldsymbol{Rule\ 1: IF\ x\ is\ A1\ and\ y\ is\ B1, THEN\ f1 = p1x + q1y + r1}\\&\boldsymbol{Rule\ 2: IF\ x\ is\ A2\ and\ y\ is\ B2, THEN\ f2 = p2x + q2y + r2}\end{aligned} \tag{3.21}$$

where

x, y = inputs,

A1, A2, B1, B2 = fuzzy sets,

f1, f2, f = outputs within the fuzzy region specified by the fuzzy rule, and

p1, p2, q1, q2, r1, r2 = design parameters that are determined during the training process.

The Sugeno fuzzy model is set into a framework of adaptive networks that can compute gradient vectors systematically in order to facilitate the learning process. The output is derived using the fuzzy reasoning mechanism from a given input vector [x, y]. Typically, the product of membership grade in the premise part of the fuzzy rules determines the firing weights w1 and w2, and the output f is obtained by the weighted average of each rule's output. Thus, the subsequent network architecture of ANFIS is shown in Figure 14, which consists of five layers. Each layer performs certain functions via nodes present in those layers. The circle indicates a fixed node, and a square indicates an adaptive node [97-98].

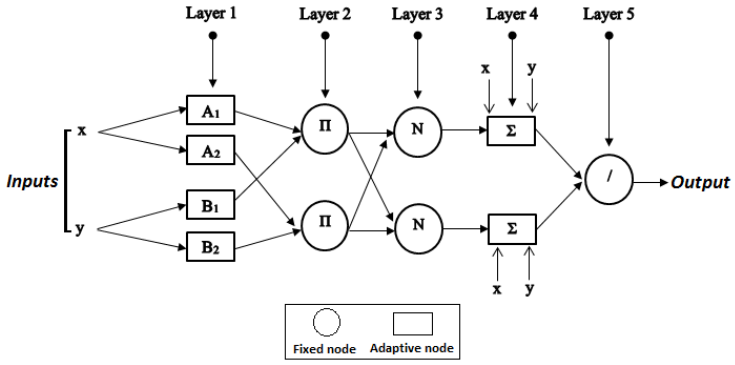

Figure 14: ANFIS Architecture [74]

The output layer has a single node. The final output is a summation of all incoming signals, expressed as follows:

$$f = \sum_i \overline{w}_i f_i = \frac{\sum_i \overline{w}_i f_i}{\sum_i \overline{w}_i} \tag{3.22}$$

3.4.3 Learning Algorithm

In the ANFIS structure, a hybrid learning approach is adopted that is a combination of back propagation and least square methods. The major advantage of using this hybrid learning algorithm is that it converges much faster by reducing search space dimensions compared to the typical backpropagation approach. The output of ANFIS expressed as an equation can be written as:

$$f = \frac{w_1}{w_1 + w_2} f_1 + \frac{w_2}{w_1 + w_2} f_2 \tag{3.23}$$

$$f = \bar{w}_1(p_1 x + q_1 y + r_1) + \bar{w}_2(p_2 x + q_2 y + r_2) \tag{3.24}$$

$$f = (\bar{w}_1 x)p_1 + (\bar{w}_1 y)q_1 + (\bar{w}_1)r_1 + (\bar{w}_2 x)p_2 + (\bar{w}_2 y)q_2 + (\bar{w}_2)r_2 \tag{3.25}$$

where

$p_1, q_1, r_1, p_2, q_2, r_2$ = Consequent parameters.

The parameters are updated in a forward backward pass method. The consequent parameters are determined with the least square technique in the forward pass of the hybrid learning, where the node outputs go forward until layer 4. The premise parameters are updated by gradient descent in the backward pass, where the error rates propagate backward, employing the backward propagation method [73], [74].

3.5 Long Short-Term Memory Network (LSTM)

3.5.1 Introduction

LSTM is a recurrent neural network architecture proposed by Hochreiter and Schmidhuber in [89]. The core idea behind LSTM is to have a memory cell that can store information for a long time and selectively decide which information to keep and

which to discard. LSTMs have been successfully applied to various tasks such as speech recognition, image captioning, natural language processing, and time series forecasting [90-93].

3.5.2 Architecture of LSTM

Recurrent neural networks, which form the basis of LSTM networks, are effective because they can recognize long-term relationships. Small weights are frequently multiplied repeatedly through a few steps in an RNN, and as a result, the gradients asymptotically approach zero. The vanishing gradient problem is another name for this RNN flaw. Cells, the memory units that make up the LSTM network, are connected by layers. In these cells, data are present in both the cell state c_t and the hidden state ht. This information is governed by gates through the sigmoid, with tanh acting as the activation function. Integers between 0 and 1 are commonly produced using the sigmoid function, with 0 denoting no information flowing through and 1 denoting that this is the focus. LSTM networks can thus conditionally add or remove information from the cell state.

In essence, the gates take the input, the hidden states from the previous time step (h_{t-1}), and the current input (x_t), and then multiply them pointwise by weight matrices (ω) and add bias (b) to the result. The three primary gates are the forgetting gate, the input gate, and the output gate. The forgetting gate, which decides the data to be removed from a specific cell state, outputs a number between 0 and 1, with 0 denoting complete deletion and 1 denoting complete retention. Equation (3.26) expresses this process:

$$f_t = \sigma(\omega_f[h_{t-1}, x_t] + b_f) \tag{3.26}$$

The input gate which has a tanh activation layer that produces a vector of prospective candidates, is shown in the following equation:

$$\widehat{c_t} = tanh(\omega_c[h_{t-1}, x_t] + b_c) \tag{3.27}$$

The sigmoid layer can then construct the following update filter as a result:

$$U_t = \sigma(\omega_u[h_{t-1}, x_t] + b_u) \tag{3.28}$$

The previous cell state c_{t-1} is then updated to:

$$c_t = f_t * c_{t-1} + U_t \times c_t^* \tag{3.29}$$

The output gate, which filters the cell state going to the output, is the final step. It has a sigmoid layer and can be expressed as follows:

$$O_t = \sigma(\omega_0[h_{t-1}, x_t] + b_0) \tag{3.30}$$

The numbers are then scaled to fall between [-1, 1] by using the tanh function on the cell state c. According to the equation, the new hidden state is made by multiplying the scaled cell state by the filtered output and then being transferred to the next cell.

$$h_t = O_t \times \tanh(c_t) \tag{3.31}$$

3.6 Novel Hybrid Forecasting Models

3.6.1 Introduction

This thesis introduces eight hybrid models combining the three-layered ANN with ANFIS and LSTM with ANFIS. In order to achieve high accuracy, all of the combinations will be applied to forecasting, and the results will be presented and compared in the following chapters. This section will describe the concept design for eight novel hybrid models generated and implemented in the thesis.

3.6.2 Model-1 – 3LCRNNL-ANFIS

The three-layered CRNNL defined in section 3.3.4 is combined with ANFIS, as demonstrated in Figure 15. The input data matrix that is used to forecast harmonics employing 3LCRNNL is cascaded to the input of ANFIS model along with the forecasting results depicted by the ANN model. Figure 15 presents the concept design.

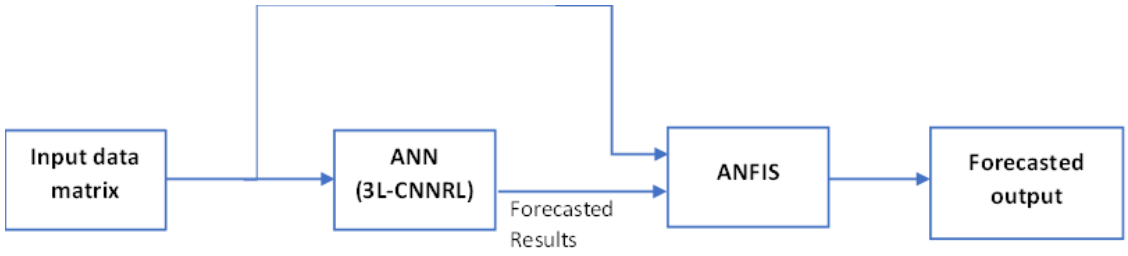

Figure 15: 3LCRNNL-ANFIS Model

3.6.3 Model-2 – 3LCRNNG-ANFIS

The three-layered CRNNG defined in section 3.3.5 is combined with ANFIS. Figure 16 depicts the proposed model.

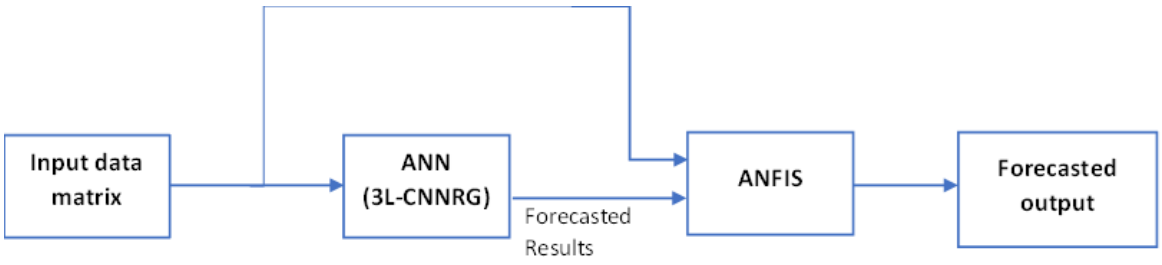

Figure 16: 3LCRNNG-ANFIS Model

3.6.4 Model-3 – 3LCRNNGL-ANFIS

This section presents a three-layered CRNNGL (section 3.3.4) combined with ANFIS. The design of the proposed hybrid model is presented in Figure 17.

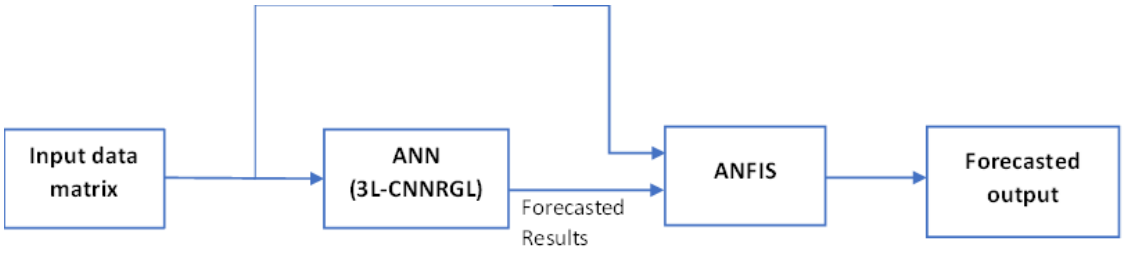

Figure 17: 3LCRNNGL-ANFIS Model

3.6.5 Model 4 – ANFIS-3LCRNNL

Similar to the above three proposed models, where ANFIS receives in its input the forecasting results from the three-layered ANN, model-4 swaps this combination. This section presents the ANFIS-3LCRNNL model where the input matrix goes to the ANFIS model to generate harmonic forecast and further cascades to the 3LCRNNL. The forecast received from ANFIS also serves as an input to the ANN model. The design of proposed hybrid model is presented in Figure 18.

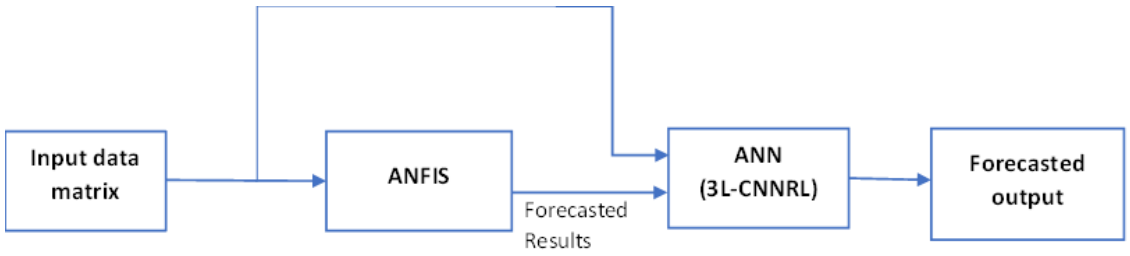

Figure 18: ANFIS-3LCRNNL Model

3.6.6 Model-5 – ANFIS-3LCRNNG Model

This section proposes the ANFIS-3LCRNNG model design in Figure 19:

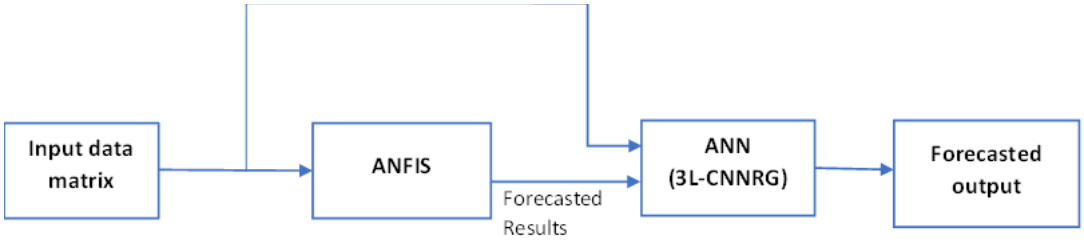

Figure 19: ANFIS-3LCRNNG Model

3.6.7 Model-6 – ANFIS-3LCRNNGL

In this section, the ANFIS-3LCRNNGL concept design is proposed in Figure 20.

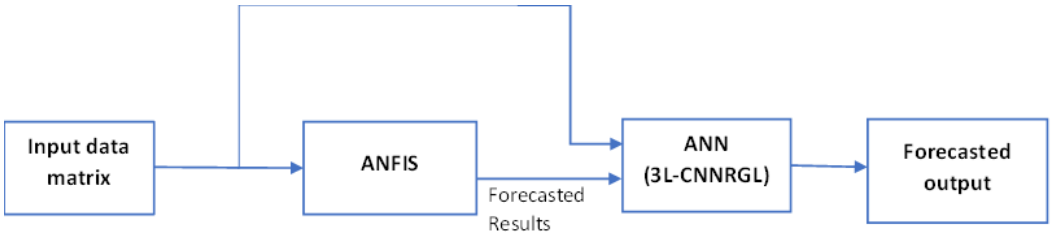

Figure 20: ANFIS-3LCRNNGL Model

3.6.8 Model-7 – LSTM-ANFIS

In this section, the ANFIS-LSTM concept design is proposed in Figure 21.

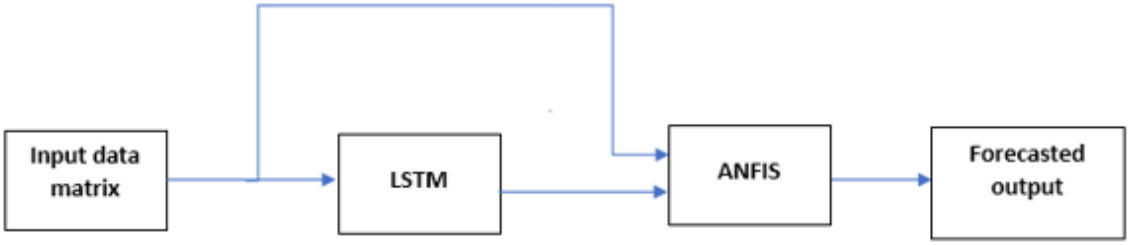

Figure 21: LSTM-ANFIS Model

3.6.9 Model-8 – ANFIS-LSTM

In this section, the ANFIS-LSTM concept design is proposed in Figure 22.

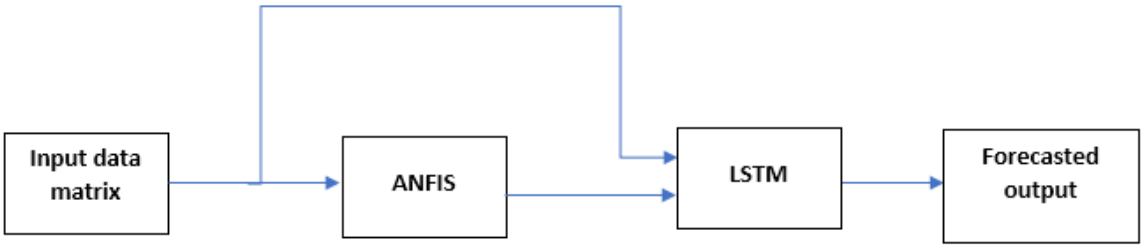

Figure 22: ANFIS-LSTM Model

3.7 K-Fold Cross-Validation

Cross-validation is a widely used technique for model evaluation. Its adaptation to time series data is crucial due to the sequential nature of such data. K-fold cross-validation is a resampling method used to assess how well a model performs on a certain dataset. In this study, the dataset is divided into K-folds of equal size. The model is tested on the remaining fold after being verified on K-1 folds. Each fold serves as the validation set precisely once during the K-fold iteration of this process. The model's

overall performance is then evaluated by averaging the performance metrics received from each fold [99-101].

Time series forecasting seeks to make future value predictions using data from the past. Each observation in a time series data set is influenced by earlier observations due to its temporal dependencies. Applying cross-validation techniques presents specific issues because of this sequential nature. As a result, the typical cross-validation approach is inapplicable to time series data, since it implies that data points are independent and equally distributed. Due to the intrinsic temporal interdependence of time series, random data splitting or rearranging can cause information leakage and produce unduly optimistic performance predictions. A modified form of K-fold cross-validation is thus utilized to overcome the difficulties presented by time series data.

The main concept in a modified K-fold cross-validation approach is to maintain the data's temporal order during cross-validation. Utilizing an expanding window system that mimics a real-time forecasting scenario is one popular strategy. For time series data, the expanding window method is a K-fold cross-validation variant. The training data window is gradually expanded throughout each fold to ensure the model is trained on historical data before generating predictions for upcoming time steps.

The following is an explanation of the algorithm used to perform expanding window cross-validation while training forecasting models on time series data:

1. Set the initial training window size, denoted as **W**.
2. Split the time series data into K folds.
3. For each fold:

a. Train the model using the data from the start of the time series up to the end of the current fold.
b. Make predictions for the next time step(s) using the trained model.
c. Evaluate the performance of the model's predictions for the current fold.
d. Slide the training window forward by one time step, incorporating the current fold's data.

4. Repeat steps 3a to 3d for all K folds.
5. Aggregate the performance metrics obtained from each fold to assess the overall model performance.

3.8 Implementation of Hybrid Forecasting Models

3.8.1 Data Generation from Generator Models

To generate harmonics forecasting using the proposed hybrid models, the two generator models discussed in section 3.2 were simulated for 31 days. Real-time data for wind speed and solar irradiation in Halifax, Canada, was used, as recorded between June 1 and July 1, 2015 [66]. The generator models produced output voltage and current waveforms, from which harmonics were extracted using FFT. These harmonics data were further analyzed and stored for use as inputs for the forecasting models. The data for the first 30 days of the test period (June 1-30, 2015) were used for training and formed the training set, while the data for the final day of the test period (July 1, 2015) were used as the test set.

3.8.2 Selection of Inputs

The selection of inputs is crucial for achieving accurate forecasting. Inputs should be carefully selected from the available data by analysing the trends for the target signal. To extract harmonics in this study, an FFT analysis was carried out on the data procured from the scope, with the MATLAB command line being used to extract harmonics information. The FFT window consisted of five cycles that extracted the samples from voltage and current waveforms. The FFT samples were extracted for 720 hours (30 days). A total of 7200 samples were recorded, with 10 samples logged per hour for both current and voltage waveforms.

The following harmonics parameters were extracted from the simulated signals, which, after statistical analysis (as detailed in Chapter 4), were selected as parameters to be forecasted for both voltage and current waveforms:

1- Total Harmonic Distortion (THD) / Total Demand Distortion (TDD)
2- Magnitude of 7^{th} (h7) harmonic component.
3- Magnitude of 11^{th} (h11) harmonic component.
4- Magnitude of 13^{th} (h13) harmonic component.

The 7^{th}, 11^{th} and 13^{th} harmonics were forecasted because of their relatively high amplitudes compared to the others. A detailed statistical analysis is presented in Chapter 4 to demonstrate their selection as forecasting parameters. Additionally, the forecasting models employed several parameters for input variables (predictors), which were used as inputs to produce a forecast. These variables are as follows:

1- Wind speed
2- Solar irradiation

3- One hour before the observation of the predicted parameter

4- One day before the observation of the predicted parameter

5- Two days before the observation of the predicted parameter.

These inputs were found to best represent the inputs for the forecasting models. The selection of wind speed and solar irradiation was obvious, as the forecasted parameters (THD/TDD, 7^{th}, 11^{th}, or 13^{th} harmonic) directly depend on the magnitude of wind speed and/or solar irradiation. As for the historical parameters, the one hour, one day, and two days before the observation of the predicted parameter have no dependencies on these inputs. Rather, they are related, as at these time intervals the conditions were observed to be similar. In order to illustrate the correlation, Figure 23 presents the plot for the voltage harmonics forecasting parameter: Total Harmonic Distortion (THD) for the Wind-DFIG-PV generator model.

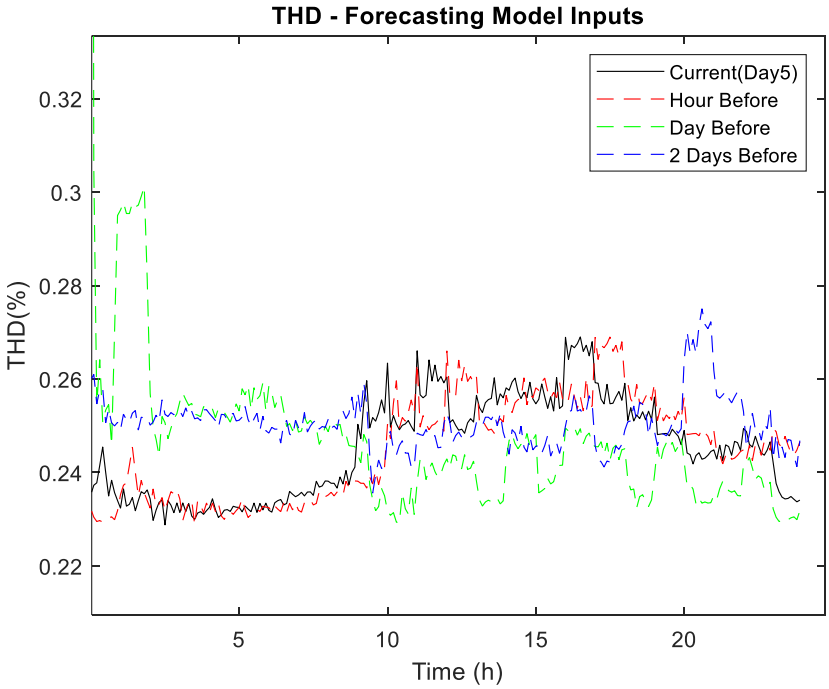

Figure 23: Total Harmonic Distortion Curves for Wind-DFIG-PV model

In Figure 23, the THD for day 5 is plotted against the THD value for one hour before, one day before, and two days before. The patterns appear to have a similar trajectory, so they are selected as inputs for the forecasting model. With the adopted training methodology, the weight adjustment should be able to train the network to produce accurate forecasts.

In further analysing the inputs, we see that days 4 and 5 wind speed and solar irradiation are plotted against respective THD in Figures 24 and 25. It can be observed that the change in both wind speed and solar irradiation have a proportionate effect on THD. For instance, in Figure 24, at hour 9, the solar irradiation and wind speed both start to increase, which also results in an increased THD.

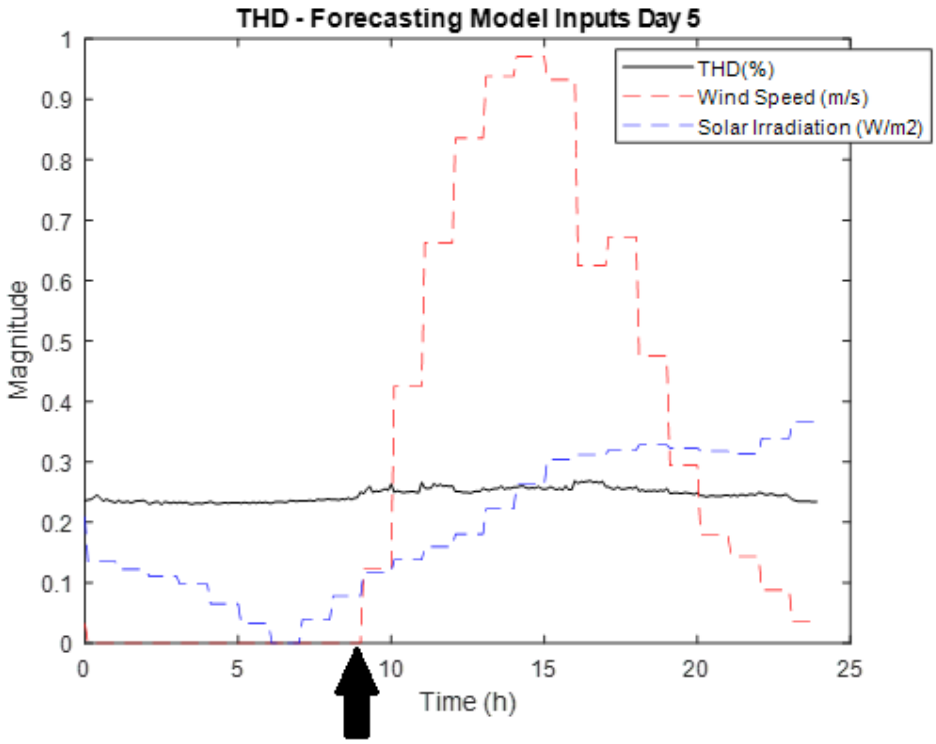

Figure 24: THD vs Wind Speed and Solar Irradiation for Wind-DFIG-PV (Day 5)

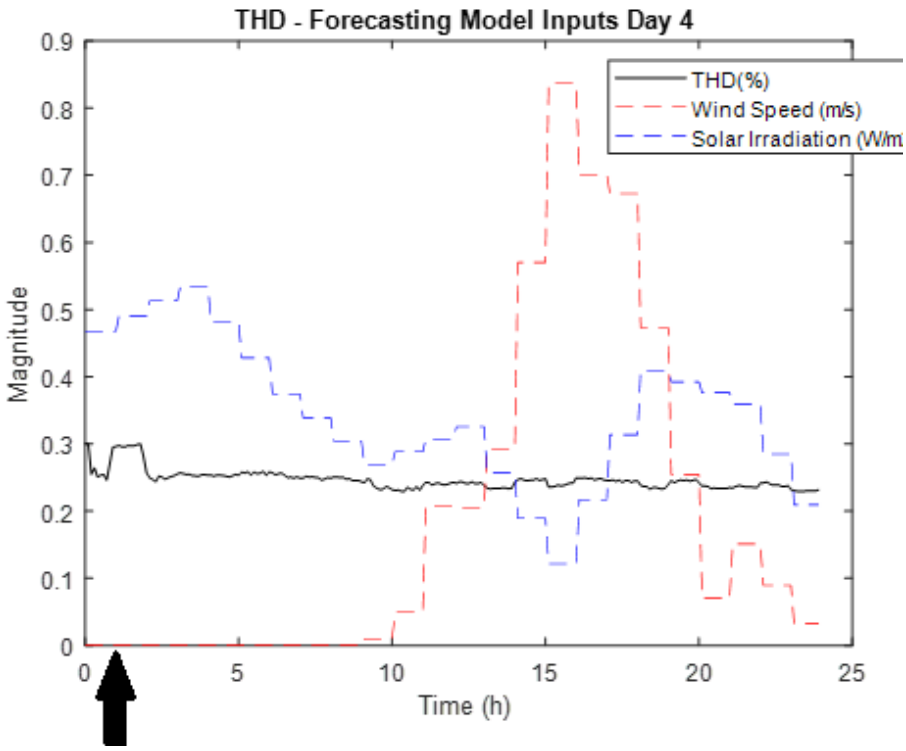

Figure 25: THD vs Wind Speed and Solar Irradiation for Wind-DFIG-PV (Day 4)

As mentioned, the increment in THD can be observed with small increases in the magnitude of THD in Figure 24. Similarly, in Figure 25, which shows day 4 curves at time of 1 hour, the wind speed increases and then falls, resulting in a similar increment and dip in the THD curve. The same type of changes can be observed in the trajectory of THD with respective changes in wind speed and solar irradiation. Hence, these parameters are also selected as an input in the forecasting model in order to train it and adjust weights accordingly to produce an accurate forecast.

3.8.3 Data Pre-processing

In the data pre-processing step, all data points are normalized between values of 0 and 1. This simplifies the calculations and uniformly presents the input parameters

under one scale. For ANN and ANFIS implementation, it is necessary to normalize data this way for better convergence. The following formula is used to normalize data:

$$x_{norm} = \frac{x - x_{min}}{x_{max} - x_{min}} \tag{3.32}$$

where

x_{norm} is the normalised data point,

x is the actual data point,

x_{min} is the minimum data point in the series, and

x_{max} is the maximum data point in the series.

Data standardization is the process of transforming data into a common scale or format that involves rescaling the data to have zero mean and unit variance. In the context of LSTM models, data standardization is crucial to ensure optimal performance and convergence during training and prediction. Data standardization is done by subtracting the mean value of the data and dividing by the standard deviation, as explained in the following steps.

1. Compute the mean (μ) of the data: Calculate the average of all data points in the dataset.
2. Compute the standard deviation (σ) of the data: Calculate the square root of the average of the squared differences between each data point and the mean.
3. Subtract the mean from each data point: For each data point (x), subtract the mean (μ) from it.
4. Divide the mean-adjusted values by the standard deviation: Divide each mean-adjusted data point by the standard deviation (σ).

This can be represented by the formula:

$$x_{standardized} = \frac{x - \mu}{\sigma} \tag{3.33}$$

where

$x_{standardized}$ = standardized dataset,

x = data set,

μ = mean value of the dataset, and

σ = standard deviation of the dataset.

Data standardization for LSTM is crucial for facilitating convergence, avoiding gradient-related issues, treating features equally, and improving the generalization and performance of the model. By standardizing the data, you ensure that the LSTM model can effectively learn and make accurate predictions on a wide range of inputs [99-101].

3.8.4 Network Training and Forecasting Methodology

3.8.4.1 Application of Artificial Neural Networks

The ANN models used in this thesis aim to predict the next-step harmonics. ANN uses previously observed harmonic patterns of simulated data for training and learning in order to provide forecasts. For the ANN to work well, however, there must be a strong correlation between the inputs and outputs. Additionally, in order to improve performance, the hidden layer and output layer weights must be carefully adjusted throughout the training phase [75]. Hence, determining the appropriate architecture—specifically, the ideal number of hidden layers, the number of neurons in each layer, and the role of each layer's activation—is crucial for optimal performance [46].

In this study, in order to improve the weight adjustment, the hyperbolic tangent transfer function was used for the hidden layers. By default, MATLAB employs the

sigmoid transfer function. For a complex and nonlinear dataset as utilized in this thesis, the selection of hyperbolic transfer function is more beneficial compared to the sigmoid function. To illustrate this point, Figure 26 superimposes the sigmoid function over the hyperbolic tangent function [84-88].

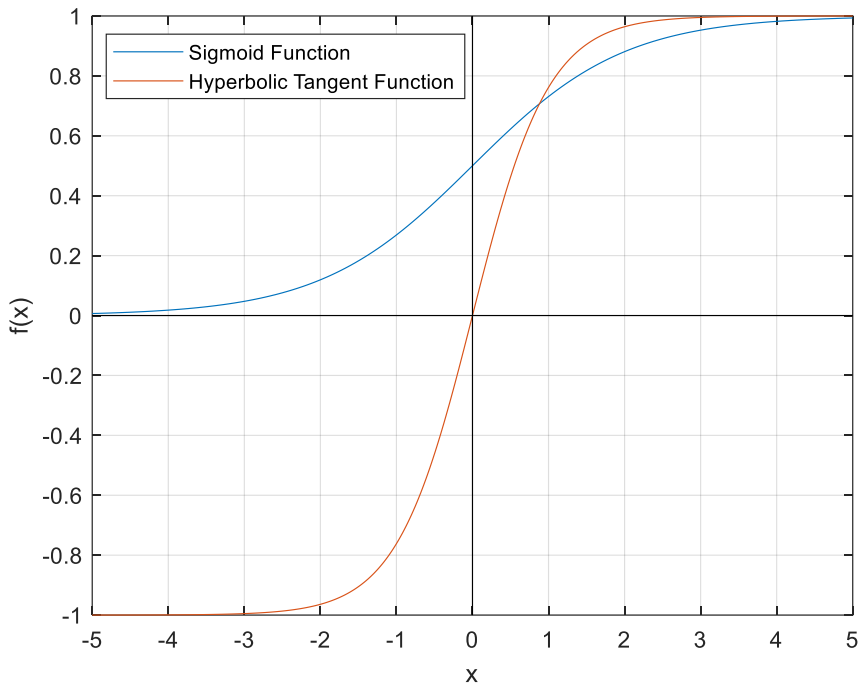

Figure 26: Superimposed Hyperbolic Function over Sigmoid Function

Figure 26 establishes two features that differentiate the hyperbolic tangent function from the sigmoid function, as explained below:

1- The sigmoid function has a substantially smaller slope than the hyperbolic tangent function.

2- The sigmoid function always responds positively, but the hyperbolic tangent function responds negatively for negative input values and positively for positive input values.

The larger slope of the hyperbolic tangent function indicates that it has a stronger response to even modest changes in the input variable. As a result, it can provide a considerably more nonlinear response and can better distinguish between subtle variations in the input variable. For network nodes, it is also crucial that the sign of the response coincide with the sign of the input in the hyperbolic tangent transfer function. Normalizing and standardizing the data to the zero mean gives the value of a node's output some meaning. A node's average state is 0, the lowest response level is -1, and the highest response level is +1. With this structure, the inputs to the nodes of the first hidden layer are similarly zero when the input variables are nominally zero. Consequently, when applying a hyperbolic tangent transfer function, the outputs of such nodes are also zero, and the output layer's inputs and outputs are likewise all zero, as are those of the other hidden layers. In other words, the network already accurately predicts the nominal situation before any training even begins, and so only needs to be trained for deviation from the nominal case.

In contrast, a 0 input to a sigmoid transfer function results in an output response of 0.5, indicating that the network must additionally modify its initial weights in order to train the nominal case, reducing the effectiveness of training. The 3LCRNNL, 3LCRNNG, and 3LCRNNGL ANN models and architecture used in this thesis employ the hyperbolic tangent transfer function in all their hidden layers. To increase the resilience of these models, linkages between inputs and outputs in various combinations are created, as discussed in section 3.5.

As mentioned previously, the ANN models employ various parameters for input variables, including solar irradiation, wind speed, and historical values for the

forecasted parameter (i.e., one hour, one day and two days before). Additionally, the ANN models have a scaled conjugate gradient as an optimizer to reduce the error function (training), which was identified by trial and error. Based on conjugate directions, Moller [76] created the scaled conjugate gradient (SCG) algorithm. Unlike other conjugate gradient algorithms, which need a line search at each iteration, this technique utilizes a network training function called "trainscg" in MATLAB. This strategy changes bias and weight variables using the scaled conjugate gradient approach. If the weights, net input, and transfer functions contain derivatives, it can train any network. The quadratic approximation of the error function is used to determine the step size in the SCG algorithm, which further increases its robustness and independence from user-defined parameters [77].

3.8.4.2 Application of Adaptive Neuro Fuzzy Inference System

ANFIS is a hybrid system that combines the advantages of both ANN and the fuzzy system [75]. As a result, ANFIS is more accurate at making predictions than ANN. In order to model data uncertainty, ANFIS essentially combines the learning capabilities of NNs with those of FIS, making it relatively easy to train an ANFIS model without the need for detailed subject-matter expertise. Furthermore, ANFIS has the benefit of utilizing both verbal and numerical information. Thus, the flexibility, nonlinearity, and quick learning of ANFIS are its benefits.

However, the system becomes exceedingly challenging to execute when the number of inputs to the standard ANFIS's fuzzy system rises. Additionally, the more inputs and membership functions are selected, the more training time is needed, and increases in the number of membership functions per input subsequently increases the

fuzzy rules. However, applying the ANFIS method for prediction, which is based on clustering, makes it simple to overcome these challenges.

Subtractive clustering is a prediction-making procedure that determines the number of clusters and their centre. It is also useful when data characteristics make clustering uncertain. The subtractive clustering method is an extension of the mountain clustering method proposed in [82]. In subtractive clustering, each data point is first evaluated as a prospective cluster centre candidate, after which each data point's potential is determined by calculating the density of the data points around it. This strategy is helpful in cases where it is unclear how many data distribution centres will be needed.

The present thesis uses subtractive clustering. Because the approach is iterative, it assumes that any point could serve as the centre of a cluster, depending on where it is in relation to other data points. Subtractive clustering involves selecting the point with the best likelihood of being the cluster centre, then deleting every other point inside the first cluster centre's radius (the radius being defined by the neighbourhoods of the centre). To find the next cluster's centre, the potential of the other spots is recalculated. The calculation proceeds until all the data are contained within a cluster centre's radius [78]. A step-by-step overview of the process is given below.

1. Based on the density of nearby data points, determine the likelihood that each data point would define a cluster centre. Measure the density index D_i corresponding to data x_i, as expressed in Equation 3.34.

$$D_i = \sum_{j=1}^{n} \exp\left(-\frac{\|x_i - x_j\|^2}{\left(r_a/2\right)^2}\right) \tag{3.34}$$

where r_a = positive number that represents the radius where all the data within it are considered neighbourhoods.

2. Pick the data point that has the best chance of becoming the first cluster centre. Hence, the data point with the highest density measure is selected as the first centre cluster denoted x_{c1} and its density is D_{c1}.

3. Eliminate all data points close to the first cluster centre. With the use of cluster influence range, the area is identified.

4. Recalculate the density measurements for each data point xi and select the final point with the greatest potential to serve as the cluster centre expressed in Equation 3.35.

$$D_i' = D_i - D_{cl}\exp\left(-\frac{\|x_i - x_{c1}\|^2}{\left(r_b/2\right)^2}\right) \tag{3.35}$$

where r_b = Kr_a (K is a positive number, usually K = 1.5 [82]). All the points near the first cluster centre x_{c1} will have a low-density degree and thus will not be considered as the next cluster centres. Rather, the next cluster centre x_{c2} will be nominated after the density measure for each data point is recalculated.

5. Reiterate steps 3 and 4 until a cluster centre can affect all of the data.

For optimization purposes, the following parameters were changed to improve the performance:

- Squash factor - Only find clusters that are far from each other.
- Accept ratio - Only accept data points with a strong potential for being cluster centres.
- Reject ratio - Reject data points if they do not have a strong potential for being cluster centres.

In this thesis, the ANFIS is utilized using subtractive clustering, which is optimized by trial and error. The input parameters used in ANFIS are the same as those used for ANN.

3.8.4.3 *Application of Long Short-Term Memory Network*

The LSTM model employed within this study comprises five sequential input layers, each dedicated to an individual input. It also includes 100 LSTM layers, organized as 20 hidden layers per input, and further incorporates a fully connected layer and a regression layer serving as the output layer. The input layer's dimensions align with the number of inputs, which is set at five. This configuration facilitates the deployment of a cumulative total of 100 LSTM layers, employed to facilitate additive interactions and the acquisition of intricate enduring relationships within sequence and time series data. To adapt to varying input dimensions, the fully connected layer employs an 'auto' setting to automatically discern the number of inputs received from the LSTM layer, executing matrix multiplication and bias vector addition as part of its operations. The regression layer is responsible for training and computational tasks, ultimately yielding the network's output. Figure 27 presents a visual representation of the LSTM network and the architecture utilized in this study.

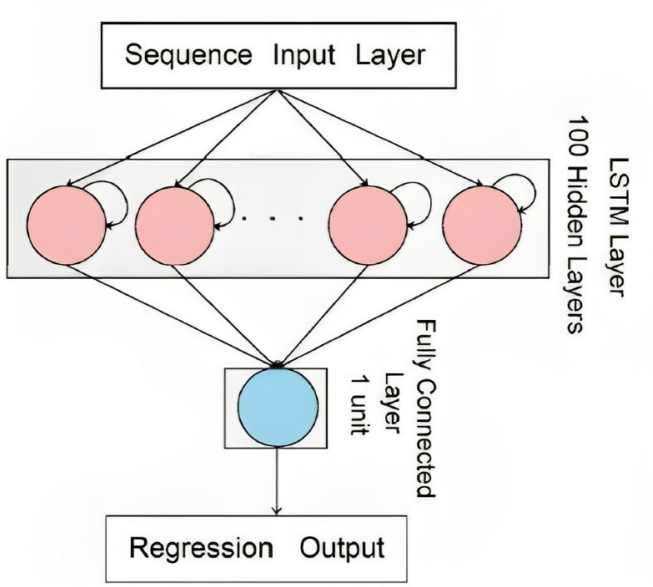

Figure 27: Structure of LSTM Model

3.8.4.4 Application of K-Fold Cross-Validation

K-fold cross-validation is applied on all the proposed models in order to improve training. The expanding window variation of K-fold is used. In this work, data for 30 days (June 1-30, 2015) are used to train the networks using K-fold cross-validation with the value of K selected as 5. The application of K-fold is explained in following steps:

1. The initial training window size is set to 25.
2. The time series data are split into K (5) folds, as shown in Figure 28. The value of K is selected based on the tests performed by setting K between 5 and 10. With K equal to 5, the training error achieved remains almost the same with higher values of K. Also, with a high K, the computation time is much longer with no significant advantage. Hence K-5 was found to result in fewer training errors and shorter simulation time.
3. For each fold:

a. The model is trained using the data from the start of the time series up to the end of the current fold.

b. The next time step (day) is predicted using the trained model.

c. The performance of the model is evaluated for the current fold.

d. The training window is slid forward by one time step (day), incorporating the current fold's data.

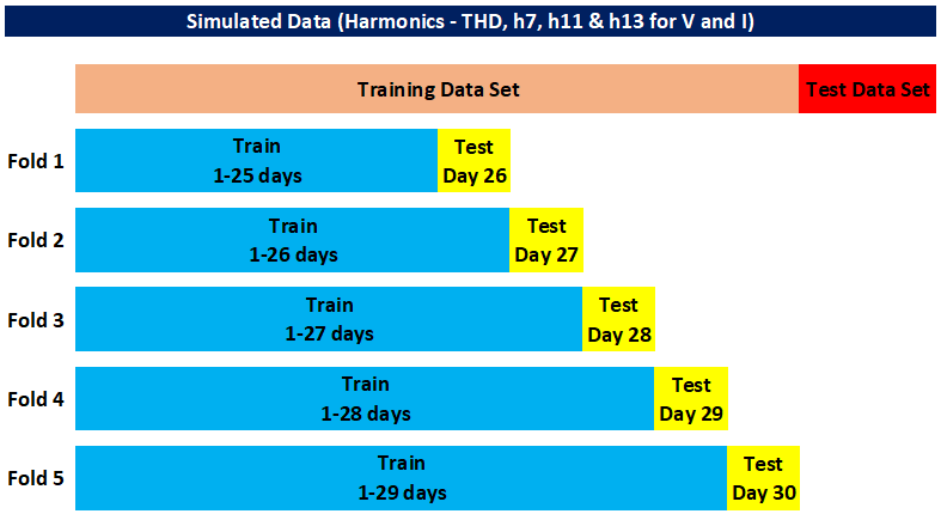

Figure 28: K-Fold Data Split Using Expanding Window for Time Series

4. Steps 3a to 3d are repeated for all K (5) folds.

5. The performance metrics obtained from each fold are aggregated to assess the overall model performance. Using this approach, all past data are assigned to the training set and successively consider each day as the test set. Using the 30-day length of the dataset and five folds, five distinct training and test divides are created, as illustrated in Figure 28. With this method, a variety of train/test splits are generated, and the error on each split is averaged to obtain a reliable prediction of the model error. In this way, the weights are adjusted to produce the most

accurate forecast and the model is trained and ready to be evaluated. The approach is presented in Figure 29.

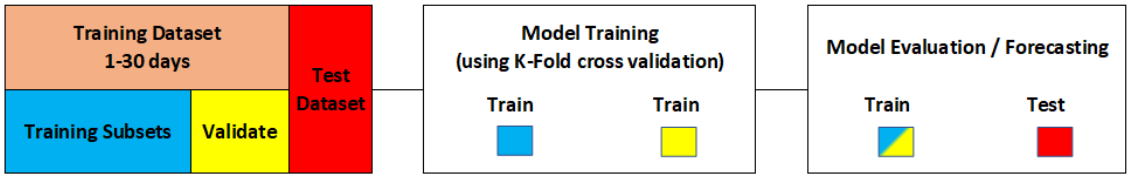

Figure 29: K-Fold Cross-Validation Methodology

6. The final step is to forecast for day 31. The trained model with adjusted weights and an improved via K-fold technique is evaluated with test data to produce a forecast. Figure 30 summarizes the whole process from steps 1 to 6, which is adopted in this work to produce forecasting results using the proposed hybrid models.

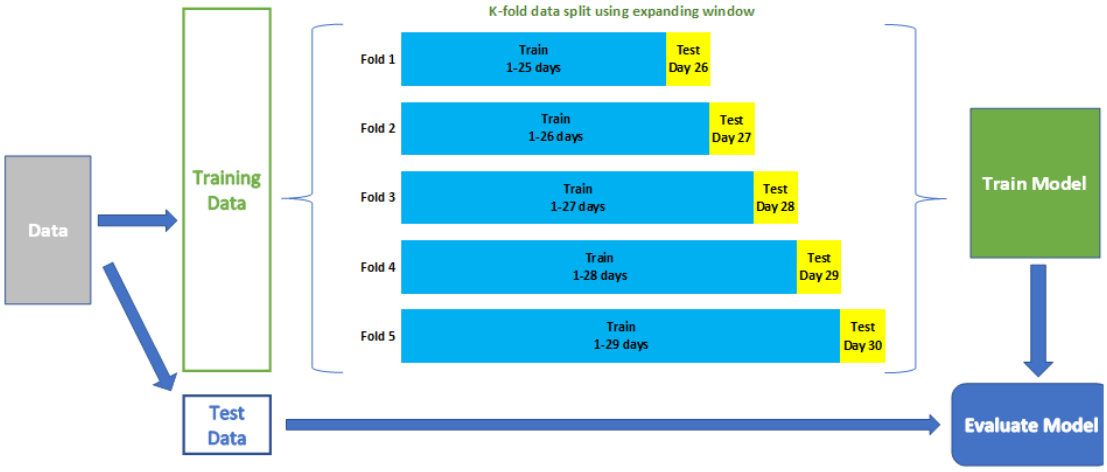

Figure 30: Forecasting Using K-Fold Cross-Validation for Model Training (for All Models)

3.8.4.5 Models 1-3: 3LCRNNL-ANFIS, 3LCRNNG-ANFIS, and 3LCRNNGL-ANFIS

The three-layered neural networks with cascaded inputs and recurrent feedbacks, as utilized in models 1-3, will have ten nodes in the first hidden layer and twenty nodes in the second hidden layer. The number of layers selected has been optimized to give the best performance. The optimization was conducted by applying the trial-and-error method, using different combinations of hidden and output layers in stage one with ANN. The training used scaled-conjugate gradient backpropagation due to its fast convergence with a large amount of data. As well, the hyperbolic tangent transfer function is used in the hidden layers to adjust weights in order to make the model synchronized with the input trends. To further improve adaptability, ANFIS is employed in the second stage of the hybrid models with subtractive clustering to make the comprehensive hybrid structure robust in order to generate accurate responses for forecasting.

The input parameters used to generate forecasting in stage one of the hybrid models 1, 2, and 3 are wind speed, solar irradiation, and one hour/one day/two days before observation of the forecasted parameters (i.e., THD, h7, h11, and h13). After the network is trained using the K-fold technique and the data from the first 30 days, the 31st day's THD, h7, h11, and h13 for voltage and current are forecasted. Once ANN in the first stage of the models is trained, the results are forecasted.

All five inputs are then fed to the ANFIS model in the second stage along with the sixth input, which are the forecasted results from stage one. This additional input from forecasting results from neural networks is expected to refine the final output. K-

fold validation is used again for ANFIS training to reduce training error and produce the final forecasting results.

3.8.4.6 Models 4-6: ANFIS-3LCRNNL, ANFIS-3LCRNNG, and ANFIS-3LCRNNGL

For the proposed hybrid models 4-6, ANFIS is used to forecast results for the 31st day in the first stage using the input variables wind speed, solar irradiation, and one hour/one day/two days before observation of the forecasted parameters (i.e., THD, h7, h11, and h13). The ANFIS results are fed into the neural networks along with the five inputs. Hence, the structure of ANN utilized in the second stage has 12 nodes in the first hidden layer and 24 nodes in the second. The scaled-conjugate gradient backpropagation method is used to train the ANNs and hyperbolic tangent is used as the transfer function to adjust weights in stage 2 for the proposed hybrid models 4-6. The K-fold technique is adopted in both stages to reduce training errors and improve the accuracy of the forecasting results.

3.8.4.7 Models 7-8: LSTM-ANFIS and ANFIS-LSTM

The proposed model-7 uses LSTM for forecasting in stage one and ANFIS in stage two. The five inputs are sent to the sequence input layer of LSTM. The LSTM model contains five input layers, 100 hidden layers in LSTM layer, one fully connected layer, and a regression layer as the output layer. K-fold validation is employed during training and the final forecast produced serves as input for stage two of hybrid model-7. In stage two, ANFIS received input from LSTM model plus the five inputs used to predict the harmonics for day 31. The K-fold technique is utilized for ANFIS training,

along with subtractive clustering of the data. In this way, the ANFIS stage produces the final forecast for model-7.

Model-8 utilizes the ANFIS model in stage one and the LSTM model in stage two. ANFIS produces forecasting results which are sent to the LSTM model. The LSTM network receives six inputs, including the five input parameters and another from the output of the ANFIS model. Hence, the LSTM network consists of six input layers, 120 hidden layers in the LSTM layer, one fully connected layer, and a regression layer, all of which combine to produce the final output, which is the forecast for day 31.

3.8.5 Evaluation of the Forecasting Models

The forecasting models described in the previous sections are validated by statistically analysing the results. In the literature, several different methods are used to evaluate the accuracy. Some of these methods are used as a measure of accuracy in the present work and are elaborated below. The results from the literature will be used to compare and validate the findings in this thesis.

3.8.5.1 Root Mean Squared Error (RMSE)

The mean squared error minimizes the variance of the error distribution. With time step N, target sequence *t,* and forecast sequence *f,* the mean squared error can be calculated as:

$$MSE = \frac{1}{N}\sum_{i=1}^{N} e_i^2 = \frac{1}{N}\sum_{i=1}^{N} (t_i - f_i)^2 \tag{3.36}$$

Similarly, the root mean squared error (RMSE) can be given as:

$$RMSE = \sqrt{\frac{1}{N}\sum_{i=1}^{N}(t_i - f_i)^2} \tag{3.37}$$

3.8.5.2 Mean Absolute Error (MAE)

MAE measures the difference between the predicted power and the actual recorded power. With time step N, target sequence *t*, and forecast sequence *f,* the mean absolute error can be computed as:

$$MAE = \frac{1}{N}\sum_{i=1}^{N}|f_i - t_i| \tag{3.38}$$

3.8.6 Use of Software

In this study, the generator models are taken from the MATLAB library and the neural network architecture figures are produced using MATLAB's neural network toolbox. Furthermore, network training and results forecasting are performed using MATLAB script in conjunction with the neural network toolbox. For ANIS, the MATLAB ANFIS toolbar is used to generate the forecasts and Microsoft Excel is employed to generate all the graphs.

3.8.7 Conclusion

This chapter opened with a brief introduction of the generator models used in the thesis, followed by an explanation of the wind speed and solar irradiation blocks utilized as inputs to these models. An overview of ANN was then presented, followed by a description of the three hybrid ANN models and their derived equations. ANN, ANFIS, and LSTM techniques were subsequently explained, along with the design concept of eight hybrid models that combined the ANFIS-ANN and ANFIS-LSTM

techniques. The closing portion of this chapter provided an overview of the implementation of several forecasting models and the methodology adopted here to utilize the data gathered from the simulation of generator models, aiming to improve model training using the K-fold cross-validation technique.

Chapter 4: Results and Discussion

4.1 Overview

In this chapter, the simulation results of generator models are presented. From these models, the harmonics are extracted and data analysis is performed to identify the dominant harmonics. Furthermore, in order to validate forecasting results, the forecasting results are compared with forecasting techniques adopted in the literature, including [36], [43], and [46] for different types of ANN, [42] for ANFIS, and [41] and [45] for LSTM network approaches.

Three neural networks are chosen from among the methods used in [36], [43] and [46] to accomplish the forecasting for this work. These networks are Cascaded Recurrent Neural Network with Local feedback (CRNNL), Cascaded Recurrent Neural Network with Global feedback (CRNNG), and Cascaded Recurrent Neural Network with Local and Global feedback (CRNNGL). In addition, the authors in [41] and [45] used the LSTM approach for prediction, whereas those in [42] used ANFIS. Later in the chapter, these five approaches are then employed to conduct a comparative analysis, in which the same data used in this thesis are utilized for all of the stated forecasting methods. Root mean squared error and mean absolute error are the indices used to compare the results.

4.2 Generator Models

The simulation of hybrid models with a total capacity of 3 MW (1.5 MW wind generator plus 1.5 MW PV array), as explained in the previous chapter, was performed to generate harmonics. To depict a real-world response, the actual wind speeds and solar

irradiance data were used as inputs for both hybrid models (Wind-DFIG-PV and Wind-PMSG-PV). Figures 31 and 32 depict the generator models used in this thesis [67], [83].

The hybrid Wind-DFIG-PV model combines the individual Wind-DFIG model and PV model taken from the MATLAB library. The Wind-DFIG model contains 1.5 MW wind turbines using a wound rotor DFIG coupled with an AC/DC/AC IGBT-based PWM converter. The stator winding is connected directly to the 60 Hz grid, while the rotor is fed at variable frequencies through the AC/DC/AC converter. For low and high wind speeds, the maximum extraction of energy is ensured by the optimization of the turbine speed. The wind speed signal in this model is generated by a signal generator block.

Furthermore, the PV model consists of a 1.5 MW-rated PV array containing 518 parallel strings. Each string has seven SunPower SPR-415E modules connected in series. The individual models for Wind-DFIG and PV were combined to be fed into the common grid. The grid is predefined in MATLAB and modelled as a typical distribution grid to add the effect of a nonlinear load. Thus, the grid acts as a nonlinear load and may have some impact on the output harmonics of the model. It is worth noting that any variations caused by the grid will not be considered in this work. The focus here is to simulate the harmonics that are generated by the generator model and study the effects of variations in the renewable sources (wind speed and solar irradiation).

Similarly, the hybrid Wind-PMSG-PV model combines the individual Wind-PMSG model and the PV model taken from the MATLAB library. The Wind-PMSG model contains 1.5 MW wind turbines directly coupled with a multipole PMSG without a gearbox. The grid connection is established via an AC/DC/AC converter consisting of

a diode rectifier, an internal DC-Link, and a PWM voltage-source inverter. This Wind-PMSG model was combined with a PV model and commonly fed into the grid, as explained in the previous paragraph. Due to the huge size of the data, time-scaling has been performed to simulate 30 days of data training and generate and capture the harmonics. One sec in the simulation represents one hour in real time. For the simulation, there is a time step of five microseconds, which means that in one second, 1/5e-6 = 200,000 steps are performed.

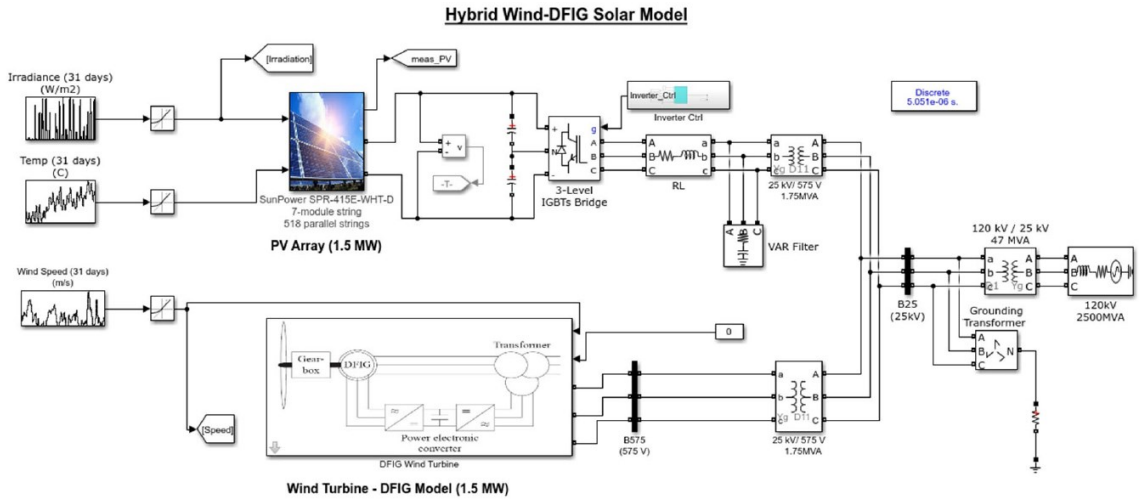

Figure 31: Wind-DFIG-PV Model

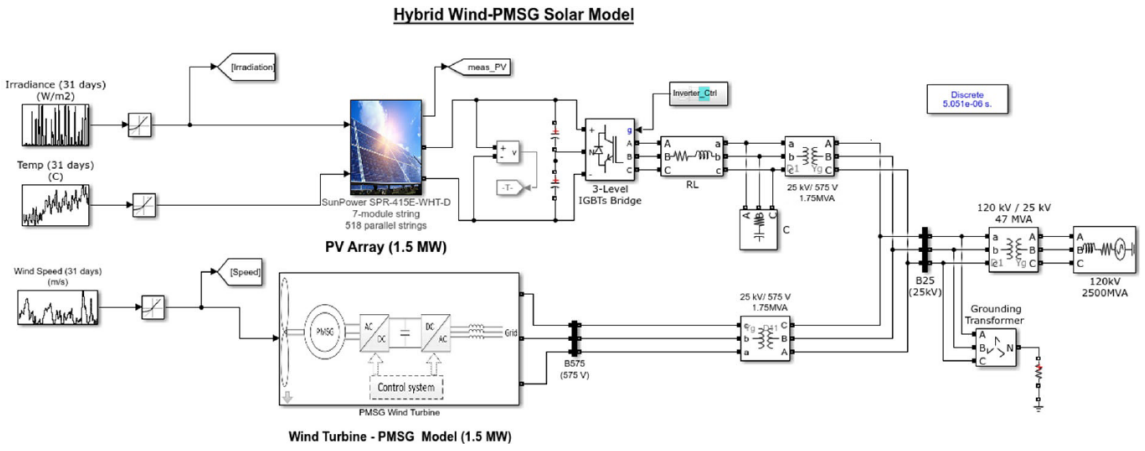

Figure 32: Wind-PMSG-PV Model

The models are taken from research in [67] and [83] and include detailed representations of power electronic IGBT converters. These models are well suited for observing harmonics and control system dynamic performance. To store and use the data for further analysis, all the data portraying variations in wind and solar parameters over 30 days (June 1-30, 2015) are split into datasets and the simulations are performed in sections.

Figures 33 and 34 present a snapshot from the voltage waveform for a Wind-DFIG-PV generator, with markers on phases 1, 2, and 3. The waveform which starts from 0 seconds is zoomed and snapped between 25 to 26 hours in order to visualize the presence of harmonics in the voltage waveform. The time frame of 25-26 hours is randomly selected to assess the condition of the output voltage waveform, as shown in Figures 33 and 34 below.

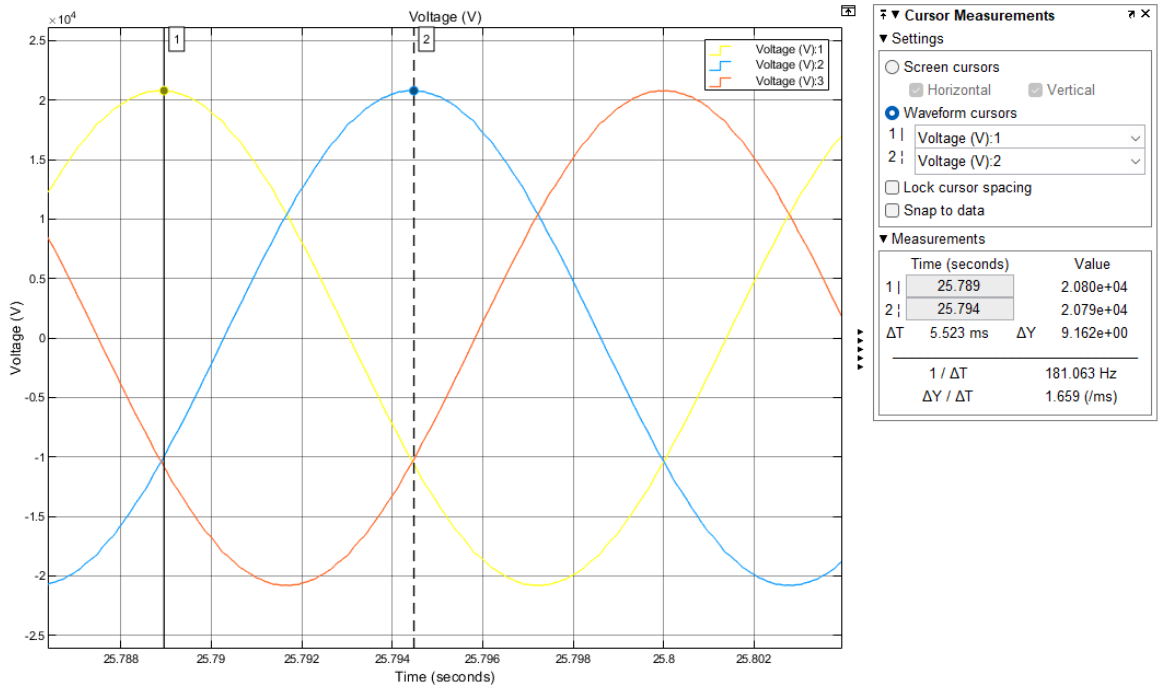

Figure 33: Sample Voltage Waveform for Wind-DFIG-PV Model (Phases 1 and 2)

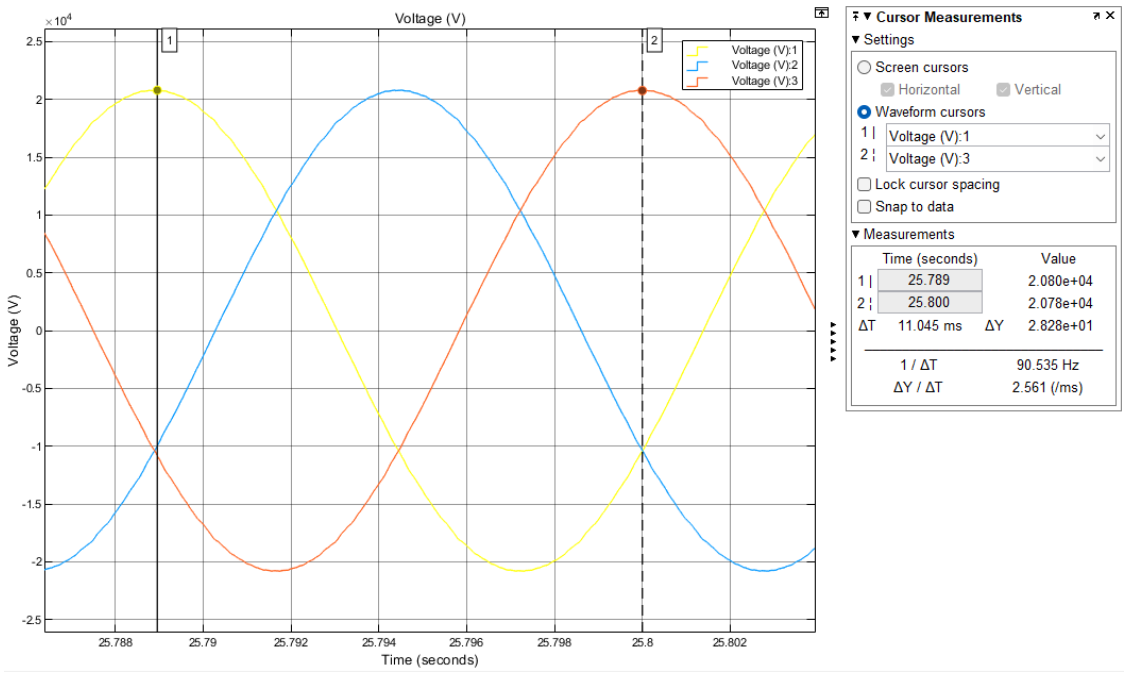

Figure 34: Sample Voltage Waveform for Wind-DFIG-PV Model (Phases 1 and 3)

Figure 33 shows the measurement markers on phases 1 and 2, while Figure 34 indicates the markers positioned at phases 1 and 3. The voltage value is displayed in the measurements window, where it can be observed that the voltages of all three phases are balanced. A 25 kV grid system is used for both generators. Figures 33 and 34 provide a profile of the output voltage, while Tables 9 and 10 later in this chapter present the amplitudes of individual harmonics and THD, as extracted from output waveforms.

The presence of harmonics can be observed in Figures 33 and 34. To log data into the workspace, the MATLAB scope feature was used. Data was stored in format structure for further analysing. Figures 35 and 36 show a sample of the three-phase current waveform visualized between 15 and 16 hours to demonstrate the presence of harmonics in the current waveform generated for the Wind-DFIG-PV model. The 15- to 16-hour timeframe is randomly selected to assess the current and is different from the

25- to 26-hour timeframe selected to analyse the voltage. This random selection of different timeframes is performed to validate that the voltage and current signals are balanced.

The presence of harmonics can also be observed in current and voltage waveforms. Figure 35 shows the markers in phases 1 and 2, while Figure 36 shows the markers in phases 1 and 3. The values of the current at the markers can be seen in the measurement window and appear to be equal. In proceeding further, our focus will remain on the single-phase voltage and current waveforms. All three-phase current waveforms are balanced, so an in-depth analysis and forecasting of single-phase current waveforms is sufficient to realize the overall impact.

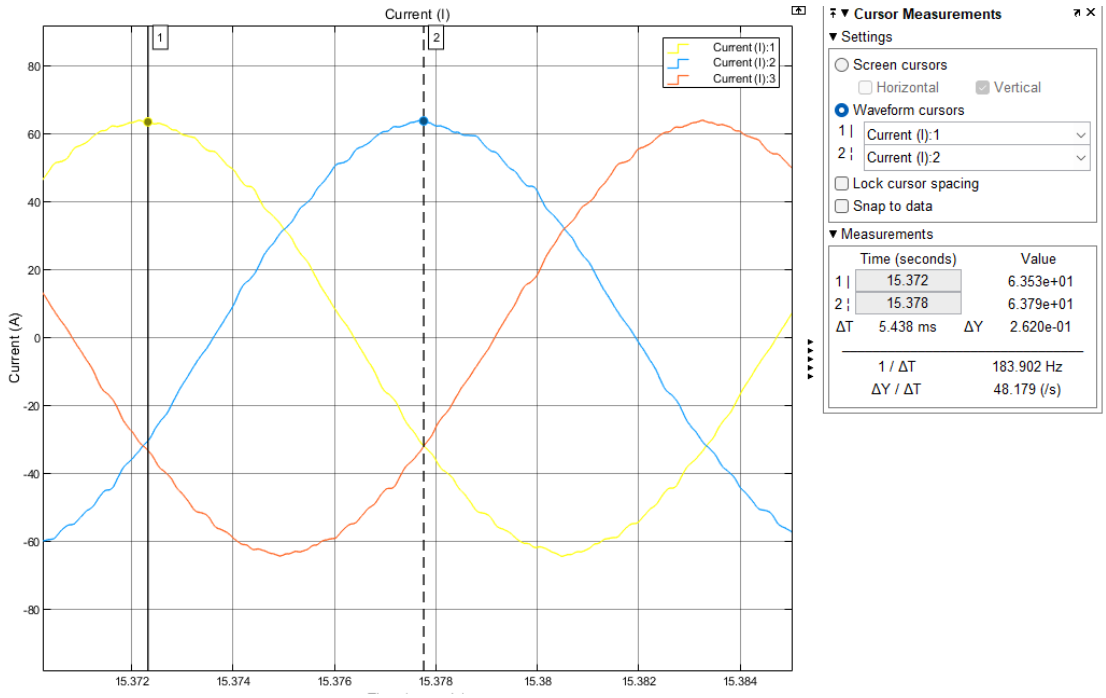

Figure 35: Sample Current Waveform for Wind-DFIG-PV Model (Phases 1 and 2)

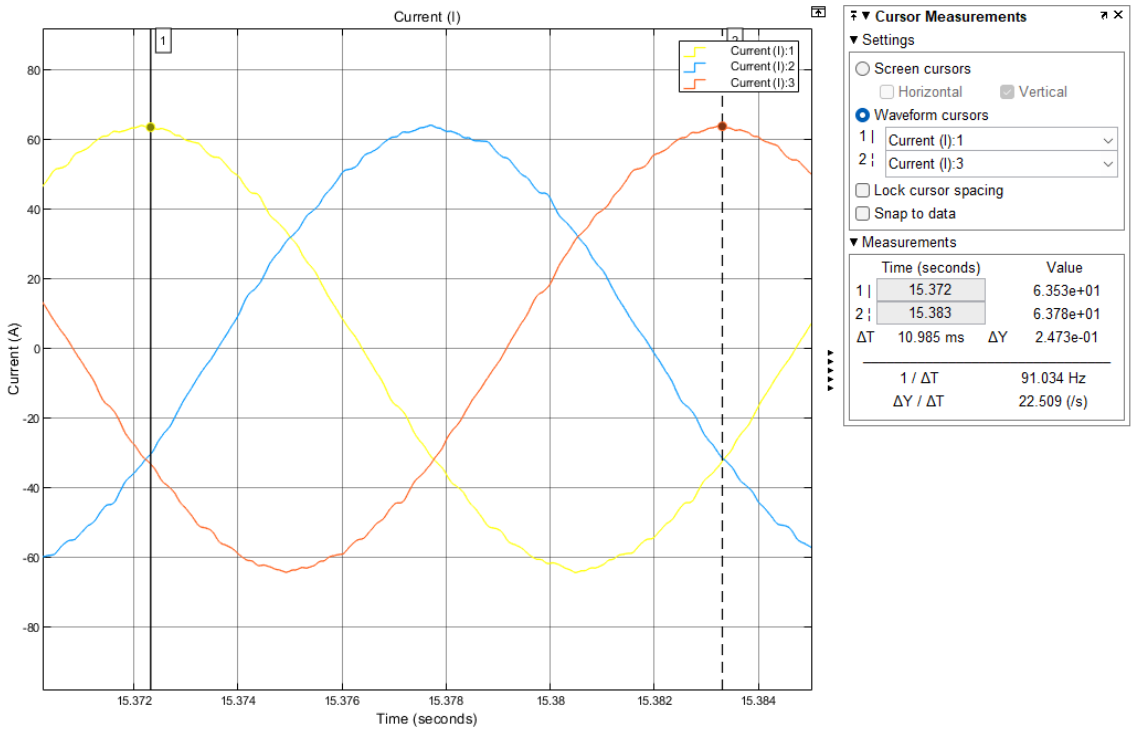

Figure 36: Sample Current Waveform for Wind-DFIG-PV (Phases 1 and 3)

In order to extract harmonics, an FFT analysis was carried out on the data procured from the scope. The MATLAB command line was used to extract harmonic information. The employed FFT window consists of five cycles that extract the samples from voltage and current waveforms. The FFT samples were extracted for 720 hours (30 days), for a total of 7,200 samples, with 10 samples logged per hour for both current and voltage waveforms. The following harmonic parameters were extracted from the simulated signals:

1- Total harmonic distortion for each sample.

2- Magnitudes of 3^{rd}, 5^{th}, 7^{th}, 9^{th}, 11^{th} and 13^{th} harmonic component.

4.3 Voltage Harmonics Results for Generator Models

The total harmonic distortion extracted for both generator models is presented in Figures 37, 38, and 39, as shown below:

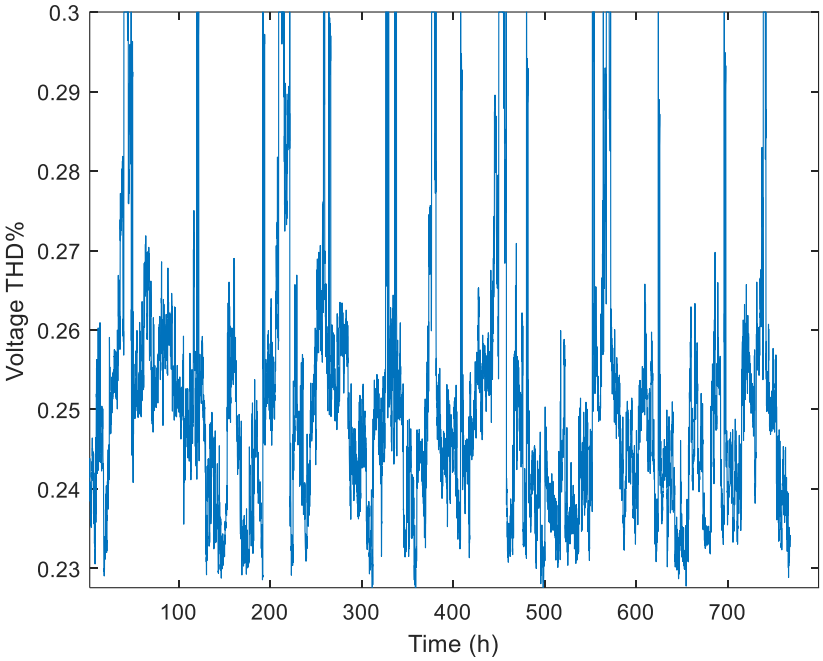

Figure 37: THD for Wind-DFIG-PV Model

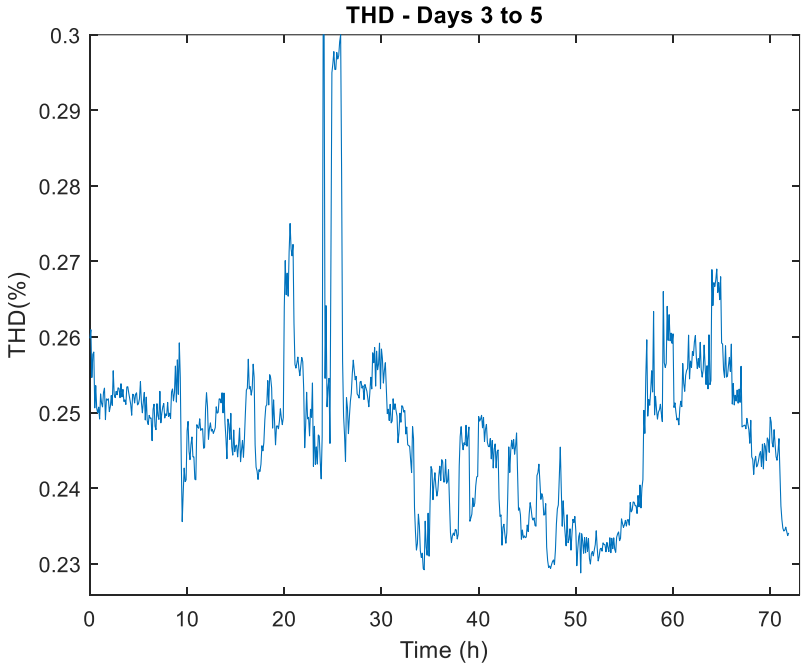

Figure 38: THD for Wind-DFIG-PV Model, Days 3 to 5

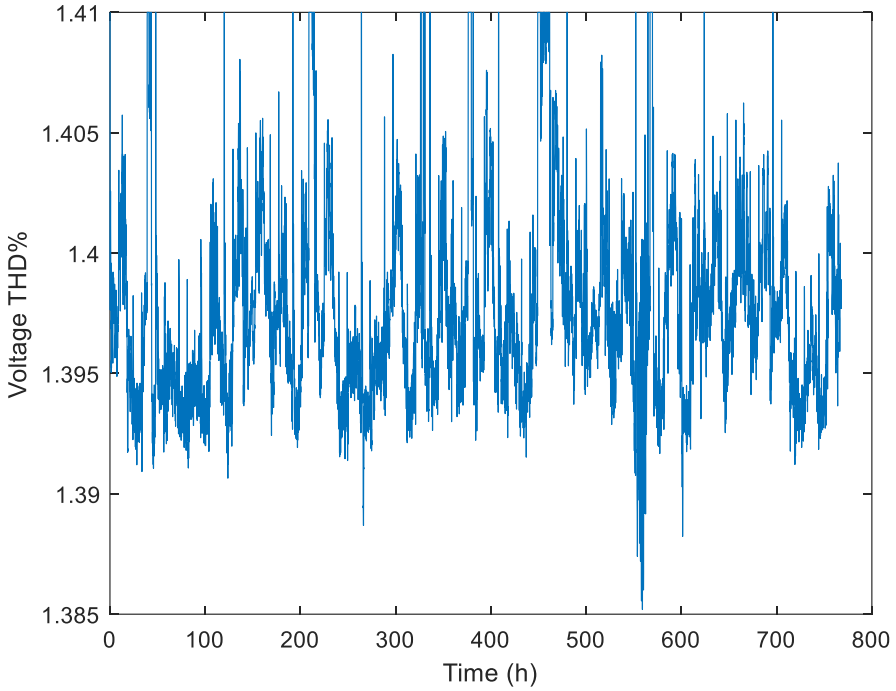

Figure 39: THD for Wind-PMSG-PV Model

Figures 37 and 39 present the THD plot for all 30 days. Figure 38 shows the plot for days 3 to 5 in order to better visualize the plot. It should be noted that the high peaks are not spikes but are the resultant high THD. This can be caused by the nonlinear nature of the grid and variations in the input parameters of the generator, i.e., wind speed and solar irradiation. Tables 9 and 10 present the statistical parameters for the simulated data.

Table 9: Statistical Parameters for Wind-DFIG-PV Generator Voltage Harmonics

Wind-DFIG-PV Model Statistics					
	THD	**h5**	**h7**	**h11**	**h13**
Mean	0.253%	3.670 V	3.792 V	7.276 V	9.988 V
Median	0.247%	1.963 V	3.767 V	6.972 V	9.284 V
Min	0.226%	0.027 V	0.025 V	0.173 V	0.054 V
Max	0.30%	40.687 V	12.539 V	30.332 V	46.67 V
Std. Deviation	0.029%	7.007 V	1.748 V	3.993 V	5.9 V

Table 10: Statistical Parameters for Wind-PMSG-PV Generator Voltage Harmonics

Wind-PMSG-PV Model Statistics					
	THD	**h5**	**h7**	**h11**	**h13**
Mean	1.398%	3.422 V	5.978 V	8.362 V	14.879 V
Median	1.397%	2.442 V	6.092 V	8.884 V	14.274 V
Min	1.385%	0.007 V	0.261 V	0.099 V	0.437 V
Max	1.492%	40.286 V	11.733 V	26.62 V	43.429 V
Std. Deviation	0.005%	5.303 V	1.814 V	3.809 V	5.675 V

The statistical indices show the distribution of simulated THD and 5^{th}, 7^{th}, 11^{th}, and 13^{th} harmonic amplitudes for the two generator models. It can be observed that the 5^{th}, 7^{th}, 11^{th}, and 13^{th} harmonics denoted by h5, h7, h11, and h13, appear to be dominant as compared to the other harmonics. It also can be observed that the voltage harmonics presented have different ranges of values. For Wind-DFIG-PV, the THDV ranges between 0.226% and 0.30%, with a mean of 0.253%, a median of 0.247%, and a standard deviation of 0.029%. For Wind-PMSG-PV, the THDV ranges between 1.385% and 1.492%, with a mean of 1.398%, a median of 1.397%, and a standard deviation of 0.005%.

Furthermore, for the individual harmonics, harmonic h13 has the largest amplitude range (0.054V to 46.67V) for the Wind-DFIG-PV model, whereas it is 0.437V to 43.429V for the Wind-PMSG-PV model with the highest mean, median, and standard deviation. It can also be concluded that h7, h11, and h13 are dominant harmonics for both generator models. The high standard deviation for THD, h7, h11, and h13 depicts the high dispersion of simulated data and these parameters will be forecasted.

4.4 Current Harmonics Results for Generator Models

In this section, the current total demand distortion results will be presented for both generator models, as shown in Figures 40, 41, and 42:

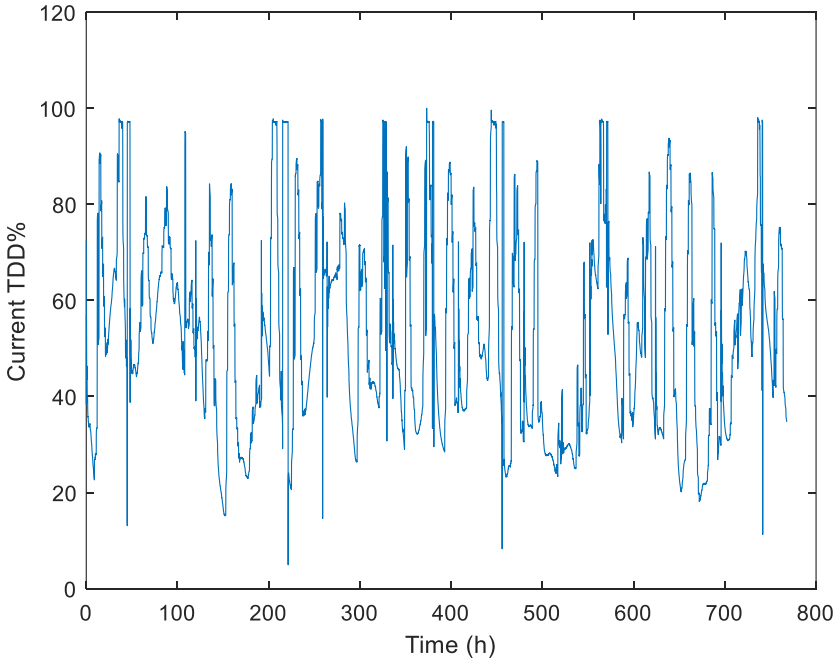

Figure 40: TDD for Wind-DFIG-PV Model

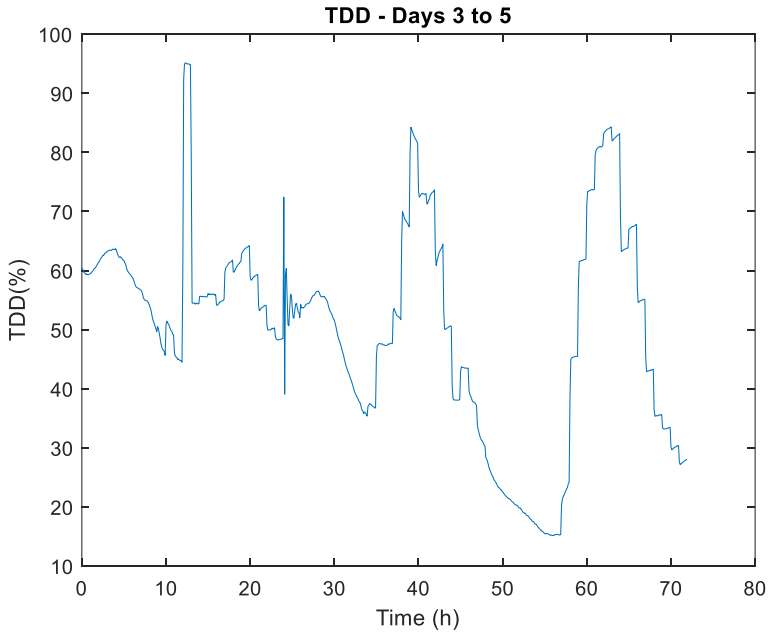

Figure 41: TDD for Wind-DFIG-PV Model, Days 3 to 5

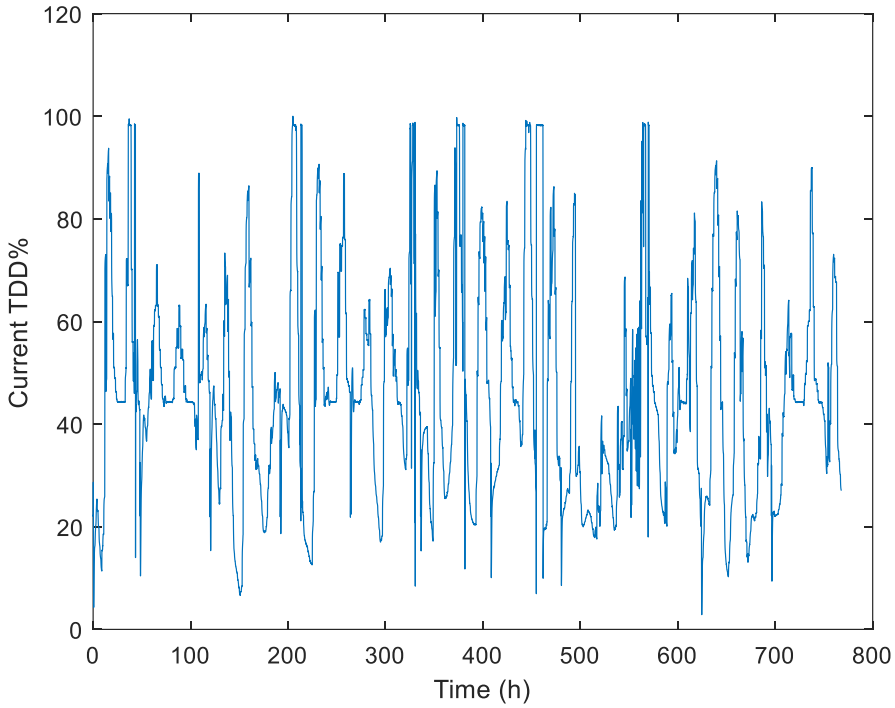

Figure 42: TDD for Wind-PMSG-PV Model

Figures 40 and 42 present the TDD plot for all 30 days. Figure 41 shows a magnified version of the plot of days 3 to 5. The high peaks are the result of the nonlinear nature of the grid and the variations in wind speed and solar irradiation. To analyse the dominant harmonics for the current waveform, the statistical indices for the results are presented in Tables 11 and 12 below:

Table 11: Statistical Parameters for Wind-DFIG-PV Generator Current Harmonics

	TDD	h5	h7	h11	h13
Mean	53.126%	0.309 A	0.230 A	0.029 A	0.323 A
Median	51.091%	0.2 A	0.228 A	0.267 A	0.300 A
Min	4.949%	0.003 A	0.002 A	0.006 A	0.003 A
Max	100%	3.439 A	0.748 A	1.158 A	1.516 A
Std. Deviation	20.706%	0.589 A	0.107 A	0.152 A	0.1913 A

Table 12: Statistical Parameters for Wind-PMSG-PV Generator Current Harmonics

	TDD	h5	h7	h11	h13
Mean	46.325%	0.288 A	0.359 A	0.320 A	0.482 A
Median	44.29%	0.205 A	0.367 A	0.339 A	0.463 A
Min	2.865%	0.002 A	0.006 A	0.004 A	0.018 A
Max	100%	3.421 A	0.703 A	1.021 A	1.406 A
Std. Deviation	21.408%	0.446 A	0.109 A	0.146 A	0.183 A

Tables 11 and 12 provide a summary of the current harmonics for the two models. As shown, the 5^{th}, 7^{th}, 11^{th}, and 13^{th} harmonics are dominant compared to the other harmonics. The spikes observed in Figures 39 and 40 indicate spikes in the current total harmonic distortion of the simulation of the generator model, caused by a sudden variation in input variables (i.e., solar irradiation and wind speed). For Wind-DFIG-PV, the current THD varies between 4.949% and 100% for the Wind-DFIG-PV model and 2.865% and 100% for the Wind-PMSG-PV model. For the current waveform, h7, h11, and h13 are the dominant harmonics for both generators.

4.5 Utilization of Artificial Neural Networks

The authors in [36], [43], and [46] applied ANN models to forecast harmonics. Three neural networks are chosen from among the methods utilized in these papers to forecast and compare. The data used to forecast is the same 30-day data employed in this thesis, generated by the simulation of two hybrid models. The five inputs used are wind speed, solar irradiation, and one hour/one day/two days before the observation of the forecasted parameters. Each version of ANN has a first hidden layer with ten nodes and a second layer with twenty nodes.

4.6 Utilization of the Long Short-Term Memory Network

The authors in [41] and [45] utilize the deep-learning LSTM method to forecast harmonics. The same simulated data and four inputs are used to generate forecasting for THD, h7, h11, and h13 for voltage and current for the two generator models. The LSTM utilized consists of five sequence input layers, 100 LSTM layers, one fully connected layer, and a regression layer as an output layer. Since there are five inputs, the size of the input layer is set to five. The 100 hidden layers of the LSTM layer are utilized to execute additive interactions and learn long-term relationships between sequence and time series data. The forecast is generated in MATLAB and presented in sections 4.8 and 4.9 for further analysis and comparison with the hybrid models used in this thesis.

4.7 Utilization of an Adaptive Neuro-Fuzzy Inference System

The study in [42] employs ANFIS architecture to forecast voltage and current THD/TDD. In order to draw comparisons, ANFIS is utilized with the data used in this thesis with the five inputs delineated in previous sections. Subtractive clustering is used to optimize the training process. THD/TDD, h7, h11, and h13 are forecasted. The results produced from the ANFIS technique are presented in sections 4.8 and 4.9 to draw a comparison with the models proposed in this thesis.

4.8 Harmonics Forecasting Results and Analysis – Wind-DFIG-PV

4.8.1 Voltage Harmonics

The actual versus forecast curves for all eight proposed hybrid models for wind DFIG-PV are presented in Figures 43, 44, 45, and 46, along with the forecasting result curves of all the forecasting techniques found in the literature, i.e., ANN – CRNNL, ANN – CRNNG, ANN – CRNNGL LSTM, and ANFIS. A total of four harmonic variables are forecasted, namely, THD followed by the dominant individual harmonics 7th (h7), 11th (h11), and 13th (h13).

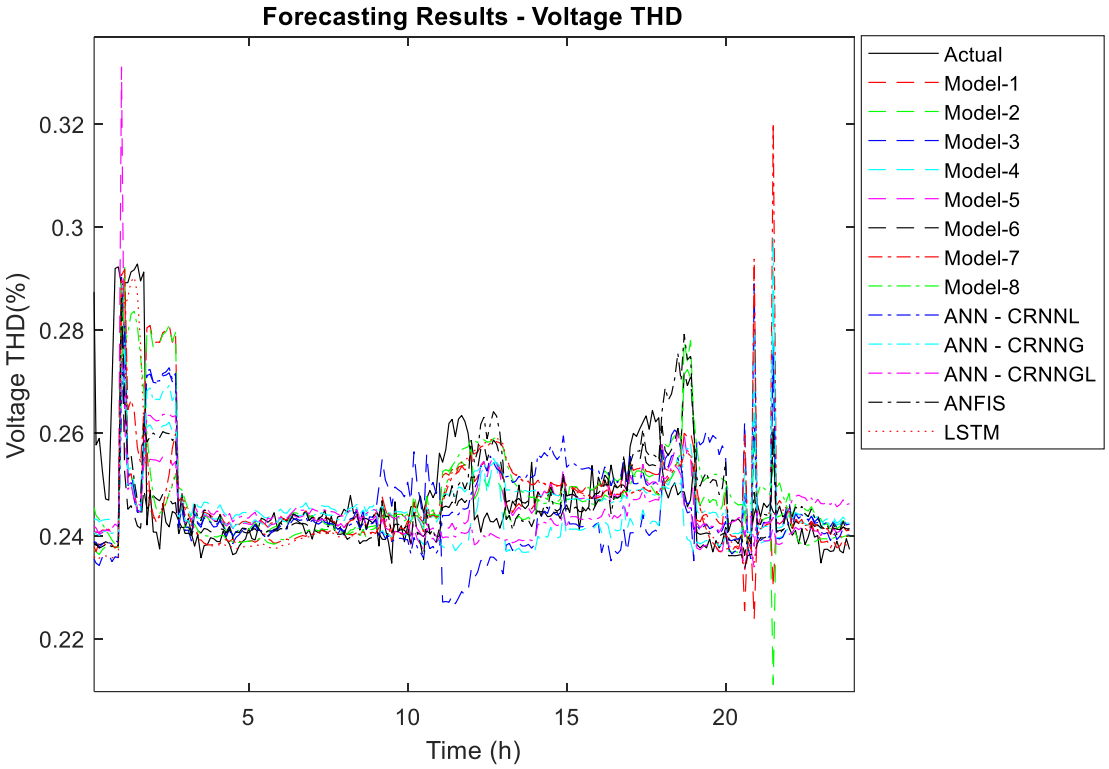

Figure 43: THDV – Actual vs Forecast curves for Wind-DFIG-PV

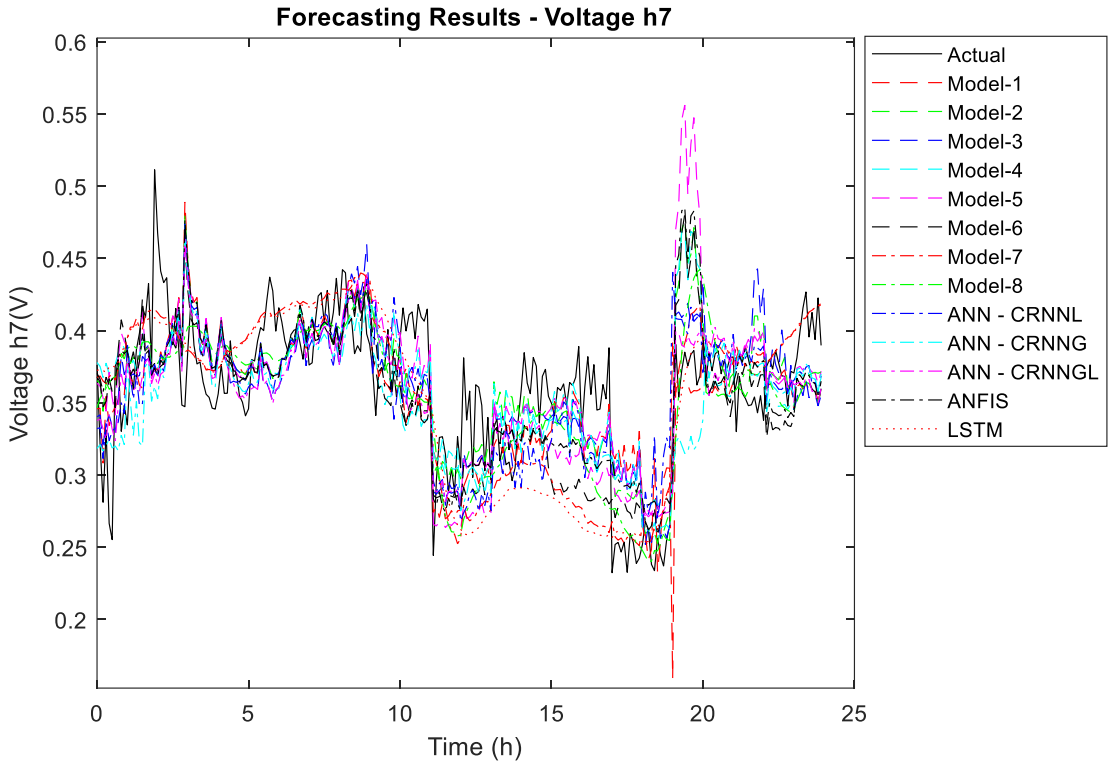

Figure 44: Voltage 7th Harmonic – Actual vs Forecast Curves for Wind-DFIG-PV

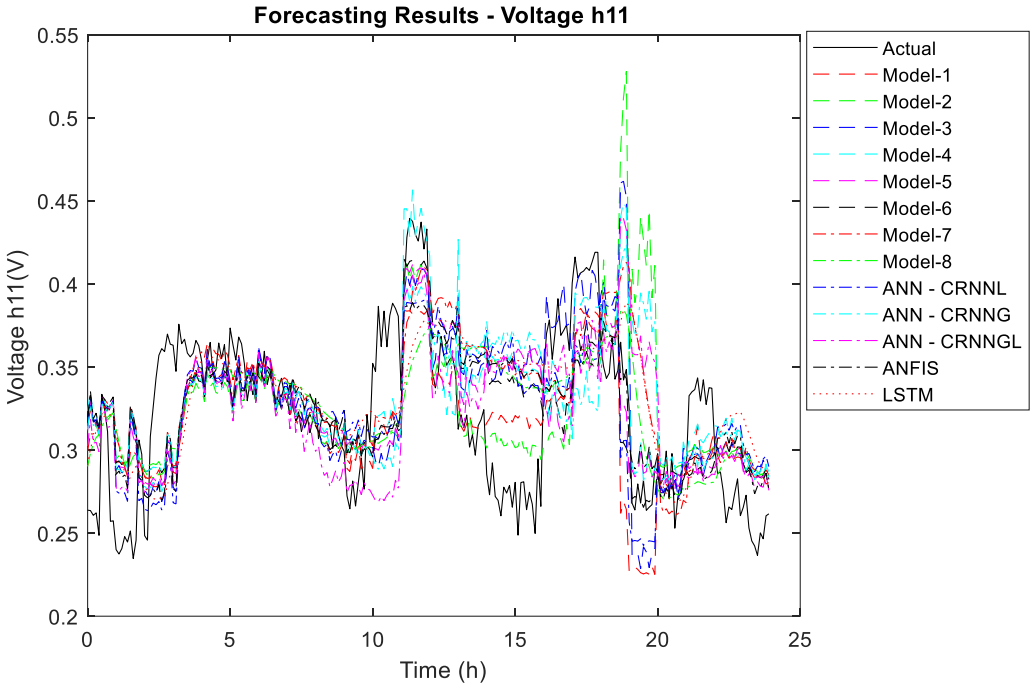

Figure 45: Voltage 11th Harmonic – Actual vs Forecast Curves for Wind-DFIG-PV

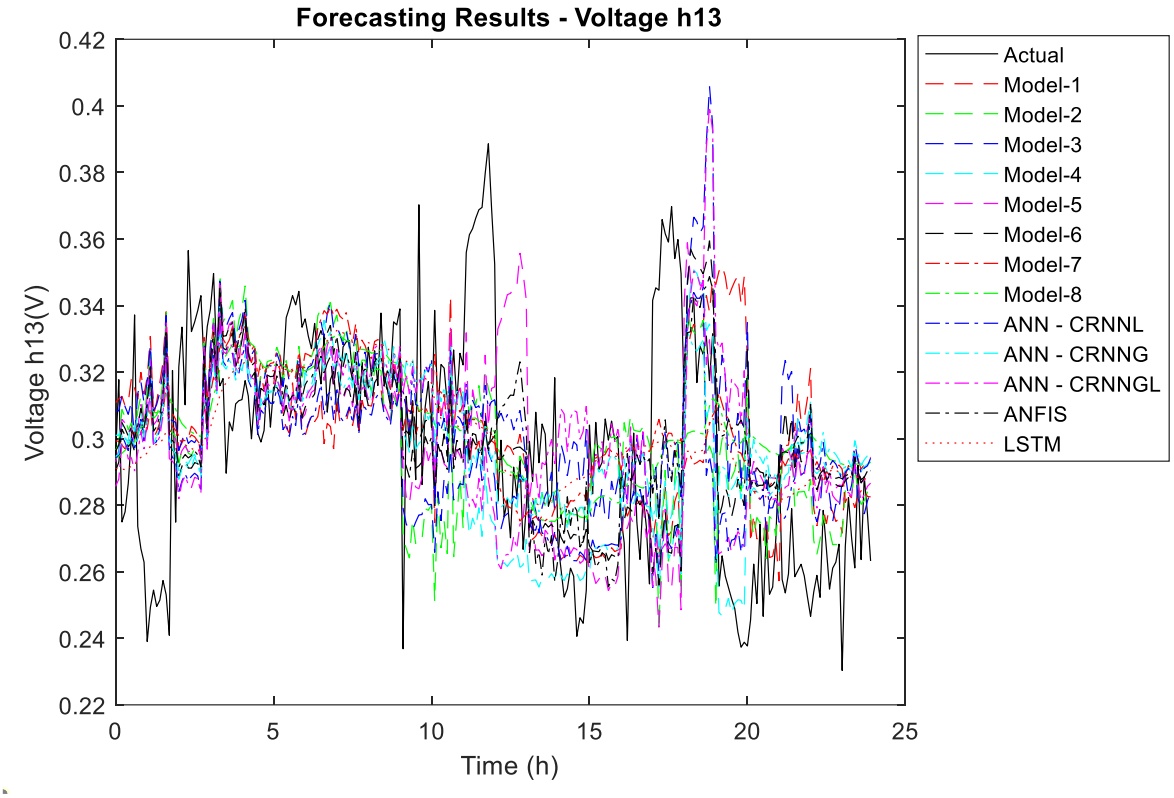

Figure 46: Voltage 13th Harmonic – Actual vs Forecast Curves for Wind-DFIG-PV

To further analyse the error profile and accuracy of these models and validate results, Table 13 presents the metrics calculated (RMSE and MAE) for the eight proposed models in this thesis and the forecasting techniques employed by other researchers in the literature. From Table 13, it can be observed that model-8 produces the best results with the lowest RMSE and MAE for THD (0.0287 and 0.0076), h7 (0.0372 and 0.03), and h13 (0.0311 and 0.0250) forecast, while model-7 produces the second-best results for THD (0.0295 and 0.0077) and h13 (0.0318 and 0.0256), and model-2 for h7 (0.0383 and 0.0304), respectively. For h11, model-1 produces the best result with the lowest THD (0.0379) and MAE (0.0307), whereas model-8 produces the second-best results, with an RMSE of 0.0396 and a MAE of 0.0324. It is obvious, therefore, that model-8 is the most accurate forecasting model for all the voltage

harmonic forecasting parameters, as it produces the best performance for THD, h7, and h13 and the second-best results for h11.

Table 13: Forecasting Results Comparison Voltage Harmonics – Wind-DFIG-PV

Forecasting Models	Voltage Harmonics								Reference / Publication
	THD		h7		h11		h13		
	RMSE	MAE	RMSE	MAE	RMSE	MAE	RMSE	MAE	
Model-1 (CRNNL-ANFIS)	0.0301	0.0084	0.0404	0.0320	**0.0379**	**0.0307**	0.0341	0.0261	Proposed Hybrid Model
Model-2 (CRNNG-ANFIS)	0.0304	0.0093	0.0383	0.0304	0.0443	0.0367	0.0350	0.0272	Proposed Hybrid Model
Model-3 (CRNNGL-ANFIS)	0.0301	0.0089	0.0386	0.0311	0.0429	0.0336	0.0322	0.0262	Proposed Hybrid Model
Model-4 (ANFIS-CRNNL)	0.0304	0.0089	0.0413	0.0331	0.0415	0.0325	0.0353	0.0289	Proposed Hybrid Model
Model-5 (ANFIS-CRNNG)	0.0301	0.0088	0.0387	0.0308	0.0436	0.0348	0.0356	0.0277	Proposed Hybrid Model
Model-6 (ANFIS-CRNNGL)	0.0302	0.0087	0.0383	0.0305	0.0435	0.0356	0.0329	0.0265	Proposed Hybrid Model
Model-7 (LSTM-ANFIS)	0.0295	0.0077	0.0403	0.0328	0.0428	0.0346	0.0318	0.0256	Proposed Hybrid Model
Model-8 (ANFIS-LSTM)	**0.0287**	**0.0076**	**0.0372**	**0.0300**	0.0396	0.0324	**0.0311**	**0.0250**	Proposed Hybrid Model
LSTM	*0.0305*	*0.0095*	0.0459	0.0344	0.0470	0.0380	*0.0368*	*0.0273*	[41] & [45]
ANFIS	0.0306	0.0099	*0.0423*	*0.0342*	*0.0448*	*0.0371*	0.0378	0.0297	[42]
ANN – CRNNL	0.0310	0.0104	0.0427	0.0329	0.0489	0.0357	0.0396	0.0314	[36], [43] & [46]
ANN – CRNNG	0.0307	0.0101	0.0481	0.0368	0.0526	0.0417	0.0394	0.0296	[36], [43] & [46]
ANN – CRNNGL	0.0321	0.0121	0.0442	0.0360	0.0473	0.0370	0.0388	0.0294	[36], [43] & [46]

- ***Yellow Highlight*** denotes the best performing model
- ***Blue Highlight*** denotes the second-best performing model

Each forecasting parameter has its own dataset, and each harmonic parameter is forecasted separately. THD has its own training and testing dataset, with the forecasting model simulated to produce forecast results for THD. A 30-day dataset containing the

training parameters for THD are used to train the model and the model is tested to produce a THD forecast. The same process is repeated for h7, h11, and h13, but the data for each parameter are different. Still, in most cases, model-8 (ANFIS-LSTM) is the best. In those few cases when model-8 is not the best, it is second best.

The results produced by forecasting techniques used in the literature are also presented in Table 13. By contrasting the results with CRNNL, CRNNG, CRNNGL, LSTM, and ANFIS, we can easily see the benefit of utilizing a hybrid technique. For THD and h13, LSTM produces the most accurate forecasting result (RMSE – 0.0301 for THD and 0.0368 for h13) compared to all other forecasting techniques. Moreover, for h7 and h11, ANFIS appears to be the most accurate individual forecasting model, with an RMSE of 0.0423 for h7 and 0.0448 for h11, respectively. Even though LSTM and ANFIS perform best among the individual models tested, the results produced by the proposed hybrid models surpass the accuracy of any other individual model. Additionally, model-7 (LSTM-ANFIS) and model-8 (ANFIS-LSTM) manifest the best forecasting results, with model-8 performing best overall.

The results indicate that the hybrid models proposed in this work produce better results than any of the individual forecasting models that were used by other authors in literature. Our analysis of the results clearly shows that model-8 performs the best among all tested models. Furthermore, LSTM (THD and h13) and ANFIS (h7 and h11) are shown to be better performing models among the individual forecasting techniques. Table 14 presents the percentage improvements offered by model-8 compared to the singular models in the literature, as tested in this thesis. The results validate the model-8 approach and illustrate the benefit of utilizing a hybrid model over singular models.

Table 14: Best Forecasting Model for Voltage Harmonics – Wind-DFIG-PV

Model / Forecasting Parameter	RMSE	RMSE (% Improvement)				
		LSTM	ANFIS	CRNNL	CRNNG	CRNNGL
Model-8 (THD)	0.0287	0.0301 ***(4.46%)***	0.0305 ***(5.9%)***	0.0301 ***(7.48%)***	0.0307 ***(6.56%)***	0.0321 ***(10.63%)***
Model-8 (h7)	0.0372	0.0459 ***(18.97%)***	0.0423 ***(12.03%)***	0.0427 ***(12.98%)***	0.0481 ***(22.67%)***	0.0442 ***(15.96%)***
Model-8 (h11)	0.0396	0.0470 ***(15.71%)***	0.0448 ***(11.53%)***	0.0489 ***(18.95%)***	0.0526 ***(24.65%)***	0.0473 ***(16.35%)***
Model-8 (h13)	0.0311	0.0368 ***(15.51%)***	0.0378 ***(17.77%)***	0.0396 ***(21.5%)***	0.0394 ***(21.13%)***	0.388 ***(19.91%)***

As shown in Table 14, model-8 offers improvements over all the individual models. For instance, for THD and h13, model-8 offer improvements of 4.46% and 15.51% over LSTM forecasting, respectively. Similarly, for h7 and h11, model-8 offers 12.03% and 11.53% improvements, respectively, over ANFIS, which is the best performing model for h7 and h11. Likewise, the percentage improvements demonstrated by model-8 over all the other models is evident and establishes the superiority of the proposed hybrid models over the forecasting techniques used in the literature.

4.8.2 Current Harmonics

This section presents the actual versus forecasted curves for the individual forecasting methods in the literature as well as the eight proposed hybrid models used to predict the TDD, h7, h11, and h13 harmonics. Figures 47, 48, 49, and 50 show the forecast curves, and Table 15 summarises the performance of each model.

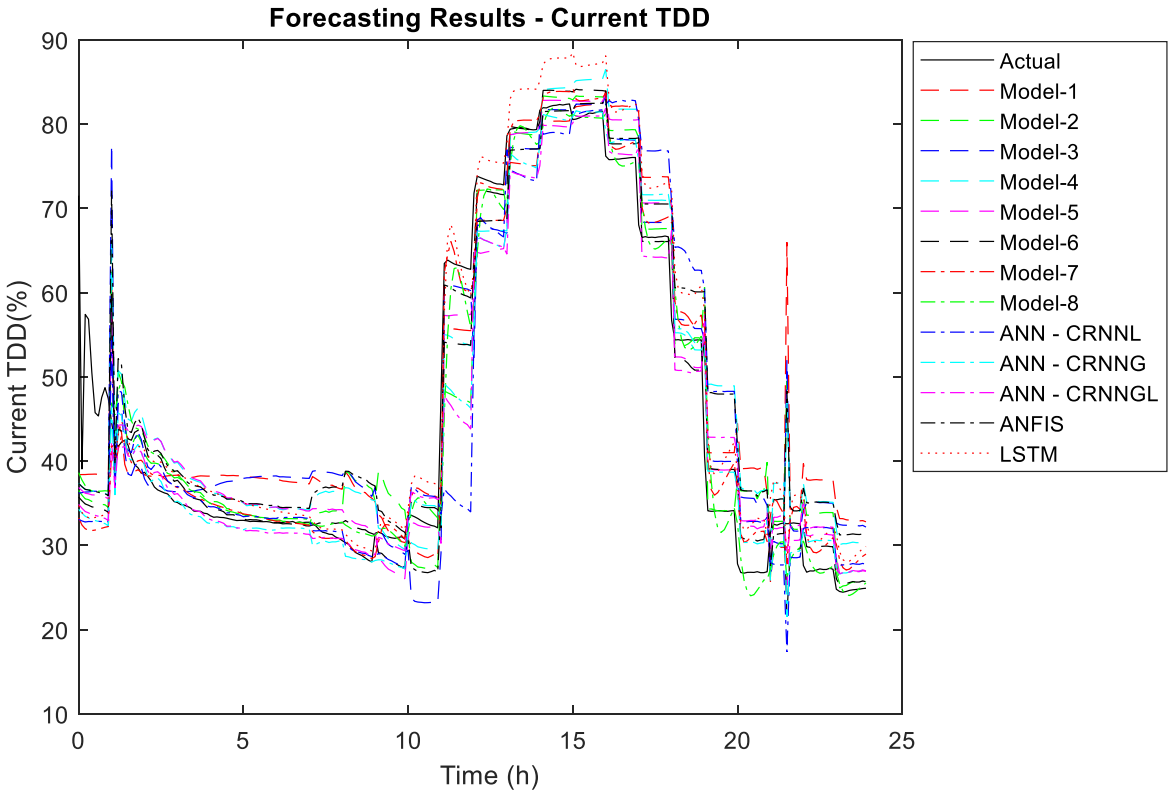

Figure 47: TDD – Actual vs Forecast Curves for Wind-DFIG-PV

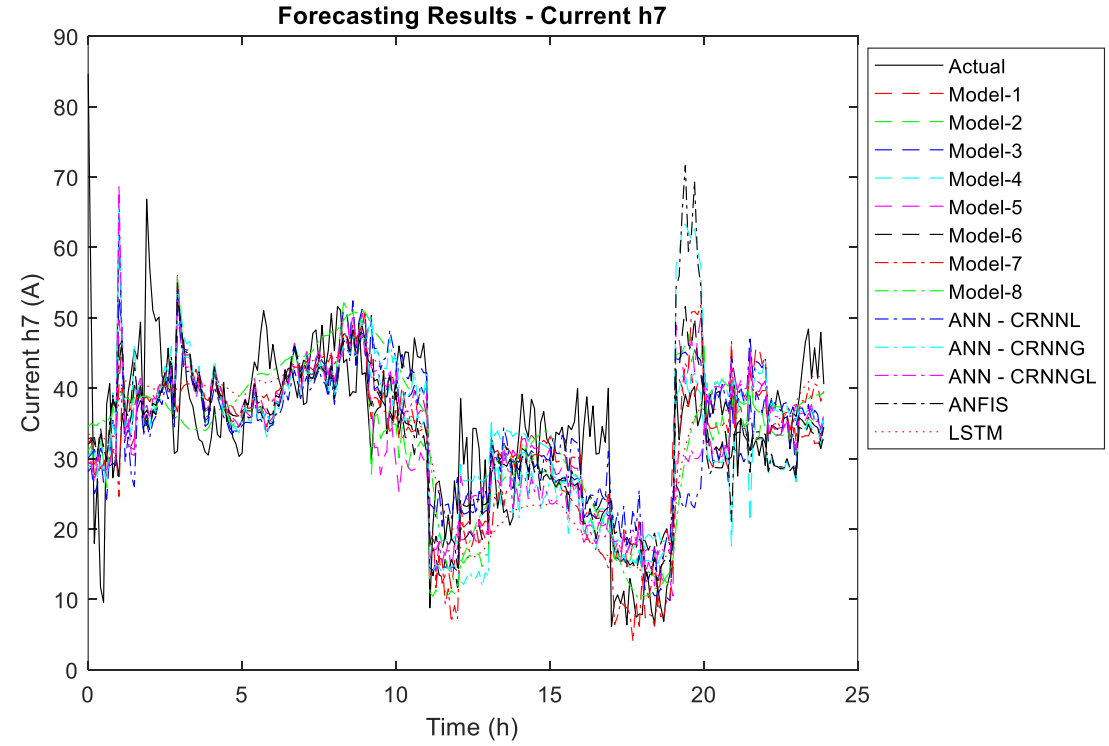

Figure 48: Current 7th Harmonic – Actual vs Forecast Curves for Wind-DFIG-PV

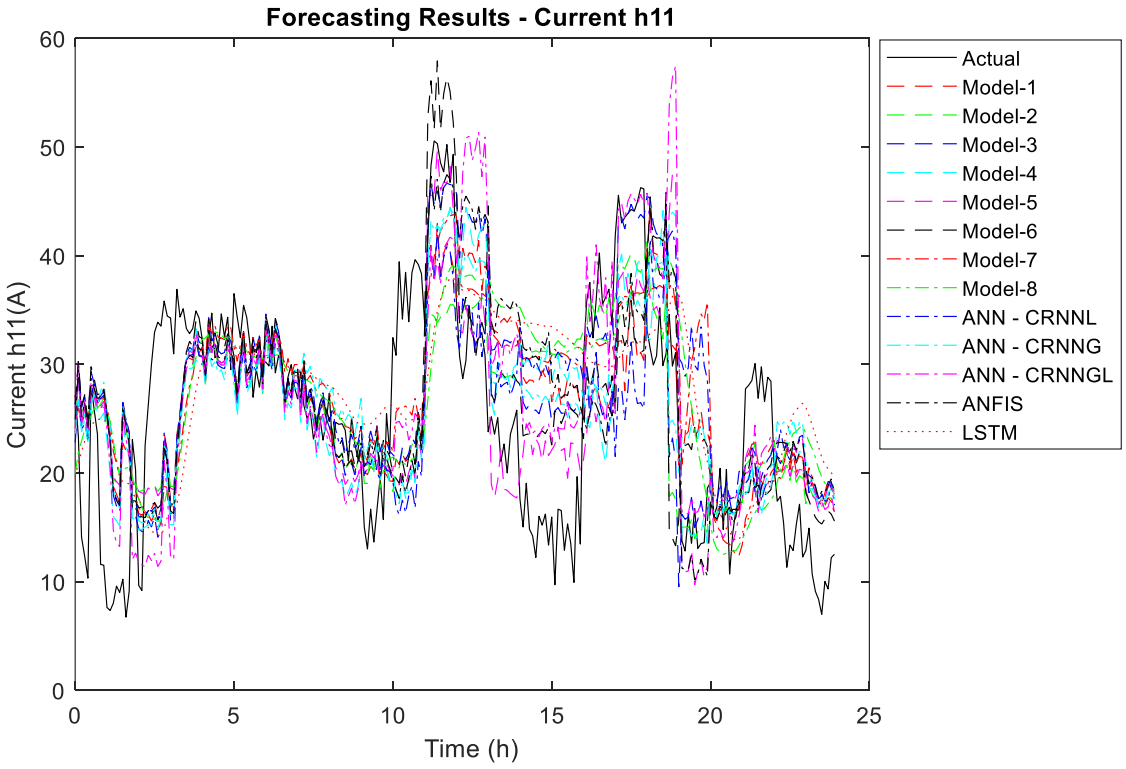

Figure 49: Current 11th Harmonic – Actual vs Forecast Curves for Wind-DFIG-PV

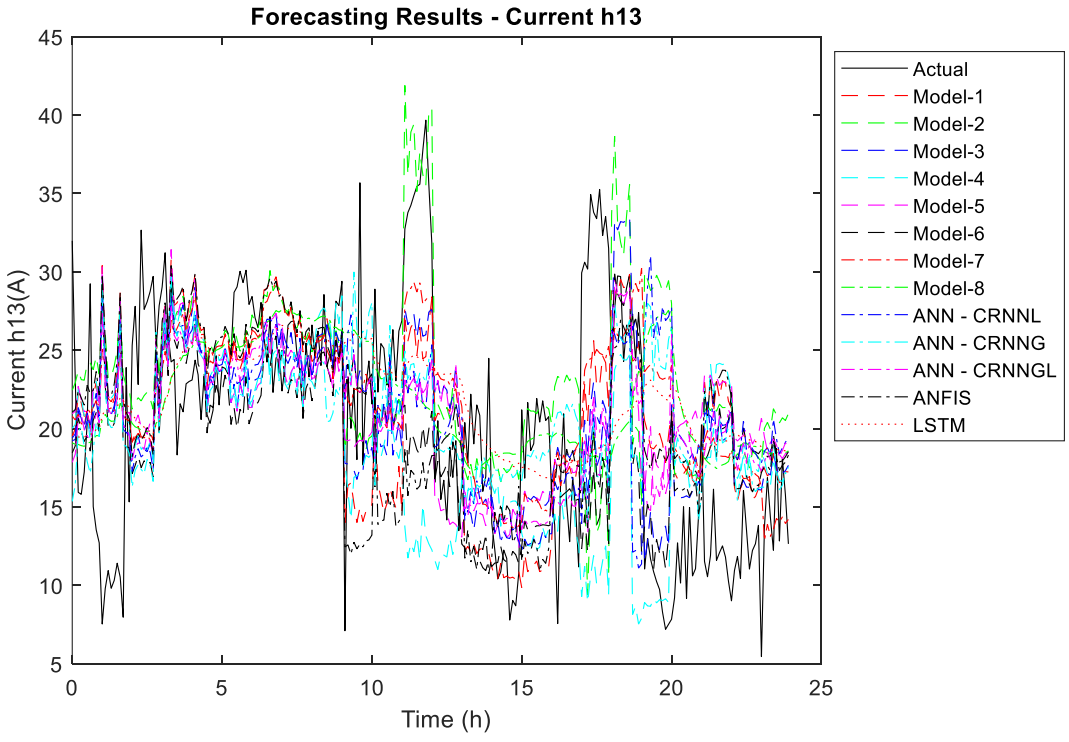

Figure 50: Current 13th Harmonic – Actual vs Forecast Curves for Wind-DFIG-PV

Model-8 fits the actual curve better than the other models for TDD and h7 forecasts, as seen in Figures 48 and 50. Table 15 shows that model-8 has the lowest RMSE and MAE recorded for TDD (4.6585 and 2.6165) and h7 (8.2918 and 5.9852), respectively. Model-8 is also the second-best performing model for h11 and h13. Model-6 produced the lowest RMSE and MAE (7.7588 and 6.1934, respectively) for h11, while model-7 had the lowest RMSE amd MAE for h11 (6.4145 and 5.2047, respectively).

For individual models, LSTM produced the best results for all current harmonic forecasting parameters. Moreover, like the results in voltage harmonics, all the hybrid models outperformed the individual models in accuracy, with the exception of TDD, where LSTM, with an RMSE of 6.5412, produced better results than model-1 (RMSE – 6.922). Other than for this case, the results clearly showed the advantage of using hybrid techniques over individual methods.

Table 15: Forecasting Results Comparison of Current Harmonics – Wind-DFIG-PV

Forecasting Models	Current Harmonics								Reference / Publication
	TDD		h7		h11		h13		
	RMSE	MAE	RMSE	MAE	RMSE	MAE	RMSE	MAE	
Model-1 (CRNNL-ANFIS)	6.9220	5.1232	8.9658	6.9100	9.0882	7.5633	7.1648	5.8910	Proposed Hybrid Model
Model-2 (CRNNG-ANFIS)	6.1819	3.8005	9.3928	7.4610	8.7084	6.7708	7.5974	5.9389	Proposed Hybrid Model
Model-3 (CRNNGL-ANFIS)	6.0481	4.4844	8.7334	6.5946	9.1029	7.1864	6.8495	5.4993	Proposed Hybrid Model
Model-4 (ANFIS-CRNNL)	6.5231	4.0152	9.5348	7.1449	9.1466	7.4102	7.6811	6.0565	Proposed Hybrid Model
Model-5 (ANFIS-CRNNG)	5.6288	4.1031	9.3329	7.2471	8.6930	7.0459	7.3543	5.8698	Proposed Hybrid Model
Model-6 (ANFIS-CRNNGL)	5.2447	3.2106	8.9654	6.5784	**7.7588**	**6.1934**	7.1701	5.8538	Proposed Hybrid Model
Model-7 (LSTM-ANFIS)	5.0956	2.7589	8.9003	6.6133	8.8975	7.4692	**6.4145**	**5.2047**	Proposed Hybrid Model
Model-8 (ANFIS-LSTM)	**4.6585**	**2.6165**	**8.2918**	**5.9852**	8.4149	6.7443	6.5160	5.2834	Proposed Hybrid Model
LSTM	*6.5412*	*4.1523*	*9.5897*	*7.3695*	*9.2142*	*7.5290*	*7.6975*	*5.8972*	[41] & [45]
ANFIS	7.2423	5.7811	9.9177	7.6614	9.5265	7.8082	8.3274	6.6013	[42]
ANN – CRNNL	8.8514	5.7865	10.0224	7.7198	10.1251	8.1193	7.9709	6.2420	[36], [43] & [46]
ANN – CRNNG	7.0190	5.3318	9.8278	7.4801	10.0475	8.2530	9.0973	6.7163	[36], [43] & [46]
ANN - CRNNGL	7.1629	5.5188	9.7003	7.3899	10.4892	8.6382	8.1300	6.2536	[36], [43] & [46]

- ***Yellow Highlight*** denotes the best performing model
- ***Blue Highlight*** denotes the second-best performing model

As previously mentioned, each forecasting parameter is associated with a dedicated dataset, and the harmonic parameters are individually predicted. In most cases, model-8 (ANFIS-LSTM) emerges as the top-performing choice, but there are a few instances where a different model outperforms it. Nevertheless, it is important to note that even when model-8 is not the best-performing option, it consistently ranks as

the second-best choice. Further, it can be shown that after model-8, model-7 was proven to be effective with accurate forecasting results. Model-7 was the best performing model for h13 and the second-best for TDD. It was also significantly accurate for forecasting h7 and h11 compared to the other tested models.

From these results, it may be concluded that all eight proposed models predicted current total harmonic distortion correctly and produced improved results in comparison to the individual models adopted in the literature, showing relatively low RMSE and MAE. Model-8 was the best performing model overall. To further analyse the results, Table 16 presents a percentage improvement of model-8 over individual methods.

Table 16: Best Forecasting Model for Current Harmonics – Wind-DFIG-PV

Model / Forecasting Parameter	RMSE	RMSE (% Improvement)				
		LSTM	ANFIS	CRNNL	CRNNG	CRNNGL
Model-8 (TDD)	4.6585	6.5412 ***(28.78%)***	7.2423 ***(35.68%)***	8.8514 ***(47.37%)***	7.019 ***(33.63%)***	7.1629 ***(34.96%)***
Model-8 (h7)	8.2918	9.5897 ***(13.53%)***	9.9177 ***(16.39%)***	10.0224 ***(17.27%)***	9.8278 ***(15.63%)***	9.7003 ***(14.52%)***
Model-8 (h11)	8.4149	9.2142 ***(8.67%)***	9.5265 ***(11.67%)***	10.1251 ***(16.89%)***	10.0475 ***(16.25%)***	10.4892 ***(19.78%)***
Model-8 (h13)	6.5160	7.6975 ***(15.35%)***	8.3274 ***(21.75%)***	7.9709 ***(18.25%)***	9.0973 ***(28.37%)***	8.13 ***(19.85%)***

Again, model-8 has been shown to produce superior results over all other models, and LSTM produces the best forecast compared to all individual models. At the same time, model-8 offers percentage improvements over LSTM forecasts of 28.78%, 13.53%, 8.67%, and 15.35% for THD, h7, h11, and h13 respectively. Likewise, the superior performance of model-8 over all other models is evident, clearly showing that the proposed hybrid models are superior to the forecasting techniques used in the literature.

4.9 Harmonics Forecasting Results – Wind-PMSG-PV Model

4.9.1 Voltage Harmonics

The actual versus predicted curves for all eight of the proposed hybrid models and the individual forecasting methods in the literature for the Wind-PMSG-PV generator model are shown in Figures 51, 52, 53, a nd 54 for Voltage Total Harmonic Distortion (THD) and 7^{th}, 11^{th}, and 13^{th} voltage harmonics (h7, h11, and h13). The forecast results are followed by Table 17, in which the error profile for each forecast made for each variable is presented.

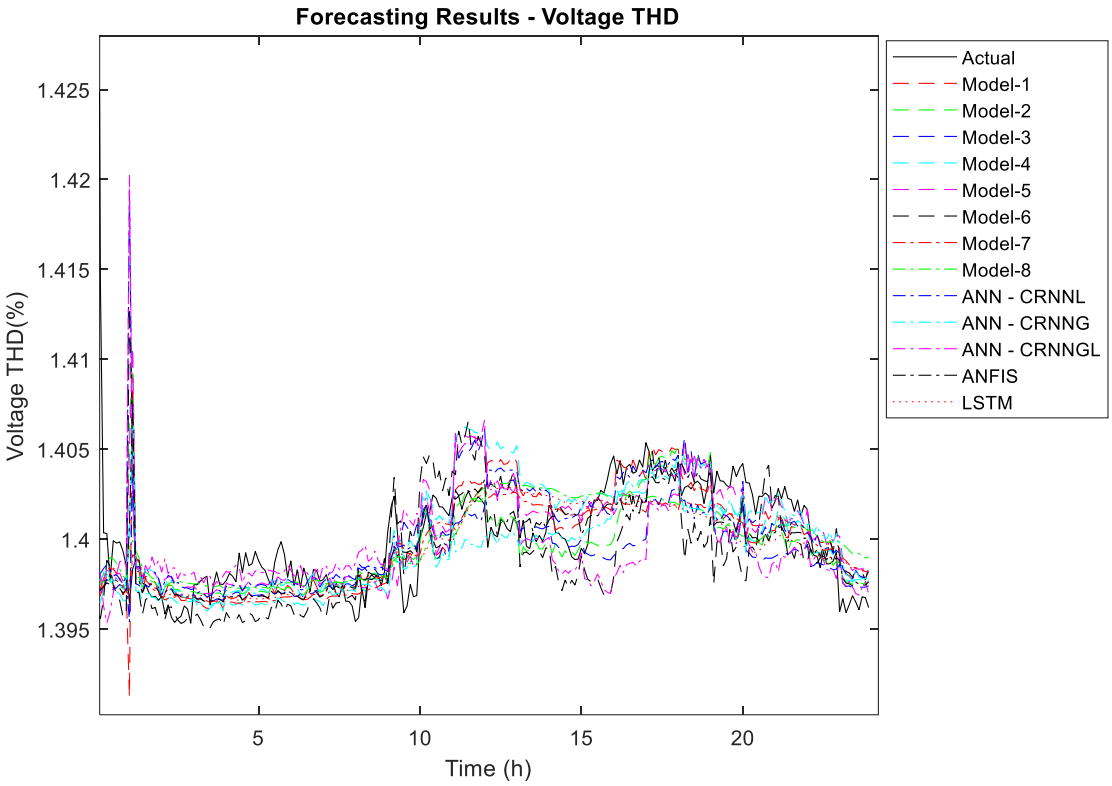

Figure 51: THDV – Actual vs Forecast Curves Wind-PMSG-PV Model

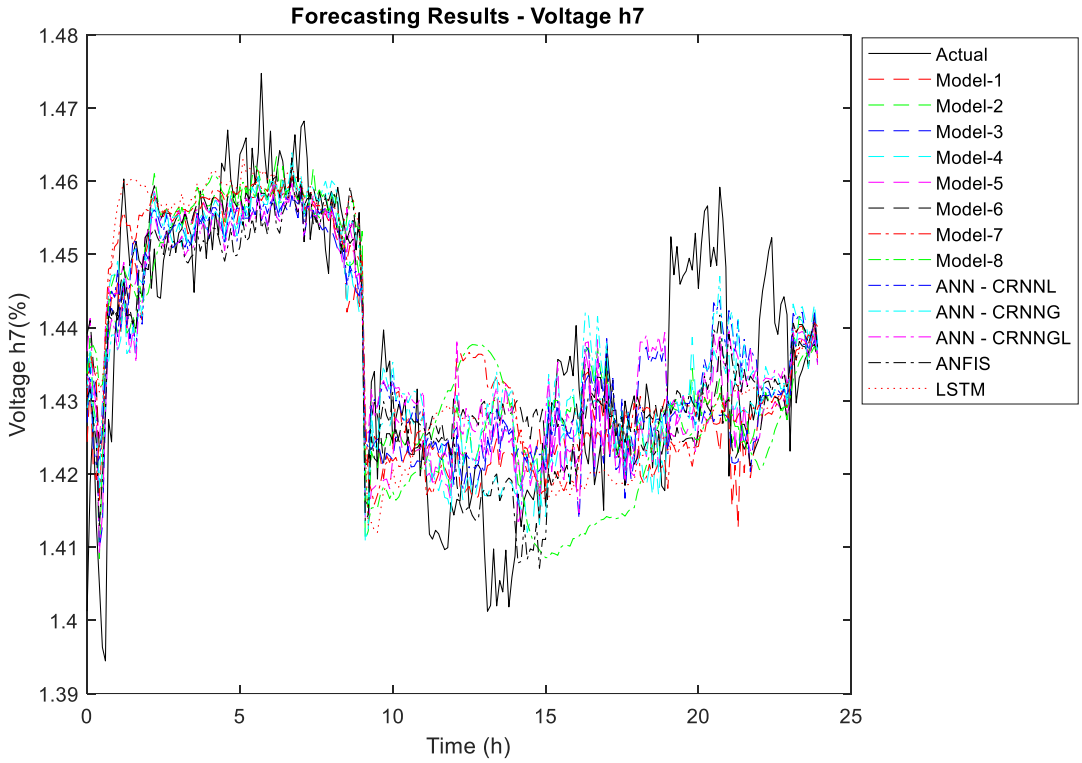

Figure 52: Voltage 7th Harmonic – Actual vs Forecast Curves Wind-PMSG-PV

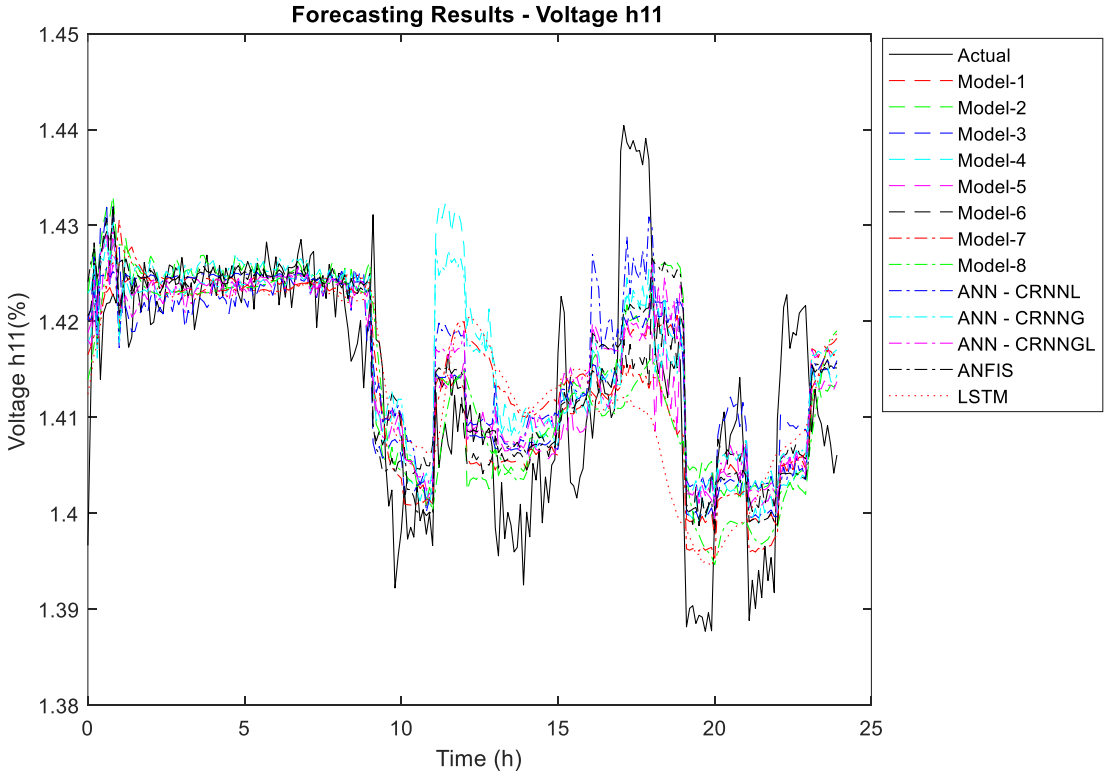

Figure 53: Voltage 11th Harmonic – Actual vs Forecast Curves Wind-PMSG-PV

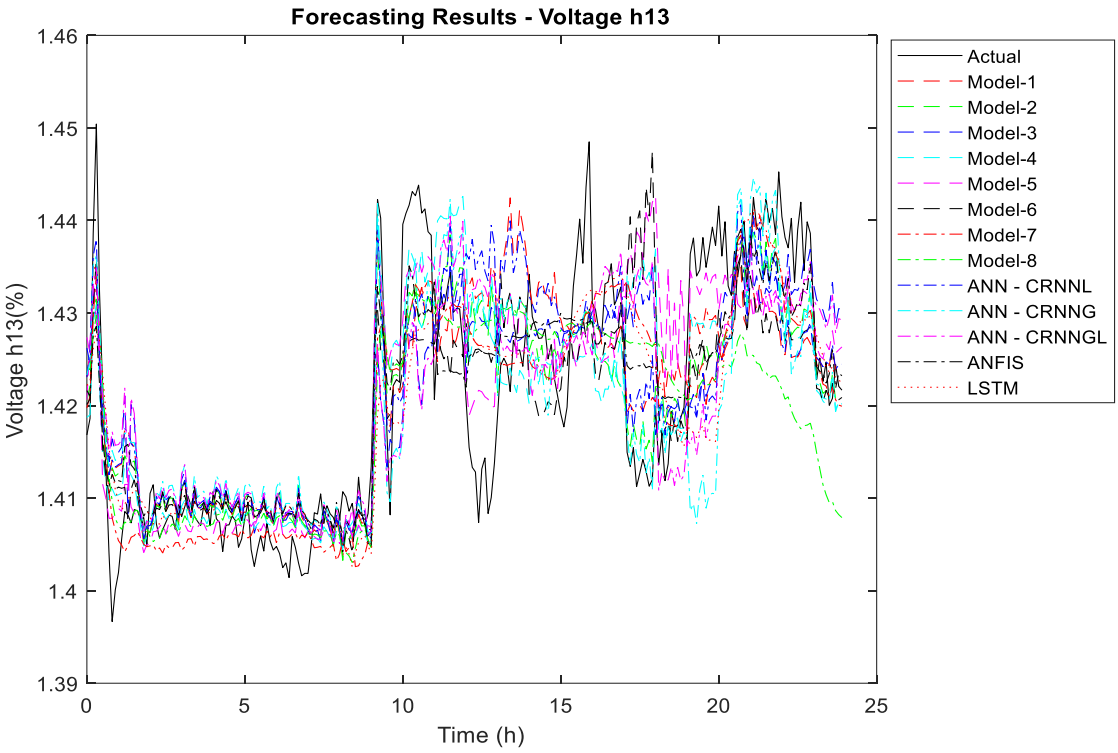

Figure 54: Voltage 13th Harmonic – Actual vs Forecast Curves Wind-PMSG-PV

As previously elucidated, each forecasting parameter is linked to its distinct dataset, and the forecasting of harmonic parameters is carried out individually. Model-8 (ANFIS-LSTM) typically exhibits superior performance across the majority of cases. Nonetheless, exceptions do occur, where an alternative model surpasses the performance even of model-8. It is noteworthy, however, that model-8 consistently maintains a commendable second-place ranking, irrespective of its relative performance. Table 17 shows that the overall performance of all hybrid models proposed in this thesis has surpassed the forecast produced by any other individual models adopted in the literature.

Table 17: Forecasting Results Comparison of Voltage Harmonics – Wind-PMSG-PV

Forecasting Models	Voltage Harmonics								Reference / Publication
	THD		h7		h11		h13		
	RMSE	MAE	RMSE	MAE	RMSE	MAE	RMSE	MAE	
Model-1 (CRNNL-ANFIS)	0.00433	0.00175	0.01114	0.00867	0.00819	0.00576	0.00864	0.00678	Proposed Hybrid Model
Model-2 (CRNNG-ANFIS)	0.00435	0.00171	0.01114	0.00831	0.00817	0.00644	0.00726	0.00557	Proposed Hybrid Model
Model-3 (CRNNGL-ANFIS)	0.00426	0.00170	0.01071	0.00835	**0.0075**	**0.00567**	0.00870	0.00649	Proposed Hybrid Model
Model-4 (ANFIS-CRNNL)	0.00430	0.00185	0.01116	0.00827	0.00816	0.00618	0.00832	0.00622	Proposed Hybrid Model
Model-5 (ANFIS-CRNNG)	0.00432	0.00175	0.01128	0.00888	0.00790	0.00591	0.00809	0.00567	Proposed Hybrid Model
Model-6 (ANFIS-CRNNGL)	0.00429	0.00174	0.01155	0.00849	0.00819	0.00602	0.00843	0.00604	Proposed Hybrid Model
Model-7 (LSTM-ANFIS)	0.00422	0.00162	0.01018	0.00808	0.00798	0.00608	**0.007**	**0.00521**	Proposed Hybrid Model
Model-8 (ANFIS-LSTM)	**0.00421**	**0.00156**	**0.0097**	**0.0075**	0.00767	0.00568	0.00704	0.00556	Proposed Hybrid Model
LSTM	*0.00436*	*0.00192*	0.01314	0.01005	0.00956	0.00734	0.00910	0.00674	[41] & [45]
ANFIS	0.00486	0.00247	0.01304	0.00962	*0.00843*	*0.00630*	0.00965	0.00742	[42]
ANN – CRNNL	0.00473	0.00220	0.01462	0.01141	0.00914	0.00690	*0.00874*	*0.00651*	[36], [43] & [46]
ANN – CRNNG	0.00447	0.00198	*0.01140*	*0.00894*	0.00894	0.00701	0.00918	0.00673	[36], [43] & [46]
ANN – CRNNGL	0.00483	0.00238	0.01209	0.00916	0.00861	0.00667	0.00983	0.00744	[36], [43] & [46]

- ***Yellow Highlight*** denotes the best performing model
- ***Blue Highlight*** denotes the second-best performing model

It is obvious that model-8 is the best performing model. It uses ANFIS-LSTM, with the lowest RMSE and MAE (0.00421 and 0.00156 for THD, and 0.0097 and 0.0075 for h7, respectively). Model-8 is the second-best performing model for h11 and h13 as well. Furthermore, model-8 outperforms all other models for h11, with an RMSE of 0.0075 and a MAE of 0.00567. For h13, model-7 is the best-performing model with the fewest errors (RMSE – 0.007 and MAE – 0.00521). As for the individual models, for

THD the best performing model is LSTM, while for h7 the best-performing model is CRNNG, for h11 it is ANFIS, and for h13 it is CRNNL.

From the results presented, it is apparent that all hybrid models perform better than any of the individual forecasting techniques. Besides model-8, the results produced by model-7 are also significant, ranking it second behind model-8 for THD and h7 on top of it being the best model for h13. Table 18 presents the percentage improvement of model-8 over the individual models.

Table 18: Best Forecasting Model for Voltage Harmonics – Wind-PMSG-PV

Model / Forecasting Parameter	RMSE	RMSE (% Improvement)				
		LSTM	ANFIS	CRNNL	CRNNG	CRNNGL
Model-8 (THD)	0.00421	0.00436 ***(3.39%)***	0.00486 ***(13.41%)***	0.00473 ***(10.99%)***	0.00447 ***(5.93%)***	0.00483 ***(12.95%)***
Model-8 (h7)	0.0097	0.001314 ***(26.18%)***	0.01304 ***(25.59%)***	0.01462 ***(33.64%)***	0.0114 ***(14.9%)***	0.01209 ***(19.75%)***
Model-8 (h11)	0.00767	0.00956 ***(19.76%)***	0.00843 ***(8.97%)***	0.00914 ***(16.06%)***	0.00894 ***(14.13%)***	0.00861 ***(10.87%)***
Model-8 (h13)	0.00704	0.0091 ***(22.58%)***	0.00965 ***(27.02%)***	0.00874 ***(19.4%)***	0.00918 ***(23.27%)***	0.00983 ***(28.3%)***

Table 18 shows the error outline and percentage improvement comparing the prediction of model-8 and individual models tested. For THD, model-8 offers a 3.39% improvement over LSTM, which is the best performing individual model. Similarly, for h7, the percentage improvement of model-8 is 14.9% in contrast with the CRNNG forecast. For h11, the results for model-8 delivers an 8.97% improvement over ANFIS. Finally, for h13 there is a 19.4% improvement compared to CRNNL.

4.9.2 Current Harmonics

The actual vs anticipated curves for the eight proposed hybrid models and five individual models adopted from the literature and used to predict the TDD, h7, h11, and

h13 for the Wind-PMSG-PV model current harmonics are presented in this section. The curves are contained in Figures 55, 56, 57, and 58, and the performance stats for forecasting are given in Table 19.

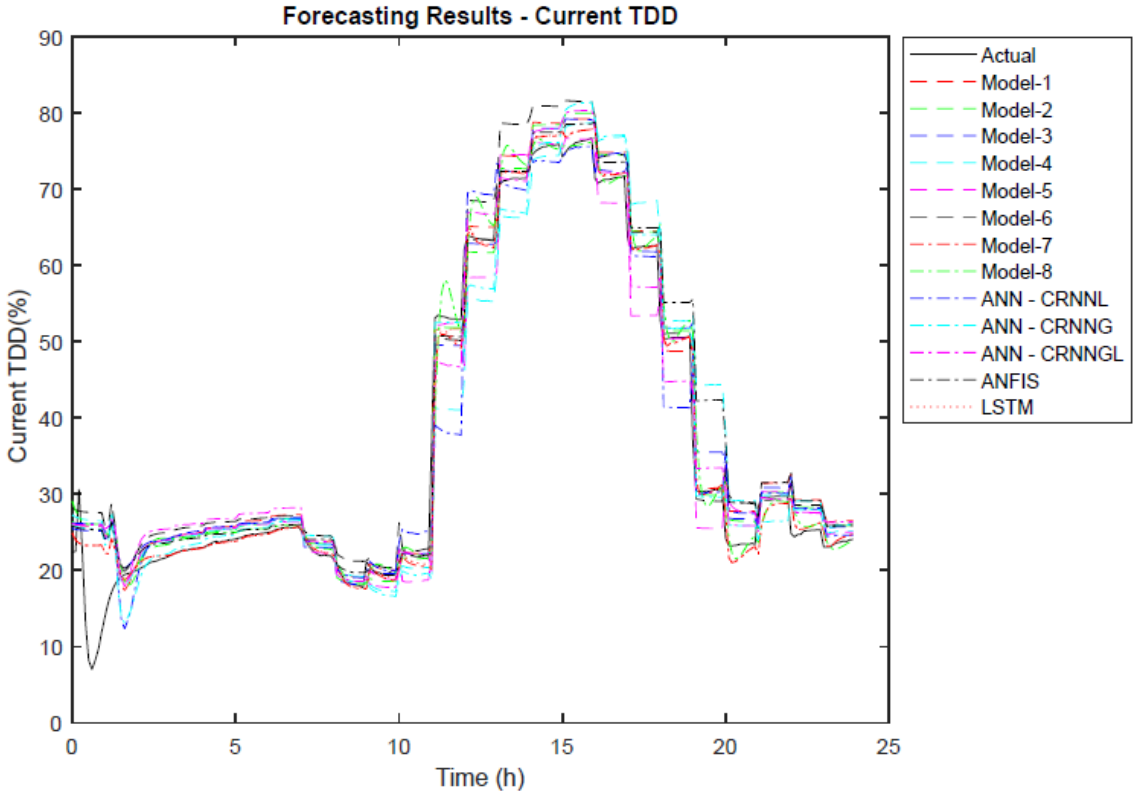

Figure 55: TDD – Actual vs Forecast Curves Wind-PMSG-PV Model

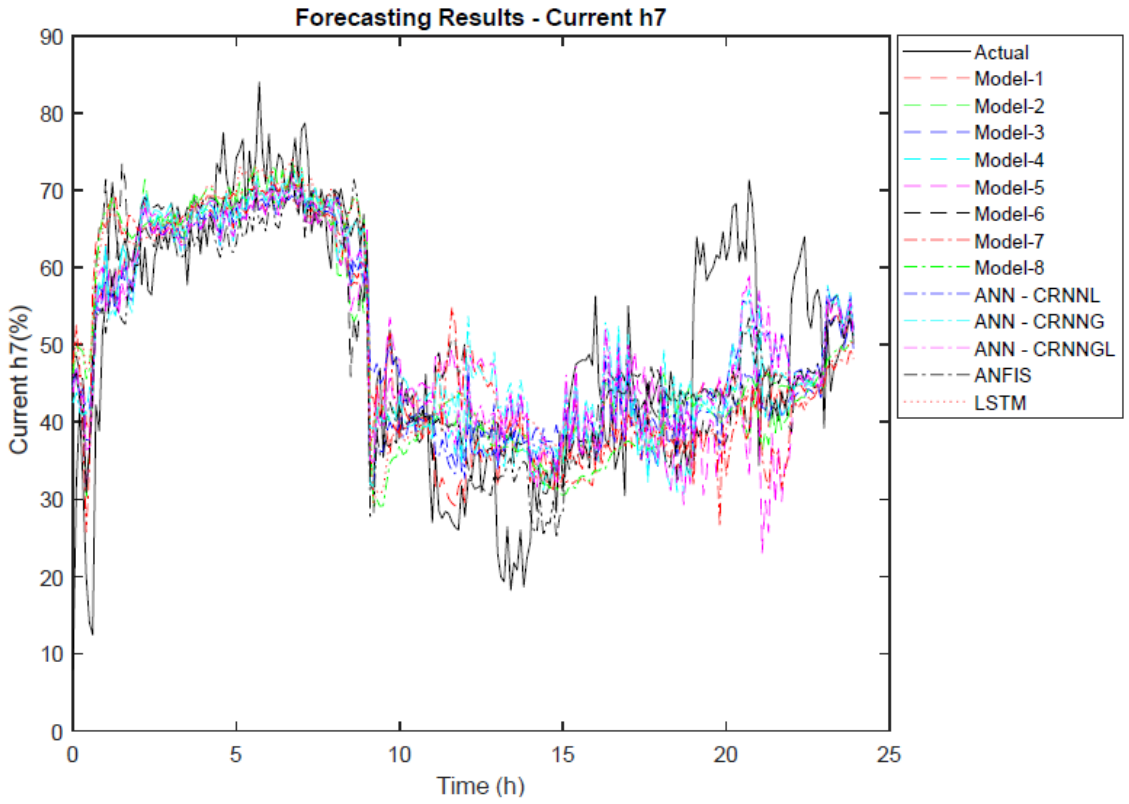

Figure 56: Current 7th Harmonic – Actual vs Forecast Curves Wind-PMSG-PV

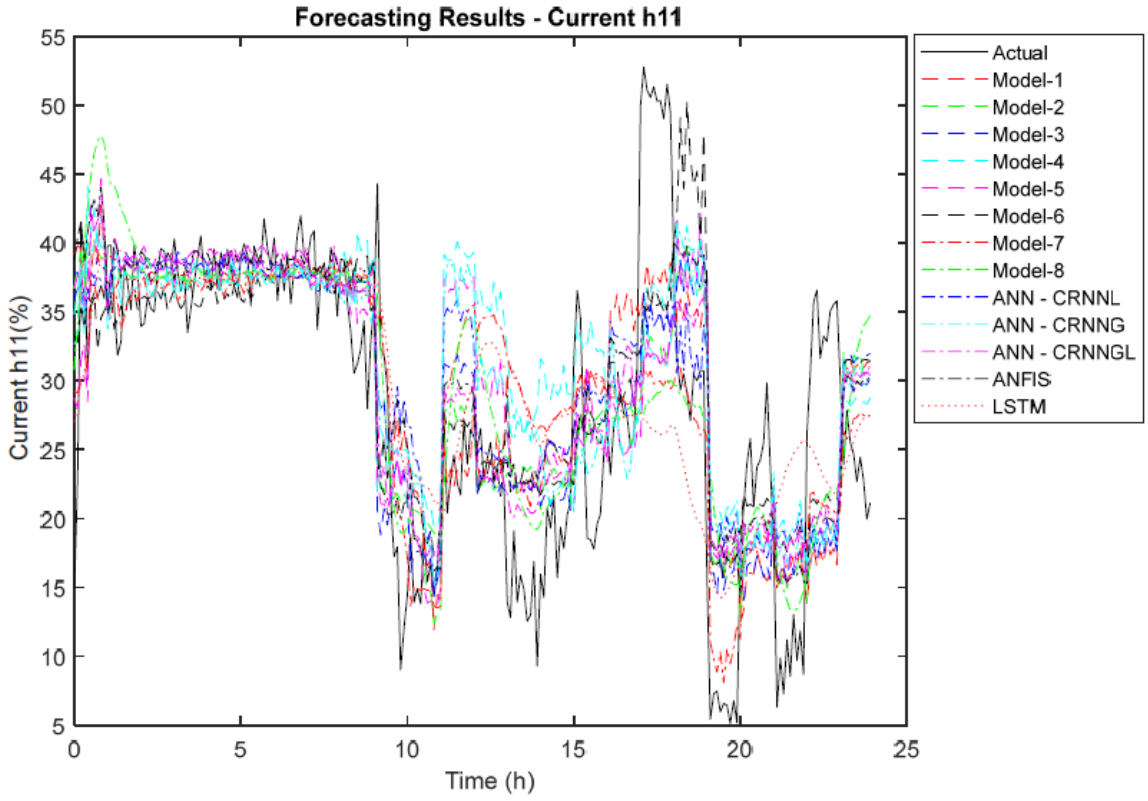

Figure 57: Current 11th Harmonic – Actual vs Forecast Curves Wind-PMSG-PV

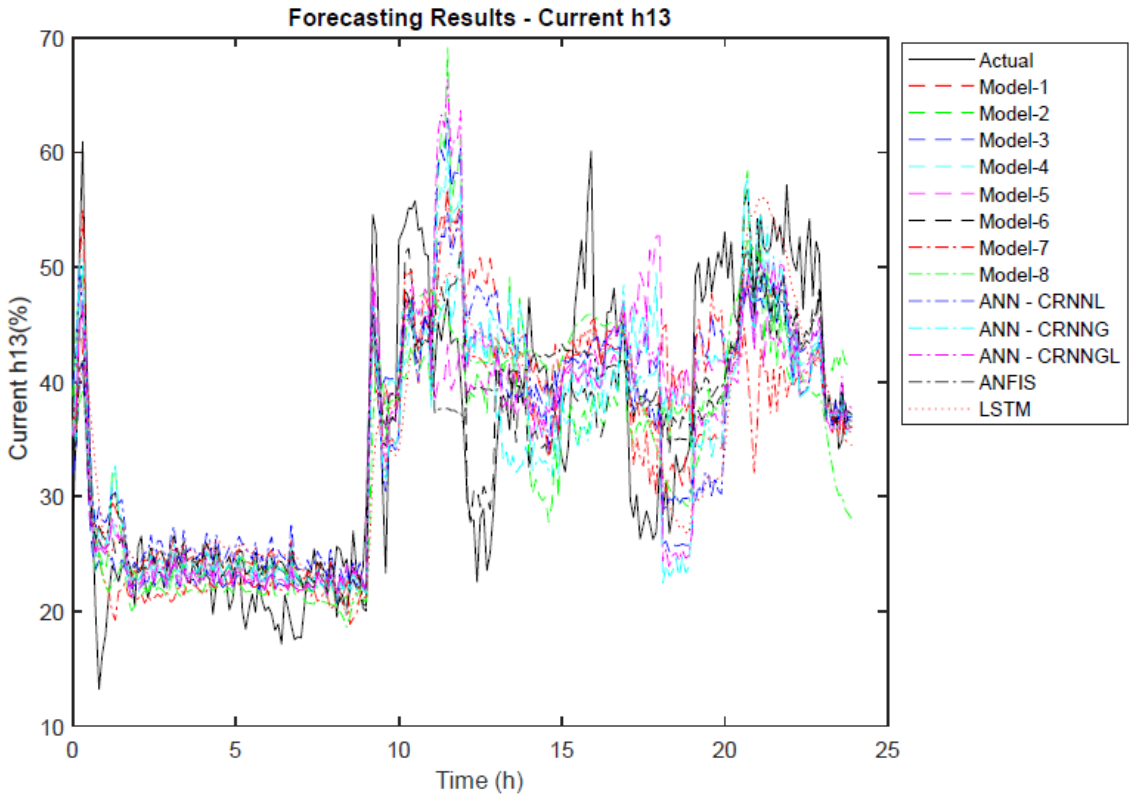

Figure 58: Current 13th Harmonic – Actual vs Forecast Curves Wind-PMSG-PV

As previously explained, every forecasting parameter is associated with its own unique dataset, and the prediction of harmonics parameters is conducted separately. Model-8 (ANFIS-LSTM) typically demonstrates superior performance usually. Nevertheless, there are occasional exceptions where an alternative model outperforms it. However, even in those cases, model-8 consistently maintains a strong second-place position.

As seen in Figures 58, 59, 60, and 61 and in Table 19, model-8 (ANFIS-LSTM) produces the best results, with the lowest RMSE for TDD (3.2011), h7 (1.5157), and h11 (7.2851) and the second-best results for h13 (6.334). Furthermore, model-6 is the best performing model for h13, with the lowest RMSE (6.3128). Among individual

models, LSTM produces the best results for TDD, with an RMSE of 3.907, while ANFIS produces the best results for h7 (11.1411) and h13 (7.9227) and CRNNGL for h11 (7.8883).

Table 19: Forecasting Results Comparison of Current Harmonics – Wind-PMSG-PV

Forecasting Models	Current Harmonics								Reference / Publication
	THD		h7		h11		h13		
	RMSE	MAE	RMSE	MAE	RMSE	MAE	RMSE	MAE	
Model-1 (CRNNL-ANFIS)	4.1810	2.8774	9.9493	7.5579	7.5972	5.7729	7.7737	5.6785	Proposed Hybrid Model
Model-2 (CRNNG-ANFIS)	4.0467	2.5420	10.0251	7.7102	7.5554	5.6338	7.3167	5.3258	Proposed Hybrid Model
Model-3 (CRNNGL-ANFIS)	4.0216	2.6187	9.9738	7.5416	7.6368	5.7169	6.9230	5.1626	Proposed Hybrid Model
Model-4 (ANFIS-CRNNL)	4.4713	2.9202	9.9783	7.6046	7.8226	5.7972	7.2860	5.4825	Proposed Hybrid Model
Model-5 (ANFIS-CRNNG)	4.4286	2.9518	10.6533	8.2755	7.8091	5.9181	7.4949	5.5060	Proposed Hybrid Model
Model-6 (ANFIS-CRNNGL)	4.4473	3.2956	9.9871	7.7436	7.4069	5.5623	**6.3128**	**4.9119**	Proposed Hybrid Model
Model-7 (LSTM-ANFIS)	3.2268	1.5521	10.2656	7.8567	7.6828	5.5971	7.0060	5.3960	Proposed Hybrid Model
Model-8 (ANFIS-LSTM)	**3.2011**	**1.5157**	**9.5301**	**7.4151**	**7.2851**	**5.5141**	6.3340	4.9965	Proposed Hybrid Model
LSTM	*3.9070*	*2.1487*	11.3811	8.2053	8.5276	6.2978	7.9486	5.8163	[41] & [45]
ANFIS	4.7846	3.0990	*11.1411*	*8.2681*	8.2793	6.4015	*7.9227*	*5.8418*	[42]
ANN – CRNNL	5.2654	3.4145	12.2311	8.9429	9.3007	7.2585	8.1233	6.1220	[36], [43] & [46]
ANN – CRNNG	6.1329	4.3554	12.0196	9.1486	8.3457	6.5548	8.1785	6.3640	[36], [43] & [46]
ANN – CRNNGL	4.8780	3.6053	11.5214	8.6189	*7.8883*	*6.0364*	7.9894	6.3652	[36], [43] & [46]

- ***Yellow Highlight*** denotes the best performing model
- ***Blue Highlight*** denotes the second-best performing model

The results indicate that the performance of the proposed hybrid models surpasses that of any individual models. Model-8 again proves to be the best performing model in comparison to the other hybrid models. To further the analysis, Table 20 presents the percentage improvement of model-8 results over all the individual models.

Table 20: Best Forecasting Model for Current Harmonics – Wind-PMSG-PV

Model / Forecasting Parameter	RMSE	RMSE (% Improvement)				
		LSTM	ANFIS	CRNNL	CRNNG	CRNNGL
Model-8 (TDD)	3.2011	3.907 **(18.07%)**	4.7846 ***(33.1%)***	5.2654 ***(39.21%)***	6.1329 ***(47.8%)***	4.878 ***(34.38%)***
Model-8 (h7)	9.5301	11.3811 ***(16.26%)***	11.1411 ***(14.46%)***	12.2311 ***(22.08%)***	12.0196 ***(20.71%)***	11.5214 ***(17.28%)***
Model-8 (h11)	7.2851	8.5276 ***(14.57%)***	8.2793 ***(12.01%)***	9.3007 ***(21.67%)***	8.3457 ***(12.71%)***	7.8883 ***(7.65%)***
Model-8 (h13)	6.334	7.9486 ***(20.31%)***	7.9227 ***(20.05%)***	8.1233 ***(22.03%)***	8.1785 ***(22.55%)***	7.9894 ***(20.72%)***

As shown in Table 20, the percentage improvement of model-8 over individual models is evident. Comparing model-8's performance with that of the best performing individual model, for TDD, model-8 shows an 18.07% improvement over LSTM, while for h7 and h13, the percentage improvement is 14.46% and 20.05%, respectively, over ANFIS. For h11, model-8 displays 7.65% improved results over CRNNGL.

4.9.3 Conclusion

This chapter examined the harmonics analysis within the context of the simulated results generated by two generator models: Wind-DFIG-PV and Wind-PMSG-PV. The results revealed variations in THD and TDD and identified the dominant harmonics as h7, h11, and h13 in voltage and current. Additionally, an extensive explanation of the forecasting methodology was provided.

Also in this chapter, the results obtained from the eight hybrid prediction models introduced in this thesis were presented. These results were subjected to validation through a comparison with the forecasting methods utilized by other researchers in the literature. Remarkably, all eight hybrid models proposed in this thesis surpassed the performance of individual models employed by the authors in [36], [41], [42], [43], [45], and [46] for predicting the same data and parameters, as evidenced by the reported outcomes. Model-8, which incorporates ANFIS-LSTM, emerged as the top-performing model among all those proposed.

Furthermore, the analysis revealed that among the individual models, the ANFIS and LSTM methods consistently delivered forecasts with higher accuracy compared to other singular forecasting techniques. For the Wind-DFIG-PV generator, model-8 demonstrated superior performance in predicting THD, TDD, voltage, and current 7th harmonic, as well as voltage 13th harmonic. As well, model-8 secured the second-best position in other cases, such as the voltage 11th harmonic and current 11th and 13th harmonics. In the Wind-PMSG-PV generator, model-8 outperformed in forecasting THD, TDD, voltage, and current 7th harmonic, along with current 11th harmonic, while ranking second-best in other scenarios, including voltage 11th and 13th harmonic and current 13th harmonic.

Ensuring the trustworthiness of the results is paramount in any scientific study, and the validity and accuracy of the outcomes are rigorously scrutinized. To verify the credibility of the results obtained from models 1-8, especially considering the observed minor discrepancies and potential deviations from actual values in figures 52, 53, 54, 56, 57 & 58, the results are compared with existing models in literature as benchmark.

This comparative analysis depicted in tables 17, 18, 19 & 20 serves as an additional layer of validation, ensuring consistency and reliability across different modelling approaches. The tables feature quantitative metrics, including Root Mean Square Error (RMSE) and Mean Absolute Error (MAE), employed for a precise evaluation of model accuracy. These metrics reveal notable distinctions in results generated by different models, underscoring the necessity for thorough scrutiny and enhancement. The identified elevated errors and deviations signal limitations in the current models, particularly evident in scenarios where the actual values experience abrupt increases or decreases. These limitations may emanate from the inherent complexities within power system dynamics or inconsistencies in input data such as wind speed and solar irradiation, elements intrinsic to the renewable energy system.

In conclusion, the advantages of employing hybrid models over individual models are evident, as no individual model proved superior to the best-performing model among the eight hybrid models proposed. Furthermore, model-8 emerged as the most accurate and consistent choice when compared to all the hybrid models presented in this study.

Chapter 5: Conclusions, and Future Works

5.1 Conclusions

In conclusion, renewable energy systems (RESs) harnessing solar and wind power represent rapidly advancing technologies for clean electricity generation. However, the integration of RESs with the grid often introduces voltage and current harmonics at the point of common coupling, thereby affecting the power quality of the system. Harmonic forecasting emerges as a valuable tool in designing harmonic mitigation solutions to mitigate these harmonics effectively.

In this study, two hybrid generator models, Wind-DFIG-PV, and Wind-PMSG-PV, were employed to simulate voltage and current waveforms and extract harmonics from real-world wind speed and solar irradiation data. The statistical analysis performed identified the dominant harmonics as the 7th, 11th, and 13th harmonics, denoted as h7, h11, and h13. We conducted forecasts for four voltage parameters (h7, h11, h13, and THD) and four current parameters (h7, h11, h13, and TDD) for both generator configurations, resulting in a total of sixteen forecasting cases.

To produce these forecasts, eight novel hybrid forecasting models were proposed, each consisting of a two-stage process that combines different forecasting techniques. For example, models 1, 2, and 3 utilized a multilayered artificial neural network (ANN) in stage 1 (3LCRNNL, 3LCRNNG, or 3LCRNNGL) and an adaptive neuro-fuzzy inference system (ANFIS) in stage 2, whereas models 4, 5, and 6 employed the reverse combination. Model-7 and model-8 integrated long short-term memory (LSTM) and ANFIS models, with model-7 utilizing LSTM in stage 1 and ANFIS in stage 2, and

model-8 adopting the opposite sequence. Additionally, five individual models (ANN CRNNL, CRNNG, CRNNGL, ANFIS, and LSTM) were also tested; these were previously proposed by other researchers for forecasting the same data.

The findings revealed that model-8 consistently outperformed all other hybrid and individual models, excelling in ten out of sixteen cases. In instances where model-8 was not the top performer, it consistently delivered second-best results. Furthermore, model-8 was compared to all individual models, demonstrating its superiority in terms of the percentage improvement it offers over these techniques.

It is worth noting that across all sixteen cases, the results produced by any of the eight proposed hybrid models consistently exhibited greater accuracy compared to any of the individual models. This underscores the effectiveness of employing hybrid models for harmonic forecasting in renewable energy systems, offering improved forecasting performance and enhanced grid power quality.

5.2 Future Works

In consideration of the objectives realized in this thesis, it is pertinent to underscore the successful development of hybrid forecasting models achieved by harmonizing the inherent capabilities of ANN, ANFIS, and LSTM techniques. The outcomes of this fusion have demonstrated their commendable nature, as elaborated upon in the preceding sections. Nevertheless, to catalyse further progress within this research domain, certain pivotal dimensions warrant our focused attention.

One of the foremost limitations encountered in the present methodology centres on the omission of the grid's influential role—a dimension of profound significance in the context of power system forecasting. It is imperative that future research endeavours

prioritise the incorporation of grid-related dynamics as a primary focus. This objective may be realized through the development of MATLAB-based modelling approaches or by harnessing historical data sourced from authentic power systems. The integration of such considerations will enable these forecasting models to ascend to a heightened level of precision and applicability, adeptly accommodating the intricate nuances associated with the grid's impact on predictive accuracy.

Furthermore, the pursuit of elevated forecasting precision should extend beyond the confines of the existing framework. It is a judicious course of action to embark on an exploration of alternative hybrid model compositions that encompass a broader spectrum of forecasting techniques, transcending the established triad of ANN, ANFIS, and LSTM. This innovative exploration holds the promise of uncovering novel synergies and methodological approaches, ultimately augmenting both the accuracy and versatility of hybrid forecasting models. Consequently, forthcoming research initiatives should maintain an unwavering commitment to the discovery of inventive hybrid model combinations, leveraging the strengths intrinsic to various forecasting techniques. In so doing, we stand poised to propel the frontiers of predictive accuracy within this dynamic and pivotal field of study.

References

[1] P. F. Keebler, “Meshing power quality and electromagnetic compatibility for tomorrow’s smart grid,” *IEEE Electromagnetic Compatibility Magazine*, vol. 1, no. 2, pp. 100–103, 2012.

[2] Fawaz Alhaddad, Hamed H Aly, Mo El-Hawary " An Overview of Active Power Filters for Harmonics Mitigation of Renewable Energies Resources*" IEEE 10th Annual Information Technology, Electronics and Mobile Communication Conference, Vancouver, BC, Canada, 2019.*

[3] N. Shah, “White paper: Harmonics in power systems: Causes, effects and control,”, Siemens Industry, Inc, May 2013. Retrieved from https://assets.new.siemens.com/siemens/assets/api/uuid:8ab2a02e-ad94-41cb-a362-438f016aa704/drive-harmonics-in-power-systems-whitepaper.pdf

[4] R. Pinyol, “White paper: Harmonics: Causes, effects and minimization,”, SALICRU, August 2015. Retrieved from https://www.salicru.com/files/pagina/72/278/jn004a01_whitepaper-armonics_(1).pdf

[5] “Product data bulletin: Power system harmonics causes and effects of variable frequency drives relative to the IEEE 519-1992 standard,” tech. rep., SQUARE D, August 1994.

[6] “IEEE Recommended practice and requirements for harmonic control in electric power systems,” *IEEE Std 519-2014 (Revision of IEEE Std 519- 1992)*, pp. 1–29, 2014.

[7] S. K. Jain and S. Singh, “Harmonics estimation in emerging power system: Key issues and challenges,” *Electric power systems research*, vol. 81, no. 9, pp. 1754–1766, 2011.

[8] T. Ortmeyer and K. Chakravarthi, “The effects of power system harmonics on power system equipment and loads,” *IEEE Trans. Power Appar. Syst.;(United States)*, 1985.

[9] V. Wagner, J. Balda, D. Griffith, A. McEachern, T. Barnes, D. Hartmann. Phileggi, A. Emannuel, W. Horton, W. Reid, R. Ferraro, and W. Jewell, “Effects of harmonics on equipment,” *IEEE Transactions on Power Delivery*, vol. 8, no. 2, pp. 672–680, 1993.

[10] IEC 61000-3-2, “Limits for Harmonics Current Emissions (equipment input current< 16 A per phase)”, 2018.

[11] IEC 61000-3-4, “Limitation of Emission of Harmonic Currents in Low- voltage Power Supply System’s Equipment with rated Current greater than 16 A,”, 1998.

[12] IEC 61000-4-7, “General guide on Harmonics and Interharmonics Measurements and

Instrumentation for Power Supply and Equipment connected thereto," 2002.

[13] J. Arrillaga and N. R. Watson, *Power system harmonics*. John Wiley & Sons, 2004.

[14] M. H. Hayes, *Statistical digital signal processing and modeling*. John Wiley & Sons, 2009.

[15] E. F. Fuchs and M. A. Masoum, *Power quality in power systems and electrical machines*. Academic press, 2011.

[16] Sankaran, C. (2002). Power Quality (1st ed.). CRC Press. https://doi.org/10.1201/9781420041026

[17] R. C. Dugan, M. F. McGranaghan, and H. W. Beaty, "Electrical power systems quality," *New York*, 1996.

[18] "IEEE recommended practice for monitoring electric power quality," *IEEE Std 1159-2019 (Revision of IEEE Std 1159-2009)*, pp. 1–98, 2019.

[19] P. Kumar and P. Prakash, "Harmonic filter design for DC lines using MATLAB," *International Journal of Computational Engineering Research*, vol. 3, no. 11, 2013.

[20] S. Chattopadhyay, M. Mitra, and S. Sengupta, "Electric power quality," in *Electric power quality*, pp. 5–12, Springer, 2011.

[21] Memon, Zubair & Uqaili, Mohammad & Unar, Mukhtiar. (2016). Harmonics Mitigation of Industrial Power System Using Passive Filters. Mehran University Research Journal of Engineering and Technology.

[22] Memon, Shafqat & Kumar, Mahendar & Memon, Abdul & Memon, Zubair & Soomro, Shakir. (2018). Total Harmonic Distortion (THD) Analysis of Grid Integrated Permanent Magnet Synchronous Generator (PMSG) With Full Scale Converter (FSC) Based Wind Farm.

[23] A. Baggini, *Handbook of power quality*. John Wiley & Sons, 2008.

[24] K. A. Stroud and D. J. Booth, *Advanced engineering mathematics*. Bloomsbury Publishing, 2020.

[25] A. Baggini and Z. Hanzelka, "Voltage and current harmonics," *Handbook of Power Quality*, pp. 228–229, 2008.

[26] A. Croft, R. Davison, and M. Hargreaves, *Engineering mathematics: a modern foundation for electronic, electrical and systems engineers*. Addison- Wesley, 1996.

[27] B. Girdwood, "Understanding power quality," Tech. Rep. 1, Energy Mad Ltd, October 2007.

[28] S. H. E. A. Aleem, A. F. Zobaa, and M. M. A. Aziz, "Optimal *c*-type passive filter based on minimization of the voltage harmonic distortion for nonlinear loads," *IEEE Transactions on Industrial Electronics*, vol. 59, no. 1, pp. 281– 289, 2011.

[29] IEC Std, "61000-2-2: Electromagnetic compatibility (EMC) - part 2-2: Environment-compatibility levels for low-frequency conducted disturbances and signaling in public low-voltage power supply systems," *IEC Commission: New York, NY, USA*, 2002.

[30] A. B. Nassif, W. Xu, and W. Freitas, "An investigation on the selection of filter topologies for passive filter applications," *IEEE transactions on Power Delivery*, vol. 24, no. 3, pp. 1710–1718, 2009.

[31] D. Bohaichuk, C. Muskens, and W. Xu, "Mitigation of harmonics in oil field electric systems using a centralized medium voltage filter," in *Ninth International Conference on Harmonics and Quality of Power Proceedings (Cat. No. 00EX441)*, vol. 2, pp. 614–618, IEEE, 2000.

[32] C.-J. Chou, C.-W. Liu, J.-Y. Lee, and K.-D. Lee, "Optimal planning of large passive-harmonic-filters set at high voltage level," *IEEE Transactions on Power Systems*, vol. 15, no. 1, pp. 433–441, 2000.

[33] A. S. Yilmaz, A. Alkan, and M. H. Asyali, "Applications of parametric spectral estimation methods on detection of power system harmonics," *Electric Power Systems Research*, vol. 78, no. 4, pp. 683–693, 2008.

[34] A. Yazdani and R. Iravani, *Voltage-sourced converters in power systems: Modeling, control, and applications*. John Wiley & Sons, 2010.

[35] N. Mohan, T. M. Undeland, and W. P. Robbins, *Power electronics: converters, applications, and design*. John Wiley & sons, 2003.

[36] Pablo Rodríguez-Pajarón, Araceli Hernández Bayo, Jovica V. Milanović, "Forecasting voltage harmonic distortion in residential distribution networks using smart meter data", International Journal of Electrical Power & Energy Systems, Volume 136, p. 107653, 2022.

[37] P. K. Ray, P. S. Puhan, and G. Panda, "Real time harmonics estimation of distorted power system signal," *International Journal of Electrical Power & Energy Systems*, vol. 75, pp. 91–98, 2016.

[38] P. Ivry, O. Oke, D. W. Thomas, and M. Sumner, "Predicting harmonic distortion of multiple converters in a power system," *Journal of Electrical and Computer Engineering*, vol. 2017.

[39] M.M. Hussam. Alhaj, Nursyarizal Mohd Nor, Vijanth S. Asirvadam, M.F. Abdullah, Comparison of Power System Harmonic Prediction, Procedia Technology, Volume 11, Pages 628-634, 2013.

[40] D. S. Braga and P. R. Jota, "Prediction of total harmonic distortion based on harmonic modeling of nonlinear loads using measured data for parameter estimation," in *2016 17th International Conference on Harmonics and Quality of Power (ICHQP)*, pp. 454–459, IEEE, 2016.

[41] H., Dong, Y., Zhang, F., Li, X., Zhang, L., Yu, J., . . . Jiang, G. (2021, May 25). Nonlinear Load Harmonic Prediction Method Based on Power Distribution Internet of Things.

[42] M. Panoiu, C. Panoiu, and L. Ghiormez, "Neuro-fuzzy modeling and prediction of current total harmonic distortion for high power nonlinear loads," in *2018 Innovations in Intelligent Systems and Applications (INISTA)*, pp. 1– 7, IEEE, 2018.

[43] H. Mori and S. Suga, "Power system harmonics prediction with an artificial neural network," in *1991 IEEE International Symposium on Circuits and Systems (ISCAS)*, pp. 1129–1132, IEEE, 1991.

[44] L. Shengqing, Z. Huanyue, X. Wenxiang, and L. Weizhou, "A harmonic current forecasting method for microgrid HAPF based on the EMD-SVT theory," in *2013 Third International Conference on Intelligent System Design and Engineering Applications*, pp. 70–72, IEEE, 2013.

[45] E. Kuyunani, A. N. Hasan, and T. Shongwe, "Improving voltage harmonics forecasting at a wind farm using deep learning techniques," in *2021 IEEE 30th International Symposium on Industrial Electronics (ISIE)*, pp. 1–6, IEEE, 2021.

[46] M. Žnidarec, Z. Klaić, D. Šljivac, and B. Dumnić, "Harmonic distortion prediction model of a grid-tie photovoltaic inverter using an artificial neural network," *Energies*, vol. 12, no. 5, p. 790, 2019.

[47] G. Todeschini and Z. Deng, "Forecasting the impact of renewable energy sources on transmission grid power quality," *11th International Conference on Renewable Power Generation - Meeting net zero carbon (RPG 2022)*, Hybrid Conference, London, UK, 2022, pp. 115-119, doi: 10.1049/icp.2022.1684.

[48] S. Li, X. Luo, Y. Li, L. Zeng and Z. He, "Harmonic current forecasting method for hybrid active power filter based on optimal linear prediction theory," *2011 International Conference on Electrical and Control Engineering*, Yichang, China, 2011, pp. 4806-4809, doi: 10.1109/ICECENG.2011.6058003.

[49] S. Vyalkova and I. Nadtoka, "Analysis of Hybrid Model Error of Short-Term Forecast of Energy Consumption in Moscow," *2021 International Conference on Industrial Engineering, Applications and Manufacturing (ICIEAM)*, Sochi, Russia, 2021, pp. 802-806, doi: 10.1109/ICIEAM51226.2021.9446344.

[50] W. Bao and W. Bin, "Real-time Tide Prediction Based on An Hybrid HA-WANN Model Using Wind Information," *2018 14th IEEE International Conference on Signal Processing (ICSP)*, Beijing, China, 2018, pp. 604-608, doi: 10.1109/ICSP.2018.8652339.

[51] M. Mansoor, Q. Ling and M. H. Zafar, "Short Term Wind Power Prediction using Feedforward Neural Network (FNN) trained by a Novel Sine-Cosine fused Chimp Optimization Algorithm (SChoA)," *2022 5th International Conference on Energy Conservation and Efficiency (ICECE)*, Lahore, Pakistan, 2022, pp. 1-6, doi: 10.1109/ICECE54634.2022.9758965.

[52] K. A. Keitsch and T. Bruckner, "Modular electrical demand forecasting framework — A novel hybrid model approach," *2016 13th International Multi-Conference on Systems, Signals & Devices (SSD)*, Leipzig, Germany, 2016, pp. 454-458, doi: 10.1109/SSD.2016.7473662.

[53] A. Inteha and Nahid-Al-Masood, "A GRU-GA Hybrid Model Based Technique for Short Term Electrical Load Forecasting," *2021 2nd International Conference on Robotics, Electrical and Signal Processing Techniques (ICREST)*, DHAKA, Bangladesh, 2021, pp. 515-519, doi: 10.1109/ICREST51555.2021.9331156.

[54] G. G. Netto *et al*., "A hybrid evolutionary probabilistic forecasting model applied for rainfall and wind power forecast," *2016 IEEE Conference on Evolving and Adaptive Intelligent Systems (EAIS)*, Natal, Brazil, 2016, pp. 73-78, doi: 10.1109/EAIS.2016.7502494.

[55] C. Ren, L. Jia and Z. Wang, "A CNN-LSTM Hybrid Model Based Short-term Power Load Forecasting," *2021 Power System and Green Energy Conference (PSGEC)*, Shanghai, China, 2021, pp. 182-186, doi: 10.1109/PSGEC51302.2021.9542404.

[56] T. Sujjaviriyasup and K. Pitiruek, "A comparison between MODWT-SVM-DE hybrid

model and ARIMA model in forecasting primary energy consumptions," *2017 IEEE International Conference on Industrial Engineering and Engineering Management (IEEM)*, Singapore, 2017, pp. 799-802, doi: 10.1109/IEEM.2017.8290001.

[57] Y. Li *et al*., "A TCN-Based Hybrid Forecasting Framework for Hours-Ahead Utility-Scale PV Forecasting," in *IEEE Transactions on Smart Grid*, vol. 14, no. 5, pp. 4073-4085, Sept. 2023, doi: 10.1109/TSG.2023.3236992.

[58] S. S. Sanz *et al*., "Short-Term Wind Speed Prediction by Hybridizing Global and Mesoscale Forecasting Models with Artificial Neural Networks," *2008 Eighth International Conference on Hybrid Intelligent Systems*, Barcelona, Spain, 2008, pp. 608-612, doi: 10.1109/HIS.2008.36.

[59] K. M. San, J. G. Singh and K. Prakash N., "Wind Speed Forecasting using Hybrid Model of CNN and LSTM with Wavelets," *2023 International Conference in Advances in Power, Signal, and Information Technology (APSIT)*, Bhubaneswar, India, 2023, pp. 297-301, doi: 10.1109/APSIT58554.2023.10201713.

[60] Guo-Feng Fan, Ying-Ying Han, Jin-Wei Li, Li-Ling Peng, Yi-Hsuan Yeh, Wei-Chiang Hong, “A hybrid model for deep learning short-term power load forecasting based on feature extraction statistics techniques”, Expert Systems with Applications, Volume 238, Part C, 2024, 122012, ISSN 0957-4174, https://doi.org/10.1016/j.eswa.2023.122012.

[61] Siwei Li, Xiangyu Kong, Liang Yue, Chang Liu, Muhammad Ahmad Khan, Zhiduan Yang, Honghui Zhang, “Short-term electrical load forecasting using hybrid model of manta ray foraging optimization and support vector regression”, Journal of Cleaner Production, Volume 388, 2023, 135856, ISSN 0959-6526, https://doi.org/10.1016/j.jclepro.2023.135856.

[62] Thomas Monahan, Tianning Tang, Thomas A.A. Adcock, “A hybrid model for online short-term tidal energy forecasting”, Applied Ocean Research, Volume 137, 2023, 103596, ISSN 0141-1187, https://doi.org/10.1016/j.apor.2023.103596.

[63] Muhammad Hamza Zafar, Noman Mujeeb Khan, Majad Mansoor, Adeel Feroz Mirza, Syed Kumayl Raza Moosavi, Filippo Sanfilippo, “Adaptive ML-based technique for renewable energy system power forecasting in hybrid PV-Wind farms power conversion systems”, Energy Conversion and Management, Volume 258, 2022, 115564, ISSN 0196-8904, https://doi.org/10.1016/j.enconman.2022.115564.

[64] Hamed H.H. Aly, “A novel approach for harmonic tidal currents constitutions forecasting using hybrid intelligent models based on clustering methodologies”,

Renewable Energy, Volume 147, Part 1, 2020, Pages 1554-1564, ISSN 0960-1481, https://doi.org/10.1016/j.renene.2019.09.107.

[65] Regita Putri Permata, Dedy Dwi Prastyo, Wibawati, "Hybrid dynamic harmonic regression with calendar variation for Turkey short-term electricity load forecasting", Procedia Computer Science, Volume 197, 2022, Pages 25-33, ISSN 1877-0509, https://doi.org/10.1016/j.procs.2021.12.114.

[66] Typical Meteorological Data access service. European Commission, Joint Research Centre (JRC) [Dataset], Retrieved from https://re.jrc.ec.europa.eu/pvg_tools/en/tools.html.

[67] Ruan Jiayang (2023). Detailed Modelling of a 1.5MW Wind Turbine based on Direct-driven PMSG, MATLAB Central File Exchange. Accessed on 2023-09-23. Retrieved from https://www.mathworks.com/matlabcentral/fileexchange/41833-detailed-modelling-of-a-1-5mw-wind-turbine-based-on-direct-driven-pmsg

[68] W. S. McCulloch and W. Pitts, "A logical calculus of ideas immanent in nervous activity," *The bulletin of mathematical biophysics*, vol. 5, no. 18, pp. 115–133, 1943.

[69] H. Demuth and M. Beale, "Neural network toolbox for use with MATLAB," vol. 9, 12 2000.

[70] S. T. Mehmood and M. El-Hawary, "Performance evaluation of New and Advanced Neural Networks for Short term load forecasting," in *2014 IEEE Electrical Power and Energy Conference*, pp. 202–207, IEEE, 2014.

[71] D. W. Marquardt, "An algorithm for Least-squares estimation of nonlinear parameters," *Journal of the Society for Industrial and Applied Mathematics*, vol. 11, no. 2, pp. 431–441, 1963.

[72] H. Yu and B. M. Wilamowski, "Levenberg–Marquardt training," in *Intelligent systems*, pp. 12–1, CRC Press, 2018.

[73] W. XiangJun and M. M. Al-Hashimi, "The comparison of Adaptive Neuro Fuzzy Inference System (ANFIS) with nonlinear regression for estimation and prediction," in *2012 International Conference on Information Technology and e-Services*, pp. 1–7, IEEE, 2012.

[74] S. Ghore and A. Goswami, "Short term load forecasting of Chhattisgarh grid using Adaptive Neuro Fuzzy Inference System," 2015.

[75] S. A. Ludwig, "Comparison of time series approaches applied to Greenhouse gas analysis: ANFIS, RNN, and LSTM," in *2019 IEEE International Conference on Fuzzy Systems*

(FUZZ-IEEE), pp. 1–6, IEEE, 2019.

[76] M. F. Møller, "A scaled conjugate gradient algorithm for fast supervised learning," *Neural networks*, vol. 6, no. 4, pp. 525–533, 1993.

[77] L. Babani, S. Jadhav, and B. Chaudhari, "Scaled conjugate gradient based adaptive ANN control for induction motor drive," in *IFIP International Conference on Artificial Intelligence Applications and Innovations*, pp. 384–395, Springer, 2016.

[78] S. M. Alam and M. H. Ali, "A new subtractive clustering based ANFIS system for residential load forecasting," in *2020 IEEE Power & Energy Society Innovative Smart Grid Technologies Conference (ISGT)*, pp. 1–5, IEEE, 2020.

[79] A. Hatata and M. Eladawy, "Prediction of the true harmonic current contribution of nonlinear loads using NARX neural network," *Alexandria engineering journal*, vol. 57, no. 3, pp. 1509–1518, 2018.

[80] Y. Pang, "Short-term Harmonics forecasting and evaluation affected by electrified railways on the power grid based on stack auto encoder neural net- work method and the comparison to bp method," in *2018 13th IEEE Conference on Industrial Electronics and Applications (ICIEA)*, pp. 1159–1165, IEEE, 2018.

[81] A. J. Zavala and A. R. Messina, "Dynamic harmonic regression approach to wind power generation forecasting," in *2016 IEEE PES Transmission & Distribution Conference and Exposition-Latin America (PES T&D-LA)*, pp. 1–6, IEEE, 2016.

[82] R.Yager and D. Filev,"Generation of Fuzzy Rules by Mountain Clustering", in 1994 *Journal of Intelligent & Fuzzy Systems,* Vol.2, No. 3, pp. 209-209

[83] "Wind Farm - DFIG Detailed Model" - MATLAB & Simulink. Accessed 2022-09-18. Retrieved from https://www.mathworks.com/help/sps/ug/wind-farm-dfig-detailed-model.html

[84] D.R. Baughman, & Y.A. Liu, "Fundamental and Practical Aspects of Neural Computing" in 1995 Neural Networks in Bioprocessing and Chemical Engineering pp. 21–109.

[85] Hamed H H Aly "A novel approach for harmonics tidal currents constitutions forecasting using hybrid intelligent models based on clustering methodologies" Journal of Renewable energy. 2020, vol 147 page 1554-1564. https://doi.org/10.1016/j.renene.2019.09.107

[86] Hamed H. H. Aly" A proposed intelligent short-term load forecasting hybrid models of

ANN, WNN and KF based on clustering techniques for smart grid" Journal of Electric Power Systems Research, Vol 182, May 2020.

[87] Hamed Aly, "Forecasting, Modelling and Control of Tidal Currents Electrical Energy Systems" Ph.D. dissertation, Department of Electrical and Computer Engineering, Dalhousie University, Halifax, N.S., 2012.

[88] D. Caputo, F. Grimaccia, M. Mussetta and R. E. Zich, "Photovoltaic plants predictive model by means of ANN trained by a hybrid evolutionary algorithm," *The 2010 International Joint Conference on Neural Networks (IJCNN)*, Barcelona, Spain, 2010, pp. 1-6, doi: 10.1109/IJCNN.2010.5596782.

[89] S. Hochreiter and J. Schmidhuber, "Long Short-Term Memory," in Neural Computation, vol. 9, no. 8, pp. 1735-1780, 15 Nov. 1997, doi: 10.1162/neco.1997.9.8.1735.

[90] Hamed H. Aly "A novel deep learning intelligent clustered hybrid models for wind speed and power forecasting" Journal of Energy, Vol 213, 2020. https://doi.org/10.1016/j.energy.2020.118773

[91] Hamed H. Aly "Intelligent optimized deep learning hybrid models of neuro wavelet, Fourier Series and Recurrent Kalman Filter for tidal currents constitutions forecasting" Journal of Ocean Engineering, Volume 218, 2020. https://doi.org/10.1016/j.oceaneng.2020.108254

[92] Aytaç Altan, Seçkin Karasu, Enrico Zio, A new hybrid model for wind speed forecasting combining long short-term memory neural network, decomposition methods and grey wolf optimizer, Applied Soft Computing, Volume 100, 2021, 106996, ISSN 1568-4946, https://doi.org/10.1016/j.asoc.2020.106996.

[93] B. Zhou, X. Ma, Y. Luo and D. Yang, "Wind Power Prediction Based on LSTM Networks and Nonparametric Kernel Density Estimation," in IEEE Access, vol. 7, pp. 165279-165292, 2019, doi: 10.1109/ACCESS.2019.2952555.

[94] Hamed H. Aly "Dynamic modeling and control of the tidal current turbine using DFIG and DDPMSG for power system stability analysis", International Journal of Electrical Power & Energy Systems, Vol 83, pages 525-540, 2016. https://doi.org/10.1016/j.ijepes.2016.03.055

[95] Hamed H. Aly "A hybrid optimized model of Adaptive Neuro-Fuzzy Inference System, Recurrent Kalman Filter and Neuro-Wavelet for Wind Power Forecasting Driven by DFIG" International Journal of Energy, 2022.

[96] Hamed H H Aly, “An intelligent hybrid model of neuro Wavelet, time series and Recurrent Kalman Filter for wind speed forecasting” Journal of Sustainable Energy Technologies and Assessments vol 41, 2020. https://doi.org/10.1016/j.seta.2020.100802

[97] Y. K. Semero, J. Zhang and D. Zheng, "PV power forecasting using an integrated GA-PSO-ANFIS approach and Gaussian process regression-based feature selection strategy," in *CSEE Journal of Power and Energy Systems*, vol. 4, no. 2, pp. 210-218, June 2018, doi: 10.17775/CSEEJPES.2016.01920.

[98] Fawaz Al Hadi, Hamed H H Aly, Timothy Little “Harmonics Prediction and Mitigation using Adaptive Neuro Fuzzy Inference System Model based on Hybrid of Wind Solar Driven by DFIG” IEEE 13th Annual Information Technology, Electronics and Mobile Communication Conference, Vancouver, BC, Canada, 2022.

[99] Ana María Peco Chacón, Isaac Segovia Ramírez, Fausto Pedro García Márquez, “K-nearest neighbour and K-fold cross-validation used in wind turbines for false alarm detection”, Sustainable Futures, Volume 6, 2023, 100132, ISSN 2666-1888, https://doi.org/10.1016/j.sftr.2023.100132.

[100] Hoang Lan Vu, Kelvin Tsun Wai Ng, Amy Richter, Chunjiang An, “Analysis of input set characteristics and variances on k-fold cross validation for a Recurrent Neural Network model on waste disposal rate estimation”, Journal of Environmental Management, Volume 311, 2022, 114869, ISSN 0301-4797, https://doi.org/10.1016/j.jenvman.2022.114869.

[101] Xinyu Zhang, Chu-An Liu, “Model averaging prediction by K-fold cross-validation”, Journal of Econometrics, Volume 235, Issue 1, 2023, Pages 280-301, ISSN 0304-4076, https://doi.org/10.1016/j.jeconom.2022.04.007.

[102] Fawaz M Al Hadi, Hamed H Aly, Timothy Little “Harmonics Forecasting of Wind and Solar Hybrid Model Driven by DFIG and PMSG using ANN and ANFIS” IEEE Access, March 2023.

[103] Fawaz Al Hadi, Hamed H H Aly, Timothy Little “A Proposed Adaptive Filter for Harmonics Mitigation based on Adaptive Neuro Fuzzy Inference System Model for Hybrid Wind Solar Energy System” IEEE Canadian Conference on Electrical and Computer Engineering, Halifax, NS, Canada, 2022.

[104] Fawaz M Al Hadi, Hamed H Aly, Timothy Little “Harmonics Forecasting of Wind and Solar Hybrid Model Based on Deep Machine Learning" IEEE Access, March 2023.

[105] Hmeda Musbah, Gama Ali, Hamed H Aly, Timothy A Little "Energy management using multi-criteria decision making and machine learning classification algorithms for intelligent system" Electric Power Systems Research 203, 107645, 2022.

[106] Gamal Aburiyana, Hamed Aly, Timothy Little "Direct net load forecasting using adaptive neuro fuzzy inference system" 2021 IEEE Electrical Power and Energy Conference (EPEC), 131-136, Ontario, Canada, 2021.

[107] Hmeda Musbah, Hamed H. Aly, Timothy A. Little 'Energy management of hybrid energy system sources based on machine learning classification algorithms" Electric Power Systems Research 199, 107436, 2021.

[108] Hamed H. H. Aly "A novel deep learning intelligent clustered hybrid models for wind speed and power forecasting", Energy 213, 118773, 2020.

[109] Fawaz Alhaddad, Hamed H Aly, Mo El-Hawary "A Proposed Adaptive Intelligent Controllers for Tidal Currents Turbine Driving DDPMSG for Improving the Output Power Generated" 2019 IEEE Electrical Power and Energy Conference (EPEC), 1-4, 2019, Montreal, Canada.

[110] Shadi H. Shehadeh, Hamed H. Aly, M. E. El-Hawary" Effect of weather conditions on harmonic performance of PV inverters" Electric Power Components and Systems 47 (14-15), 1233-1246, 2019.

[111] Fawaz Alhaddad, Hamed H Aly, Mo El-Hawary "An Overview of Wind-Solar System Output Power" 2019 IEEE Canadian Conference of Electrical and Computer Engineering,2019, Edmonton, Canada.

[112] Hamed H. H. Aly "A Proposed Intelligent Adaptive Controllers for Wind Turbine Driving DFIG for Improving the Output Generated Power" 2019 IEEE Canadian Conference of Electrical and Computer Engineering, 2019, Edmonton, Canada.

[113] Shadi H. Shehadeh, Hamed H. Aly, M. E. El-Hawary "PV harmonic distribution analysis for various conditions" 2016 IEEE Canadian Conference on Electrical and Computer Engineering, 2016 Vancouver, Canada.

[114] Hamed H. Aly, Mo E. El-Hawary "Tidal current turbine, wind turbine and their dynamic modelling Transactions on Engineering Technologies: Special Issue of the World Congress on Engineering and Computer Science 2013.

[115] Hamed Aly "Offshore Wind and Tidal Current Energy Resources: Forecasting, Modeling, and Control" 2013, https://www.amazon.ca/Offshore-Tidal-Current-Energy-Resources/dp/365937167X.

[116] Hamed H. Aly, Mo E. El-Hawary "The current status of wind and tidal in-stream electric energy resources" American Journal of Electrical Power and Energy Systems" 2 (2), 23-40, 2013.

[117] Hamed H H Aly, M E El-Hawary" Stability and control of tidal current energy with DFIG using PI controllers" 2012 25th IEEE Canadian Conference on Electrical and Computer Engineering, 2012, London, Canada.

[118] Hamed H. Aly, Mo E. El-Hawary "Small signal stability analysis of tidal current turbine using ddpmsg with and without controller"2011 IEEE Electrical Power and Energy Conference, 239-243, 2011, Winnipeg, Canada.

[119] Hamed H. Aly, Mo E. El-Hawary "State of the art for tidal currents electric energy resources" 2011 24th Canadian Conference on Electrical and Computer Engineering, 2011, Niagara Falls, Calgary, Canada.

[120] Hamed H. Aly, Mo E. El-Hawary "An overview of offshore wind electric energy resources" Canadian Conference on Electrical and Computer Engineering, 2010, Calgary, Canada.

Appendix A: NON-EXCLUSIVE DISTRIBUTION LICENSE

I, Fawaz Al Hadi grant Dalhousie University the non-exclusive right to reproduce and distribute your submission worldwide in any medium.

I agree that Dalhousie University may, without changing the content, reformat the submission for the purpose of preservation.

I also agree that Dalhousie University may keep more than one copy of this submission for purposes of security, back-up, and preservation.

I agree that the submission is your original work, and that I have the right to grant the rights contained in this license. I also agree that my submission does not, to the best of my knowledge, infringe upon anyone's copyright.

I agree that I have obtained the unrestricted permission of the copyright owner to grant Dalhousie University the rights required by this license, and that such third-party owned material is clearly identified and acknowledged within the text and content of the submission.